Study on Electromagnetic Crimping of Tube-to-Rod for Axial and Torsional Joint

A Thesis Submitted in Partial Fulfillment of the Requirements

for the Degree of

DOCTOR OF PHILOSOPHY

Submitted by

Getu Tilahun Areda

(Roll No. 146103039)

Department of Mechanical Engineering

Indian Institute of Technology Guwahati

Guwahati-781039, India

October 2019

Department of Mechanical Engineering

Indian Institute of Technology Guwahati

Guwahati-781039,

India

Declaration

I hereby certify that the information presented in the dissertation "***Study on Electromagnetic Crimping of Tube-to-Rod for Axial and Torsional Joint***" is entirely my own account of research performed under the guidance of Dr. Sachin D. Kore. Any part of this work has not earlier been submitted for the award of any degree, diploma, associate-ship, fellowship or it's equivalent to any University or Institution. The entire procedure implemented, text and figures used to discuss and explore results are my own.

18/10/2019

Getu Tilahun Areda

Roll No. 146103039

Department of Mechanical Engineering

Indian Institute of Technology Guwahati

Assam-781039, India

Department of Mechanical Engineering

Indian Institute of Technology Guwahati

Guwahati-781039,

India

Certificate

To whomsoever, it may concern it is to certify that the work contained in this thesis entitled "***Study on Electromagnetic Crimping of Tube-to-Rod for Axial and Torsional Joint***" submitted by ***Mr. Getu Tilahun Areda (Roll No. 146103039)*** to the Indian Institute of Technology Guwahati for the award of the degree of Doctor of Philosophy. This work has been carried out under my supervision in the Department of Mechanical Engineering, India Institute of Technology Guwahati. The contribution of this work has not been submitted partly or entirely elsewhere for the award of any other degree or diploma.

18/10/2019

(**Dr. Sachin D. Kore**)

Associate Professor

Department of Mechanical Engineering

Indian Institute of Technology Guwahati

Assam-781039, India

To my beloved wife (Mekdiye) and boys (Dany & Eyosi)

For their unconditional love, support, and patience

Acknowledgments

I would like to thank ***almighty God*** for bringing hope through even the toughest of times and strengthening me to reach where I am right now. I take this opportunity to express my sincere appreciation to many people for their support and inspiration during the various stages of my doctoral research work in IIT Guwahati.

I wish to express my deepest gratitude to my supervisor, ***Dr. Sachin D. Kore*** for his continuous guidance, inspiration, and support throughout my research work. It was privileged to have had the opportunity to learn from and work with him. I have been given full freedom to explore my ideas, discuss any aspect of the work and encouragement when I was faced with challenges. I express my sincere appreciation to my administrative supervisor and doctoral committee members, i.e., ***Dr. Arup Nandy, Dr. R. Ganesh Narayanan, Dr. Swarup Bag,*** *and* ***Dr. Sisir Kumar Nayak*** for their valuable suggestions, encouragement, and support during the period of my research work.

I am thankful to the Ministry of National Defence of Ethiopia, Defence Engineering College of Ethiopia and Government of India for giving me this opportunity to carry out my study in one of the prestigious technological institute in engineering. I am also thankful to all faculty and staff of the Department of Mechanical Engineering of the Indian Institute of Technology Guwahati for extending their cooperation regarding technical and official support.

I would like to thank my seniors ***Dr. Chandrahas Patel, Dr. J. K Doley, Dr. Ashish Kumar Rajak***, and labmates ***Dr. Ramesh Kumar, Mr. Piyush Singh, Mr. Sagar Pawar***, ***Mr. Deepak Kumar*** for their support during ups and downs of my work. I am also thankful to all Ethiopian scholars for their friendship and support to overcome any encountered problems.

Finally, I would like to thank my ***beloved wife (Mekdiye) and kids (Dany & Eyosi)*** for their unconditional love, support, and patience until the completion of my research work. I don't have any single word to express the sacrifice that my wife made for me to complete my research work in the way it should be. ***It is impossible to imagine my success without her sacrifice***.

Getu Tilahun Areda

Abstract

Dissimilar metal joints are widely used for the technical and economical reason in various industrial applications which involves lightweight design. The capability to join aluminum tube and a steel rod are highly desirable, but challenging to achieve expected joint quality using conventional means like by arc welding or mechanical crimping. To deal with all those challenges, advanced joining technology like electromagnetic crimping becomes prominent. Electromagnetic crimping (EM crimping) is a high-speed joining process that deforms electrically conductive material by discharging high-voltage from the capacitor bank at room temperature. Primarily, experiments were carried out to investigate the feasibility of EM crimping of aluminum tube with steel rod using a single rectangular groove which includes the effects of discharge energies on the strength of a joint, radial displacement, and tube thickness reduction respectively. This study was further extended to a numerical and experimental approach. A numerical study was carried out initially to find a suitable coil dimension. A validated model was used to predict the effects of discharge energies on process parameters and to determine the best energy levels. Based on the result obtained from simulations, three among seven levels of discharge energy were chosen for the experiment. For improving joint strength to support an axial load, a double rectangular groove was used. The numerical simulation is reasonably predicting mode of failure and process parameters. A significant effect of groove depth on the strength of the joint, groove filling, wrinkling, and tube thickness reduction was also studied. A practical design guideline that describes the effects of the width-to-depth ratio on the strength of a joint was proposed.

The concentrated discharge energy enhances the uniformity of deformation at the joining zone which can be achieved using a tool called field-shaper. The effects of two field-shapers on the strength of a joint manufactured for torsional and axial load bearing were investigated experimentally. From this study, it can be concluded that a single stepped field-shaper is better than a tapered one regarding deformation uniformity in the joining zone and joint quality. Besides that, the joint strength of aluminum to steel rod with a knurled profile was found better compared to plain profile. Further, the effects of rectangular groove parameters on joint quality that can support both torsional and axial load simultaneously were investigated. A new technique in mechanical strength testing is introduced for the crimped sample which can resolve challenges faced so far in this regard. The optimum groove parameters predicted using response surface

methodology (RSM) were found in a good agreement with actual measured parameters. Different modes of failure which signify joint quality were explored during mechanical strength tests. Finally, a guideline is proposed to design a rectangular groove to transfer maximum torsional and axial load simultaneously. The developed method has great importance to identify groove parameters which significantly affect the strength of a joint manufactured by EM crimping process. The results found in this study have vital significance in automotive and spaceframe structure industries practically use EM crimping as alternative joining techniques.

Contents

Abstract v

Contents vii

List of Figures x

List of Tables xv

CHAPTER 1

1 Introduction 2

1.1. Metal Forming Processes 2

1.1.1. Conventional Forming Processes 2

1.1.2. High Strain Rate Forming Process 3

1.2. Motivation 5

1.3. Objectives 6

1.4. Organization of the Thesis 7

2 Literature Review 11

2.1. Introduction 11

2.2. Experimental Studies on Joining by EMF 11

2.3. Numerical Studies on Joining by EMF 12

2.4. Analytical Studies on Joining by EMF 14

2.5. Application Oriented Studies on Joining by EMF 16

2.6. Field-shaper 17

2.7. Advantage and Disadvantage of EMF 19

2.8. Theoretical Background of EMF Processes 21

2.9. Gaps in the Literature 27

3 Electromagnetic Crimping for Tube-to-Rod Configuration to Support Axial Load 30

3.1. Introduction 30

3.2. Methodology 30

3.2.1. Finite Element Modeling 32

3.2.2. Material and Experimental Setup 33

3.3. Mechanical Pull-out Test Condition 36

3.4. Results and Discussion 36

3.4.1. Process Parameters 36

3.4.2. Tube Thickness Reduction at the Groove Edge 37

3.4.3. Radial Displacement 38
3.4.4. Groove Filling....39
3.4.5. Comparison of Effective Plastic Strain and Resultant Displacement 40
3.4.6. Resultant Velocity and Effective Plastic Strain....41
3.4.7. Resultant Displacement....42
3.4.8. Lorentz Force, Current Density and Magnetic Field 43
3.4.9. Mechanical Pull-out Strength....43
3.4.10. Prediction of Possible Failure Region 49
3.4.11. Relation between Resultant Pressure and Displacement 49
3.5. Summary 50
4 Mechanical Interlock Made by EM crimping for Axial Load Resistance using Double Rectangular Groove 53
4.1. Introduction 53
4.2. Experimental Detail 53
4.2.1. Materials and Experimental Method....53
4.2.2. Experimental Setup....55
4.3. Mechanical Pull-out Test....56
4.4. Results and Discussion....56
4.4.1. Mechanical Pull-out Strength Analysis....58
4.4.2. Effects of Width-to-Depth Ratio on Joint Strength 62
4.4.3. Failure Mode 63
4.4.4. Effect of Groove Depth on Wrinkling and Tube Thickness Reduction....64
4.4.5. Hardness Analysis....66
4.5. Summary 66
5 Electromagnetic Crimping Using Double Rectangular Groove for Axial Joint: Experiment and Numerical Simulation....69
5.1. Introduction....69
5.2. Material and Method 69
5.3. Numerical Modeling....70
5.4. Analysis and Discussion 71
5.5. Experimental Work 72
5.6. Summary....77
6 Effect of Field-shaper and Groove Profile on Torsional and Axial Joint Strength 79

6.1. Introduction 79
6.2. Experimental Methods 79
6.2.1. Materials and Profile 79
6.2.2. Experimental Procedure and Setup 80
6.3. Mechanical Strength Testing Conditions and Setup 82
6.4. Results and Discussion 83
6.4.1. Deformation with and without Field-shaper 83
6.4.2. Effect of Voltage on Current 84
6.4.3. Effect of Field-shaper on Torsional strength 85
6.4.4. Effect of Field-shaper and profile on Pull-out Strength 89
6.4.5. Tube Thickness Reduction and Contact Length 91
6.4.6. Effects of Energies on Deformations 92
6.4.7. Failure Mode in a Torsion and Pull-out Test 92
6.5. Summary 93
7 Analysis of Effect of Groove Parameters on Axial and Torsional Joint Strength 96
7.1. Introduction 96
7.2. Experimental Methodology 96
7.2.1. Experimental Procedure 96
7.2.2. Material and Experimental Setup 97
7.3. Testing Condition 99
7.4. Result and Discussions 99
7.4.1. Cause and Effect Matrix 99
7.4.2. Model Validation 101
7.4.3. Effect of Groove Parameters on Torque and Pull-out Load 103
7.5. Summary 108
8 Conclusions and Future Scope of the Work 111
8.1. Conclusions 111
8.2. Future Scope of the Work 113
9 References 114
10 Publications Out of this Work 123

List of Figures

Fig. 1. 1 Schematic representation of (a) sheet and (b) tube EHF process 3
Fig. 1. 2 Schematic representation of (a) sheet and (b) tube explosive forming process.....4
Fig. 1. 3 Three major electromagnetic forming processes 5
Fig. 1. 4 Schematic representation of the simplified electromagnetic forming circuit 5
Fig. 2. 1 EMC setup using single stepped field-shaper.....19
Fig. 2. 2 Schematic representation of EM crimping 21
Fig. 2. 3 Workpieces shape (a) before and (b) after deformation.....23
Fig. 2. 4 The research plan implemented to achieve the objectives 28
Fig. 3.1 Flow chart of the implemented procedure.....31
Fig. 3.2 Dimension of (a) rod (b) aluminum tube and (c) coil (All dimensions are in mm).....32
Fig. 3.3 (a) side view and (b) cross-sectional view of assembled models 32
Fig. 3.4 Boundary condition for the tube, rod, and coil 33
Fig. 3.5 Experimental setup.....34
Fig. 3.6 EMF system and experimental setup 35
Fig. 3.7 Pull-out testing condition for (a) crimped sample and (b) tube (All dimensions are in mm) 36
Fig. 3.8 (a) The measured current curve for 5.7 kV and 10.2 kV (b) a solenoid copper coil and (c) crimped sample 36
Fig. 3.9 Effects of discharge energy on tube thickness reduction at groove edge.....37
Fig. 3.10 Final shapes obtained in (a) experiment and (b) simulation.....38
Fig. 3.11 Radial displacement in experiment and simulation 38
Fig. 3.12 Radial displacement at 3.4 kJ, 4.1 kJ, and 4.7 kJ discharge energy.....39
Fig. 3.13 Prediction of groove filling at different time value for 4.1 kJ discharge energy 39
Fig. 3.14 Selected elements along the joining zone.....40
Fig. 3.15 Variations of effective plastic strain and resultant displacement along the joining zone 41
Fig. 3.16 Effect of discharge energies on resultant velocity and effective plastic stain 41
Fig. 3.17 Effect of discharge energies on resultant displacement for different energy levels 42
Fig. 3.18 Tube cracking at the groove edge for 5.0 kJ.....43
Fig. 3.19 Pull-out strength of crimped sample and tube 44

Fig. 3.20 Pull-out loads for 3.4 kJ, 4.1 kJ, and 4.7 kJ discharge energy.....45
Fig. 3.21 Load versus extension for all samples.....45
Fig. 3.22 Crimped sample after the pull-out test 46
Fig. 3.23 Effect of discharge energy on (a) radial displacement and (b) thickness reduction at groove edge.....47
Fig. 3.24 (a) effect of discharge energy on pull-out strength and (b) discharge energy for the respective voltage.....47
Fig. 3.25 Effect of radial displacement on pull-out strength.....48
Fig. 3.26 (a) Cross-sectional view of joining zone and (b) metallographic image at the joining zone 48
Fig. 3.27 Effect of energy on maximum shear stress distribution along the joining zone 49
Fig. 3.28 Relation between resultant pressure and displacement at (a) 3.4 kJ (b) 4.1 kJ (c) 4.7 kJ, and (d) comparison.....50
Fig. 4. 1 Dimension and nomenclature of (a) rod (b) tube and (c) coil (All dimensions are in mm) 54
Fig. 4. 2 (a) Experimental setup and (b) coil inside Teflon made a fixture 55
Fig. 4. 3 Schematic representation of pull-out test for a crimped sample (All dimensions are in mm) 56
Fig. 4. 4 Tube necking at the groove edge due to discharging (a) 4.7 kJ and (b) 5.6 kJ for groove which has 2 mm depth.....57
Fig. 4. 5 Measured current waveform obtained at 4.7 kJ of discharge energy.....57
Fig. 4. 6 Pull-out strength vs. extension for (a) S_1-S_6 (b) S_7-S_{12} (c) S_{13}-S_{18} (d) S_{19}-S_{24} 58
Fig. 4. 7 Predicted and actual pull-out load for (a) S_7-S_{12} and (b) S_{19}-S_{24}.....59
Fig. 4. 8 (a) UTM pull-out test setup for a crimped sample and (b) pull-out strength of tube and samples failed at the joining zone.....60
Fig. 4. 9 Gap measured for (a) 0.5 mm (b) 1 mm (c) 1.5 mm (d) 2 mm (e) 2.5 mm and (f) 3 mm groove depth 61
Fig. 4. 10 Effect of groove depth on percentage gap filling.....61
Fig. 4. 11 Effect of groove depth on joint strength for all samples 62
Fig. 4. 12 Effect of width-to-depth ratio on joint strength (a) S_1-S_6 (b) S_7-S_{12} (c) S_{13}-S_{18} (d) S_{19}-S_{24}.....63

Fig. 4. 13 Failed sample (a) on Al tube and (b) on groove edge (joining zone).....64
Fig. 4. 14 Wrinkles for a sample which has (a) 3 mm and (b) 0.5 mm groove depth 65
Fig. 4. 15 Tube thickness reduction at groove edge for various depths.....65
Fig. 4. 16 (a) Hardness distributions across the interface of the crimped sample and (b) indentation locations 66
Fig. 5. 1 Workflow chart implemented in this procedure 70
Fig. 5. 2 (a) Side view and (b) cross-sectional view of assembled parts 71
Fig. 5. 3 Detail dimension of (a) tube (b) rod and (c) coil (All dimensions are in mm) 71
Fig. 5. 4 The waveform of the current curve obtained from the experiment 71
Fig. 5. 5 Resultant displacements for different groove depth.....72
Fig. 5. 6 (a) Experimental setup (b) coil with Teflon fixture and (c) crimped sample 72
Fig. 5. 7 Crimping in (a) simulation and (b) experiment for the different groove depth.....73
Fig. 5. 8 Radial displacement comparison using simulation and experiment for 0.5 mm groove depth. 73
Fig. 5. 9 Radial displacement comparison using simulation and experiment for 2 mm groove depth.....74
Fig. 5. 10 Contours of maximum shear strain at a different time value.....74
Fig. 5. 11 A contour of (a) magnetic pressure maximum at different time value and joining zone failure in (b) simulation and (c) experiment.....75
Fig. 5. 12 (a) pull-out strength of tube and crimped sample with different groove depth and (b) effect of groove depth on pull-out load.....75
Fig. 6. 1 Geometry and dimensions of (a) single-stepped field-shaper (b) tapered field-shaper (c) rod and (d) tube (All dimensions are in mm) 80
Fig. 6. 2 Steel rod with (a) plain and (b) knurled profile 80
Fig. 6. 3 Experimental procedure implemented.....81
Fig. 6. 4 Experimental setup (a) a top (b) left side and (c) right side view.....82
Fig. 6. 5 Tapered and single-stepped field-shaper 82
Fig. 6. 6 Testing condition for torsion and pull-out test (All dimensions are in mm) 82
Fig. 6. 7 (a) Torsion and (b) pull-out test set up.....83
Fig. 6. 8 Peak current for C_1 without and C_2 with single-stepped field-shaper.....83
Fig. 6. 9 Deformation using (a) C_1 without field-shaper and (b) C_2 with field-shaper.....84

Fig. 6. 10 Typical waveform of the current for various voltages used in (a) aluminum-to-aluminum and (b) aluminum-to-steel configuration 85
Fig. 6. 11 Effect of discharge energy on torque using (a) single-stepped and (b) tapered field-shaper 86
Fig. 6. 12 Effect of field-shaper geometry on torque resistance (Aluminium-to-aluminium) 87
Fig. 6. 13 Effect of discharge energy on torsional strength 88
Fig. 6. 14 Crimped sample with (b) plain and (c) knurled profile 89
Fig. 6. 15 Effect of knurled and plain profile on torque resistance (Aluminium-to-steel).....89
Fig. 6. 16 Effect of field-shaper geometry on pull-out strength 90
Fig. 6. 17 Pull-out strength for (a) plain and (b) knurled profiles 91
Fig. 6. 18 Tube thickness reduction and contact length.....91
Fig. 6. 19 Deformation at (a) 2.3 kJ (b) 2.7 kJ and (c) 3.0 kJ.....92
Fig. 6. 20 Samples (a) before the test (b) after torsion test and (c) after pull-out test 93
Fig. 6. 21 Joint failure (a, b) using plain groove surface and (c) knurled groove surface 93
Fig. 7. 1 Implemented procedure for an experiment and analysis 97
Fig. 7. 2 Geometrical shape and dimensions of (a) tube (b) rod and (c) single-stepped field-shaper (All dimensions are in mm) 98
Fig. 7. 3 Experimental setup (a) side and (b) top view 98
Fig. 7. 4 Current waveforms measured from the experiment 98
Fig. 7. 5 Test condition for (a) torsion, pull-out and (b) three-point bending 99
Fig. 7. 6 Groove parameters (a) length (b) width and (c) depth 100
Fig. 7. 7 Predicted versus actual (a) torque and (b) pull-out strength.....101
Fig. 7. 8 (a) Comparison of predicted and actual torque and (b) absolute percentage error of respective trials 102
Fig. 7. 9 (a) Comparison of predicted and actual pull-out load and (b) absolute percentage error of respective trials 102
Fig. 7. 10 Tube shearing at groove edge for (a) 1 mm (b) 2 mm and (c) 3 mm groove depth....103
Fig. 7. 11 Effect of depth on (a) torque and (b) pull-out strength for 8 mm and 10 mm width ..104
Fig. 7. 12 Effect of width on (a) torque and (b) pull-out strength 104
Fig. 7. 13 Effect of groove length on (a) torque and (b) pull-out strength.....105
Fig. 7. 14 Response surface plot of the effect of groove parameters on torque 106

Fig. 7. 15 Response surface plot of the effect of groove parameters on pull-out load 106
Fig. 7. 16 Failure mode in torsion test for (a) 1 mm (b) 2mm and (c) 3mm groove depth.....107
Fig. 7. 17 Failure mode in the pull-out test for (a) 1mm (b) 2 mm and (c) 3 mm groove depth.107
Fig. 7. 18 Three-point bending (a) setup and (b) failure mode.....108

List of Tables

Table 2. 1 Different designs of field-shaper, corresponding advantages, and disadvantages (Psyk et al., 2011) 18
Table 3. 1 Johnson-cook constants for Al 1050 and 4340 Steel (Rajak et al., 2018, Johnson, and William, 1983) 33
Table 3. 2 Chemical composition of Al 1050 tube and 4340 steel (Dhar et al., 2006) 34
Table 3. 3 Circuit parameters of EMF system 35
Table 3. 4 Sample numbers and process parameters 35
Table 3. 5 Detail process parameters for best energy levels 37
Table 3. 6 Maximum Lorentz force, current density and magnetic field 43
Table 4. 1 The chemical composition of aluminum tube and steel rod (Kumar and Kore, 2017) 53
Table 4. 2 Mechanical properties of the material used (Rajak and Kore, 2018, Kumar and Kore, 2017) 54
Table 4. 3 Groove geometrical parameters 55
Table 5. 1 Property of coil and tube material 69
Table 5. 2 Johnson-cook constants for Al1050 and DP steel (Melby and Eide, 2013, and Vedantam et al., 2006) 70
Table 5. 3 Predicted parameters 76
Table 6. 1 Chemical composition of Al1050 and Al 6061 tube 79
Table 6. 2 Coils parameters 81
Table 7. 1 Cause and effect matrix 100

CHAPTER 1

INTRODUCTION

1 Introduction

1.1. Metal Forming Processes

The ability to join tubular aluminum and steel is highly desirable to meet the demands of lightweight design for automotive and aerospace parts. However, to attain the expected joint quality using conventional means like arc welding or mechanical crimping is difficult. Besides that, dissimilar-metal joints are widely used for various industrial applications due to a technical and economical reason. Joining of dissimilar material is feasible by welding, riveting, bolting, soldering, mechanical crimping, forming, etc. Currently, several studies are undergoing to industrialize different joining by forming processes for the benefit of producing the upcoming lightweight engineering products. A general overview of the metal forming process is covered in this chapter.

Metal forming is one of the manufacturing processes in which a workpiece undergoes deformation beyond its elastic limit to take the shape of a die. An external load applied either manually or automatically is used to deform the workpiece plastically. A set of punches and dies with a static or dynamic load are used in the conventional and non-conventional forming process. However, there are non-conventional forming processes characterized as punch-less and die-less respectively. In general, metal forming processes can be classified as conventional and high strain rate which are briefly discussed as follows.

1.1.1. Conventional Forming Processes

Several conventional forming processes like rolling, forging and extrusion, wiredrawing, bending, deep drawing, and shearing can be done with maximum strain rate up to 5.0 s^{-1}. A set of dies and punches is the feature of this process. Besides that, a means for applying loads are mechanical or hydraulic which is known as the static load. These processes can successfully deform materials that have high formability such as alloys of steels. Lower formability limit of the material, wrinkling and spring back effect are critical factors that significantly affect the quality of a final product. Moreover, there are some common defects observed in the final product made by conventional forming processes such as poor surface finish, buckling, instability, etc. These defects occur due to the difficulty to control local deformation in the quasi-static forming process which can be resolved using a high strain rate forming method.

1.1.2. High Strain Rate Forming Process

In most of high strain forming process, the workpiece is given kinetic energy early in the process and then forming is mostly inertial as kinetic energy dissipated as plastic deformation. The applied load in the high strain forming process is dynamic that makes the workpieces to accelerate with greater kinetic energy. A high strain rate up to $10^4\,s^{-1}$ can be achieved in most of these processes (Woodward et al., 2010). Magnesium alloys have high potential as structural materials since magnesium is the lightest of all structural alloys (Watanabe et al., 2001). Aluminum and magnesium alloys are normally exhibited low formability in the quasi-static forming process. However, the formability of metals like aluminum and magnesium shows improvement while deformed using a high strain rate forming process. At large, three processes are categorized under high strain rate forming process based on sources of energy, i.e., electrohydraulic, explosive, and electromagnetic forming process. A brief description is provided in the following subsections.

1.1.2.1. Electrohydraulic Forming

Electrohydraulic forming (EHF) is a high-speed forming process that has a considerable effect on the formability improvement for different metal. Figure 1.1 (a) and (b) show some configurations of the electrohydraulic sheet metal forming and tube bulging respectively.

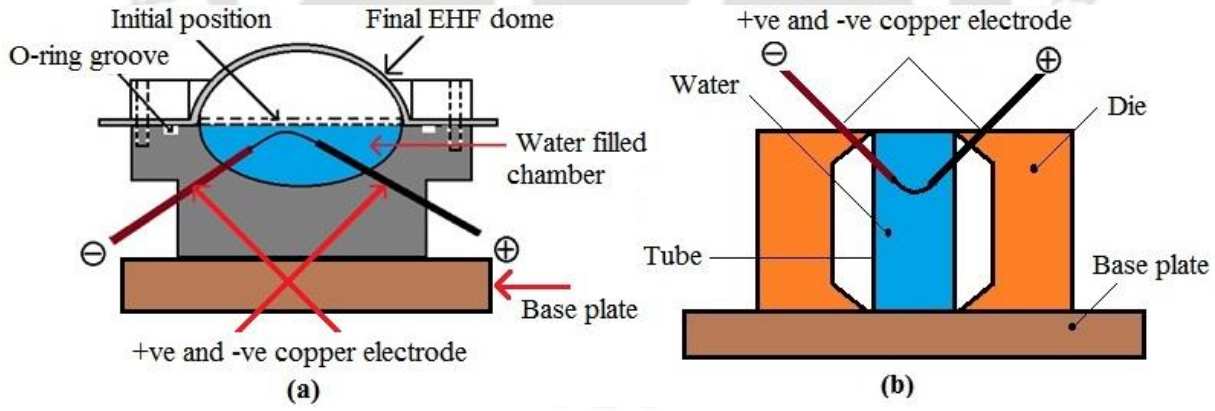

Fig. 1. 1 Schematic representation of (a) sheet and (b) tube EHF process

In this process, the electrical energy stored in a bank of capacitors discharges between a pair of electrodes submerged in a fluid and forms the sheet metal (Zia et al., 2017). When a high electric current passes through the electrodes, the spark will generate and vaporizes a small volume of liquid, and in turn, a shock wave will be produced which is responsible for plastic deformation.

Several processes like bulging, forming, flanging, drawing and piercing can be done successfully, but this process is not suitable for tube compression and swaging.

1.1.2.2. Explosive Forming

Explosive forming is a high-velocity forming technique that utilizes chemical energy of explosives to generate shock waves through a medium for the purpose of workpiece deformation. Some configurations in explosive forming process are demonstrated as Fig. 1.2 (a) and (b). Explosive forming is a broad term covering many process variations. Early patents relating to explosive forming appeared at the end of the 19th and the beginning of the 20th century. An increasing number of economically successful applications were being seen in the early 1970s, with the manufacture of large aluminum and high strength steel parts (Mynors and Zhang, 2002).

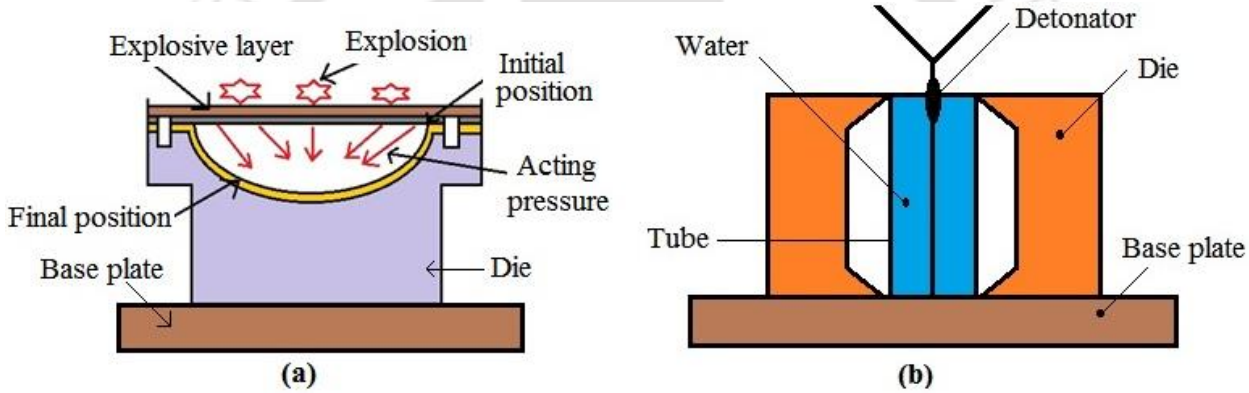

Fig. 1. 2 Schematic representation of (a) sheet and (b) tube explosive forming process

This process was designed to transfer chemical energy to mechanical and deform metals into dies and molds. The explosives are typically either detonated underwater or in direct contact with the materials. The method is useful for short production runs of conventionally difficult-to-manufacture parts. Because of process flexibility, explosive forming has historically been employed in the aerospace industry for prototyping of complex parts. This process used for forming parts on the scale of a few inches up to 15 feet and shows limitations like the lack of initiation of uniform detonation and the size of the holding tank.

1.1.2.3. Electromagnetic Forming

Electromagnetic forming (EMF) processes were invented in the late 1960s, which can overcome problems related to the joining of dissimilar materials (Oliveira et al., 2005). Figure 1.3 shows

different processes which are categorized under electromagnetic forming process, i.e., tube compression, tube expansion, and sheet metal forming based on workpiece and coil arrangement.

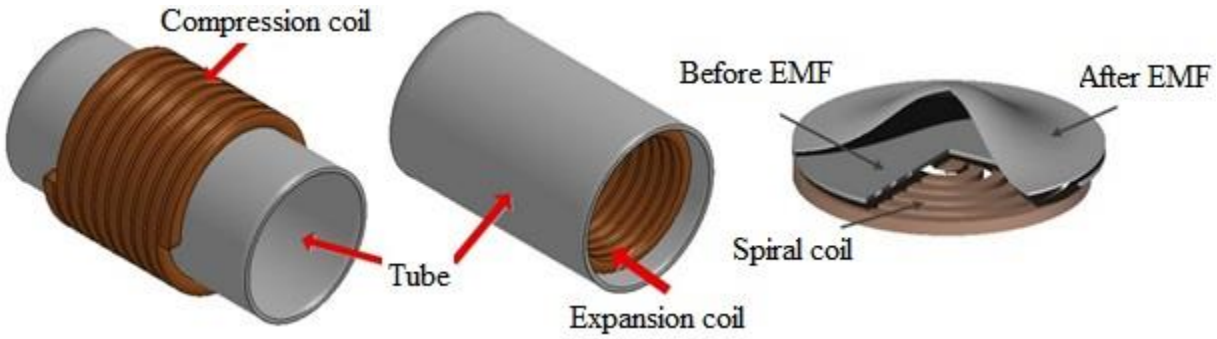

Fig. 1. 3 Three major electromagnetic forming processes

Figure 1.4 demonstrates a schematic representation of a magnetic pulse forming process. In Fig.1.4, a current will start to flow through the coil once electrical energy is discharged from the capacitor bank, and in turn magnetic field on the workpiece surface generated due to an induced current according to Faraday's law. This process is based on the repulsive forces generated by two opposing magnetic fields of the coil and a tube. A metal that has high electrical conductivity such as copper, aluminum, and magnesium can be easily deformed. However, alloys that have poor electrical conductivity can also be deformed using drivers made of metals like copper (Fenqiang et al., 2013 and Chansun et al., 2008).

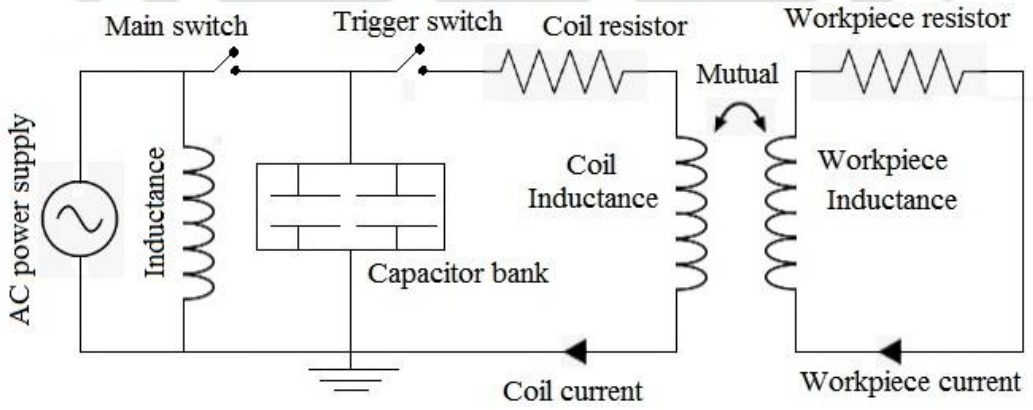

Fig. 1. 4 Schematic representation of the simplified electromagnetic forming circuit

1.2. Motivation

Traditional joining methods such as bolts and nuts, screws, pegs, and rivets must use additional joining elements, but the reliability of a joint made is questionable when functional for an extended

period. For the technical and economical reason, dissimilar metal joints are widely used in various applications that required an efficient joining technology. Besides that, joining of aluminum tube with a steel rod is challenging using a thermal-based welding process due to oxides formation which requires a higher melting temperature than the parent metal. The electromagnetic crimping process which is a high-speed and waste-free process was developed to address the problems mentioned above. Hence, electromagnetic impulse forming and joining process becomes prominent in the aerospace and automotive industries where the weight aspect ratio is the most critical.

In this thesis, crimping of the aluminum tube on aluminum and steel rod was investigated using EMF technology. The effect of rectangular groove parameters on joint strength to support axial and torsional load is investigated. For the analysis, a combined experimental investigation and numerical strategy, as well as the design of experiment (DOE) method have been chosen. The number of grooves and groove length were revealed as important parameters which can affect torsional strength significantly. Consecutively, increasing the mentioned parameters were leads to an increase in torsional resistance. However, the research result showed that the effect of increasing groove depth revealed unclear, and the effects of levels of energy were found less. Limited numbers of research works were found related to applications of EM crimping process. Hence, detail studies on the effect of groove and process parameters on joint quality using different approaches were found critical as a newly emerging joining technology. Finally, design guidelines to manufacture a joint that can support axial and torsional load were proposed for the benefit of lightweight design.

1.3. Objectives

The principal aim of this thesis is to investigate the effects of geometrical and processes parameters of EM crimping on joint strength using DOE, experimental, and numerical approaches. Finally, a design guideline is proposed to determine the best geometrical and process parameters to achieve better joint quality.

The following specific objectives were planned to be accomplished in this thesis.

1. Study on the feasibility of EM crimping process to join aluminum tubes to aluminum and steel rods for different applications using single and double rectangular grooves.

2. Experimental and numerical study on EM crimping of aluminum tube with a steel rod to predict the effect of discharge energies on process parameters.
3. Study the effect of groove depth on joint quality and propose a design guideline based on the effect of width-to-depth ratio on joint strength for the double rectangular groove.
4. Study the effects of field-shaper which has different geometry on joint strength to support axial and torsional loads. Investigate the effect of discharge energy on torsional joint strength made by aluminum to aluminum and steel configuration using EM crimping process for the automotive drive shaft.
5. Design a guideline to optimize rectangular groove parameters for joint manufactured that can support torsional and axial load simultaneously using a design of experiment method.

1.4. Organization of the Thesis

The thesis has been organized into eight chapters, and each chapter is briefly introduced as follows:

Introduction of conventional and high strain rate forming process, motivation and the primary objectives along with how the thesis is organized are covered in chapter 1.

Chapter 2 presents a review of the literature on electromagnetic forming in a particular EM crimping process. The review of work done related to EM crimping is organized based on research methodology and findings, i.e., experimental studies on joining by electromagnetic forming, numerical studies on joining by electromagnetic forming, analytical studies on joining by electromagnetic forming, and application-oriented studies on joining by electromagnetic forming respectively. Research on a different aspect of a field-shaper, advantage, and disadvantage of the process with the working principle of EMF are included in this chapter.

Chapter 3 provides numerical modeling and experimental study of EM crimping for a single rectangular groove. The best discharge energy levels were found from the simulation and used in the experiment. The effect of discharge energy on process parameters was predicted and studied in detail using a validated model. The feasibility of EM crimping of aluminum tube with steel rod using a single rectangular groove was realized in this study. The effect of discharge energy on joint strength and process parameters were explored. The experiment was carried out to find the best discharge energy among seven levels which can give higher joint strength. A joint strength of 90 % compared to the strength of a parent tube was found. The hardness at the interface was found

more than the tube. The joint strength achieved in this process was based on mechanical interlock at the groove edge which is examined and verified using microscopic study.

In chapter 4, the experimental study which aims the effect of groove parameters on joint strength manufactured by EM crimping using a double rectangular groove has been covered. A suitable groove depth was found using central composite design method, and a design guideline was proposed based on the effect of width-to-depth ratio on joint strength that is obtained from different geometrical configurations of groove parameters. Groove filling, tube thickness reduction at groove edge, and hardness at the joining zone were covered in this chapter.

Chapter 5 is concerned with the extension of previous work to predict different process parameters using numerical modeling and simulation which are difficult to measure experimentally. FE analysis and modeling were carried out using LS-DYNA^{TM} software which has EM module coupled with the mechanical, thermal and structural solver. A possible failure zone, effective plastic strains, resultant velocity, resultant displacement, magnetic field, Lorentz force, current density were predicted based on a validated model with the experiment.

Chapter 6 presents the effect of two field-shapers on joint strength which has different geometrical shapes. Pull-out and torsional strength of a joint manufactured which is obtained at different energy levels were considered and compared for aluminum to aluminum and aluminum to steel configuration. The effects of knurled profile in enhancing joint strength were also included for aluminum to aluminum and aluminum to steel configuration. The failure modes observed during each mechanical strength test were investigated.

Chapter 7 introduces a central composite design (CCD) method and response surface methodology (RSM) to find the best groove parameters that are significant in affecting axial and torque joint strength manufactured using EM crimping process for the first time. A combined effect of groove parameters on joint strength manufactured to resist axial and torsional load was studied in detail. Furthermore, the most significant groove parameters affecting joint strength also identified using the model developed.

Chapter 8 provides conclusions and future scope of the presented work which is followed by references and a list of publications.

Throughout the thesis, each chapter describes the experiment, simulation or both have been written in a self-sufficient manner. For these, each chapter comprises an introduction, methodology, results and discussion, and summary respectively.

CHAPTER 2

LITERATURE REVIEW

2 Literature Review

2.1. Introduction

In this chapter, the state of the art of joining by electromagnetic forming mainly EM crimping is reviewed as per the nature of the works and its findings. Moreover, gaps in the literature along with the research plan used to achieve the objectives are also provided. Intensive studies are required to understand clearly and use electromagnetic crimping as the production tool in the industries. Several research contributions are focusing on different aspects of this process and conclusively revised based on their approach and findings. Hence, an extensive literature survey has been conducted to know the scopes and researchers' focus areas on joining by electromagnetic forming. Literature is reviewed and organized based on their approaches, i.e., experimental studies, numerical studies, analytical studies, application-oriented studies on joining by electromagnetic forming, field-shapers and advantage and disadvantage of EMF process respectively.

2.2. Experimental Studies on Joining by EMF

The strength of the joint manufactured by EMF mainly depends on process parameters, material property, and joining mechanisms respectively. Three joint mechanisms which are categorized under joining by electromagnetic forming, i.e., interference fit, EM crimping, and electromagnetic welding (Weddeling et al., 2010). Residual stress between workpieces to be joined, the area of the contact zone and coefficient of friction affect the joint quality manufactured by interference fit (Kleiner et al., 2006 and Homberg et al., 2006). As reported by a few researchers, the joining of tubular components can be the most promising application field of an electromagnetic joining by forming process (Hammers et al., 2009). Effects of the surface profile like thread and knurled of the rod in enhancing the strength of a joint manufactured in electromagnetic crimping were studied. In this study, the threaded profile sample shows maximum pull-out strength comparing to plain and knurled (Kumar and Kore, 2017). The joints mechanical properties were analyzed using tensile tests after joining by electromagnetic compression due to the influence of different mandrel's surface conditions (Barreiro et al., 2006). A joint strength achieved from electromagnetic welding was found higher than which is obtained using interference fit and crimping, but it requires higher discharge energy. Comparable joint strength can be manufactured using EM crimping which is free from welding-related defects and mainly depends on the profile made on the rod. Even though

joint strength obtained by electromagnetic welding is stronger than the remaining two techniques, concerning energy efficiency in many cases EM crimping is the best alternative.

Axial loads were primarily transferred by a mechanical resistance against the deformation of an undercut section of the rod. The effect of rectangular, triangular and circular geometry of grooves on joint strength made by EM crimping process was investigated. As a result, a rectangular groove shape was found better in providing the highest joint strength due to the shearing effect at the groove edge (Mori et al., 2013). Another study shows how crimping onto 'textured' surfaces such as screw threads and different knurled geometry affect the joint quality. The achievable joint strength exceeded the strength of the tube in torsional loading (Faes et al., 2014). Both axial and torsional load were transferred simultaneously using a knurled profile at the joining interface which is its advantage in EM crimping process (Weddeling et al., 2012).

As the number of grooves increases, the joint strength also increases but the weight of the joining zone becomes more which is not recommended from the lightweight design perspective. EM crimping using a double groove subjected to an axial load was experimentally investigated, and its design was optimized using a Design of Experiments Methods. The optimized design was tested, and tensile strength was found more than 90 % comparing to the base metal (Faes et al., 2012). EM crimping of aluminum tube with two different types of steel mandrels was investigated experimentally, and geometrical parameters for double grooves were optimized for axial load-bearing. Besides that, EM crimping of steel to steel using a single rectangular groove also investigated as a case study (Vanhulsel et al., 2011). In general, small groove edge angle and large length were preferred for highest torque strength. The number of grooves and lengths were revealed as important parameters which can affect torque strength significantly. Moreover, increasing the mentioned parameters were leads to an increase in torque resistance (Park et al., 2005). Direct proportionality between torque strength of the joints and number of grooves were determined, but the effect of increasing depth revealed unclear, and the impact of levels of energy was found less (Faes et al., 2014).

2.3. Numerical Studies on Joining by EMF

The study on EMF and joining process using different approaches is still going on for better understanding. A combination of the Finite Element Method (FEM) for the conductor parts and the Boundary Element Method (BEM) for the insulators (including air) as implemented in the LS-

DYNA^{TM} commercial software used to simulate EM forming process (L'Eplattenier et al., 2009). Few researchers reported the high capability in simulating EMF process using LS-DYNA^{TM} (3-D coupled electromagnetic-structural simulation) for torque joint between steel tube and the steel rod (Neugebauer et al., 2012). The load-bearing capacity of an axially loaded joint was improved by adding the second rectangular groove, and that was found by studying the magnitude and distribution of the stresses and deformations at each groove edge using ABAQUS software (Vanhulsel et al., 2011). The effect of a sequential coupling method on the accuracy of radial displacement of the Al6061-T6 tube in inside-bead forming was studied (Chaharmiri and Arezoodar, 2016). Results show 8.2% differences between experimental and simulation. Maxwell and ABAQUS software was used for electromagnetic for mechanical analysis. Authors are strongly recommended to use a sequential coupling approach to obtain good result especially during deformation at higher discharge voltage.

Dynamic explicit FE code LS-DYNA becomes the main simulation software using in research related to joining by EMF. Solid elements are 3D that can model solid bodies and structures without any prior geometric simplifications. The capability of the EM module of LS-DYNA for solving EMF problem numerically for designing the systems has been reported by comparing it with the result found by the experiment. Flanging processes were considered for comparison of simulation and experimental results and found in good agreement (Shang et al. 2010).

EM crimping process was demonstrated to join an aluminum terminal with copper wire for industrial application. Numerical simulations were carried out using LS-DYNA^{TM} software to optimize coil design and discharge energy for uniform deformation. A trapezoidal cross-section coil was proposed as best suitable comparing with rectangular and circular (Rajak and Kore, 2018). Modeling and simulation of electromagnetic crimping of Al6016-T6 tube on a steel rod with single and double rectangular grooves were carried out, and process parameters are predicted using LS-DYNA^{TM} software (Areda and Kore, 2017). Besides that, numerical modeling and simulation were carried out to find a maximum transmittable moment of joint manufactured and found in a good agreement with the experiment. In this study, the EM-module in a beta version of the LS-DYNA structural explicit code was used (Neugebauer et al. 2012).

2.4. Analytical Studies on Joining by EMF

Analytical studies become very helpful for understanding the effect of the different parameter on the achievable result. Joining parameters in electromagnetic crimping are approximated analytically. The model was used to predict a magnetic pressure and thus the discharging energy required to fill specific groove geometry. Besides the joining zone characteristics, the model considers major workpiece, coil, and circuit properties. For validation of the analytical approach, experimental investigations were performed (Weddeling et al., 2015). The results of the analytical model deviate from experimentally applied discharge energies due to neglection of strain hardening and a strain rate sensitive. The author recommended combining the introduced model with the experimental methodology to minimize the difference and analytically approximated pressure will be valuable for the process design. This model is beneficial mainly to determine processes parameters for electromagnetic crimping. The following equations are being used in this analytical approach. Acting magnetic pressure $P_m(t)$ in electromagnetic compression determined using Eq. 2.1 which describes how pressure is directly proportional to charging energy and inversely proportional to coil length. The plastic deformation starts if the acting magnetic pressure $P_m(t)$ exceeds collapse pressure P_y described by Eq. 2.2 for the fully clamped cylindrical shell. Moreover, the movement of the shell element and function of the radial displacement $h_d(t)$ was described by Eq. 2.3 and 2.4.

$$P_m(t) = \frac{1}{2}\mu \frac{n^2}{l_{coil}^2} \frac{U^2}{(\omega . L_{res})^2} . e^{-2\delta t} \sin^2(\omega t) \tag{2.1}$$

$$P_y = \frac{2\sigma_y . s}{\sqrt{3} r_T} (1 + \frac{4 r_T . s}{w^2}) \tag{2.2}$$

$$\frac{\partial^2 M_z(z,t)}{\partial_z^2} + \frac{N_\theta(z,t)}{r_T} + P(z,t) - \rho_A \partial^2 \frac{h_d(z,t)}{\partial_t^2} = 0 \tag{2.3}$$

$$h_d(t) = \frac{3}{2\rho_A} \left[\int_{t_y}^{t} p_m(\tau) d_\tau - \int_{t_y}^{t} \tau . p_m(\tau) d_\tau - \frac{1}{2} P_y (t - t_y)^2 \right] \tag{2.4}$$

Where μ is permeability, l_{coil} is length of coil, n is number of turn, L_{res} is resultant inductance, ω is frequency, δ is damping coefficient, u is initial voltage, ρ is density, t is time, σ_Y is yield stress, r_T is the inner radius of the workpiece, S is wall thickness, N_θ is circumferential stress resultant, and M_Z is axial bending stress resultant across the shell thickness respectively.

Finally, applying the introduced analytical approach can avoid extensive experimental studies required and makes it easy to understand the process economically (Weddeling et al., 2015). Hence, this approach leads to a less expensive and time-consuming design process and can also be used as a valuable tool for the optimization of the EMF systems. Further, prediction of the possible strength of electromagnetically crimped joints under quasi-static tensional loads is introduced, and the effect of the compressive strength of the inner joining partner on the achievable joint strength is also analyzed. As a result, design strategies and an approach for establishing process windows for the manufacturing of electromagnetically joined form-fit connections featuring hollow mandrels are developed. A result found analytically and experimentally shows an 18% mean absolute error which is in a good agreement. Analytical and experimental studies are carried out on the joinability of aluminum tubes on polyurethane cores using joining by electromagnetic forming (Hwang et al., 1992). The governing equations which can estimate the joining strength were proposed and shown in Eq. 2.5 & 2.6.

$$q = q_0 - q_f = \frac{a}{(1-\upsilon)^b}(\varepsilon_{r0}^b - \varepsilon_{rf}^b) \tag{2.5}$$

$$F = \pi r^2 \frac{2l\mu a}{(1-\upsilon)^b \bullet r + 2l\mu\upsilon^b}\varepsilon_{r0}^b \tag{2.6}$$

Where q is resultant contact stress, q_0 is contact stress, q_f is reduced radial stress, υ is Poisson's ratio, ε_{ro} is an initial residual strain, ε_{rf} is a final residual strain, l is contact length, μ the is coefficient of friction, r is the radius of the core and *a* & *b* are constant.

The computational procedure has been used for estimating the joining strength, and its values have been compared with the experimental results for validation. Process variables are chosen for the joining of aluminum tubes on polyurethane cores using EMF and characterize this process.

Moreover, estimated values are agreed well with experimental results. How joint strength increases by increasing charging energy and decreases as length increases were investigated (Hwang et al., 1992). Furthermore, joint strength and radial strain decrease as the length of the outer tube increases. The analytically computed result using proposed governing equations were agreed with experimentally found.

2.5. Application Oriented Studies on Joining by EMF

The application of lightweight materials like aluminum and magnesium is becoming prominent in the automotive and aerospace industries. As a recently developed system, more application-oriented studies have to be done for addressing several manufacturing problems to cop up with the limitation of conventional methods. The application of an electromagnetic forming (EMF) process for joining automotive parts was started in early 1964 (Zittel, 2010). These processes can be completed within a fraction of seconds which has a significant impact on maximizing the rate of production. Hence, an electromagnetic pulse technology is the best alternative for mass production which gives better economic benefit due to its processes feature (Schäfer, and Pasquale, 2010).

The effect of process variables on joint strength has been studied. Those variables were estimated experimentally and theoretically on the structural body for marine applications which are composed of three members (copper tube/polyurethane tube/aluminum core. The magnitude of the residual radial strain of the polyurethane tube govern joint strength, and it will increase as the number of discharges and as the level of discharged energy increases, but decreases in the case of uneven deformation in which large wrinkles occur. The contact pressure between the polyurethane tube and the aluminum core reduces due to the radial shrinkage of the tube which leads to the decreasing of joint strength. The roundness of the polyurethane tubes is improved by increasing energy and the number of discharges (Hwang et al., 1993). Tooling provided for the following three processes, i.e., restrike operation to fill sharp corners of automotive panels, low energy method of spring back calibration and joining of closed frames with an openable coil was demonstrated, and also applications are described. The design of an openable coil which consists of two independent multi-turn coils are connected in series and each of which was mounted in its shell. This coil was employed for joining a cylindrical tube to a cylindrical mandrel and also a rectangular tube to an inner rectangular mandrel (Golovashchenko, 2006).

There are several processes like forming, welding, cutting, crimping and clinching, claimed as feasible in EMF and joining process (Schäfer et al., 2009 and Schäfer et al., 2014). Crimping wires for different electrical applications using EM crimping were also found better comparing to mechanical or conventional approach (Rajak, and Kore, 2017). Joining tubular aluminum profiles made of EN-AW6060 for axial load resistance were experimentally investigated (Marré et al., 2009). Aluminum tube and inner workpiece made of (S235) was crimped with different groove designs for torsional load resistance (Bogaert et al., 2012). The performance of this process makes several industries to prefer EMF as the best alternative, but it is not yet studied completely and requires more research to be done.

2.6. Field-shaper

A coil used in EMF comes in different models based on the required applications; the same is true for field-shaper. Equipment and tools which are frequently used in joining by EMF like drivers and field-shaper have different geometrical configurations to enhance the performance of the process. A field-shaper is a current-carrying conductor, inductively coupled to the forming coil and used to concentrate the magnetic pressure at the point were forming is desired (Mamalis et al., 2004). Uniformity of pressure distribution in the joining zone also improved. The way how the geometry of a field-shaper affects tube bulging was studied. Performance of cylindrical-type, convex-type, and concave-type field-shapers in tube bulging was investigated experimentally (Suzuki et al., 1987). The effect of a geometrical parameter of a stepped field-shaper on magnetic pressure and radial displacement during tube compression was studied using 2D and 3D Maxwell simulation. The magnetic flux density found while using field-shaper is more (Bahmani et al., 2009). The significant effect of field-shaper on pressure distribution during tube compression was investigated using a numerical approach. Distribution of magnetic pressure with and without field-shaper was also compared for the same (Haiping et al., 2005). Taguchi and 3D simulation were used to study the effect of slit made on field-shaper in concentrating Lorentz force for deforming sheet metal and results were found in good agreement (Chu and Lee, 2013).

An improvement of uniform distribution of magnetic pressure at the deformation zone and addressing the end-effect of the tube is a contribution of field-shaper. As the electrical pulse is transferred, the magnetic field of coil induces an eddy current in the skin of the field-shaper which

passes to the inner cross-section using radial slit made. At the interior cross-section of a field-shaper, current density and magnetic pressure significantly increased in comparison to the outer face (Haiping et al., 2005). The primary role of field-shaper in electromagnetic compression is to concentrate the magnetic field on the point of interest so that the peak pressure increases and causes severe plastic deformation (Marré et al., 2008). A different construction of field-shaper for compression and expansion with their features are shown in table 1.

Table 2. 1 Different designs of field-shaper, corresponding advantages, and disadvantages (Psyk et al., 2011)

Construction	**Symmetric-conic shaper**	**Symmetric-cylindrical shaper**	**Asymmetric-conic shaper**	**Asymmetric-cylindrical**
Compression	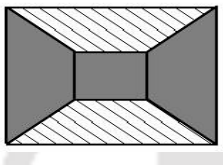	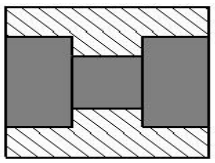	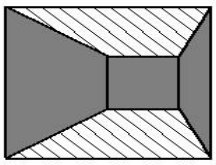	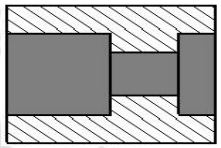
Expansion	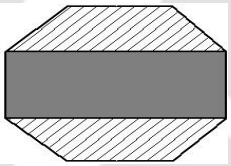	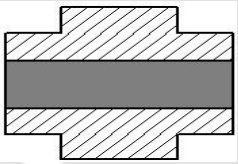	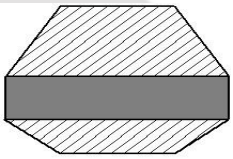	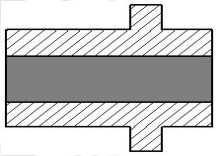
Features	▪ Poor efficiency ▪ High strength	▪ High efficiency ▪ Low strength	▪ Poor efficiency ▪ Very sensitive to deformation	▪ High efficiency ▪ Very sensitive to deformation

A simplified EM crimping circuit and setup is shown in Fig. 2.1 where *R* and *C* represent circuit resistance, and capacitance. The current flows in the coil induced in the outer surface of field-shaper and change direction due to the slit and flows to the internal section in the opposite direction. The interior surface area of a field-shaper is smaller than the exterior which leads to generating high current and magnetic field density. The magnetic field generated on the surface of the workpiece due to induced current will interact with a magnetic field of the field-shaper to produce radial force. The force generated can be used for forming, welding, joining, perforating, cutting, and embossing, etc. (Schäfer et al., 2014).

The current (I_c) flows in the coil when the high current switch is closed. A discharged energy from a capacitor bank generates a magnetic field to induce a current (I_p) in the outer surface of a field-shaper. The slit which is made on field-shaper changes the direction of current (I_s) flow into the

interior section. The interaction of a magnetic field generated on the surface of the workpiece and internal surface of field-shaper produces a Lorentz force. The force produced is used for the crimping process. The workpiece undergoes permanent plastic deformation if the stress generated due to Lorentz's force exceeds its flow stress.

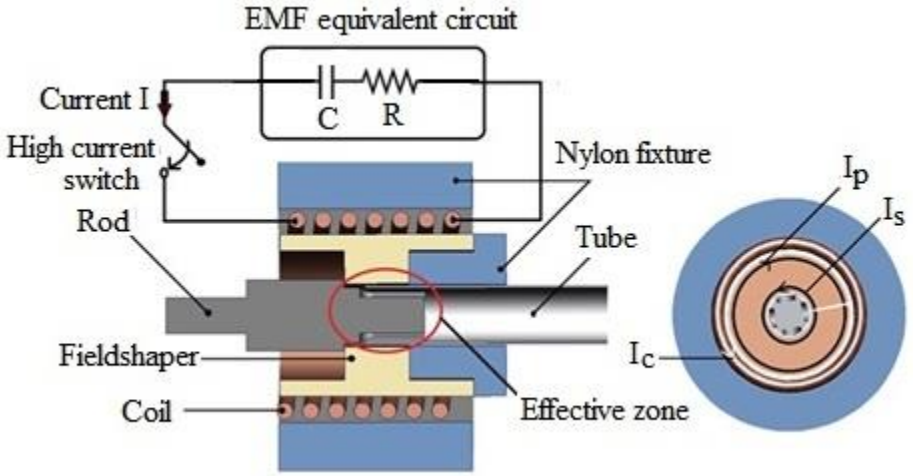

Fig. 2. 1 EM crimping setup using single stepped field-shaper

2.7. Advantage and Disadvantage of EMF

EMF is one of the high-speed forming processes which deform electrically conductive materials like aluminum and copper (Kamal and Daehn 2007). However, metals that have poor electrical conductivity require drivers made up of electrically conductive metals like copper to be deformed (Fenqiang et al., 2013 and Shin et al., 2008). The flexible design of a product is possible using different materials efficiently which requires the adoption of dissimilar-metal combinations that are benefiting from the specific properties of each in a useful way. Traditional joining methods such as bolts and nuts, screws, pegs, and rivets must use additional joining elements, but the reliability of the joint made is questionable when functional for an extended period (Varis, 2002). Welding dissimilar tubes require coating the weld seams to avoid bimetallic corrosion of the welded zone in moist environments. Joining two tubes with metallurgical differences by their end using brazing and adhesive bonding is not recommended particularly for the tubes exposed to high service temperatures. Flanges or bulkhead joints used as alternative solutions for connecting two tubes by their ends based on its advantage like simplicity to design, easiest to assemble and disassemble. However, aesthetic and geometrical constraints limit its application, and also

additional tube end preparation requirements (e.g., threaded tube ends) that may increase the overall weight and cost of tubular trusses and piping systems (Silva et al., 2015).

Heat affected zone generated due to the thermal joining process distorts the joining area which can significantly degrade the quality of the joint manufactured. Besides that, the intermetallic compound created at the joint interface which has different mechanical and chemical properties affect the strength of a joint by introducing voids and pores at the joining zone. In general, the formation of brittle phases, the segregation of high- and low-melting phases due to chemical incompatibility, and possibly significant residual stresses from the physical mismatch are defects associated with an arc welding (Sun and Karppi, 1996). Cracks at the interface of electromagnetically welded parts were investigated (Faes et al., 2010). Therefore, advanced joining methods such as electromagnetic crimping process are the best option to overcome those limitations. The electromagnetic crimping process is one of the high-speed processes which can complete joining within 100 μs (Weddeling et al., 2011). Besides a high rate of production, an excellent dimensional accuracy of the final product can also be achieved (Psyk et al., 2011, Schäfer and Pasquale, 2010). A high strain rate can be achieved using EMF process which is difficult to obtain in static deformation (Unger et al., 2008). The formability of aluminum and magnesium was enhanced due to the speed involved and associated strain rate of EMF process (Imbert et al., 2005 and Golovashchenko, 2007).

Deforming energy required for joining can be controlled and monitored effectively to give high process repeatability. Material combinations like metals and glass, polymers, composites or different metals can be easily joined with high production rates. Forming of sensitive materials can be realized, and the possibility of operating using remote for safety issues are some of the advantages of this process as discussed by few researchers (Psyk et al., 2011). The fact that tubes that needed to be deformed must have a good electrical conductivity which is considered as one of the major limitations of EMF processes in addition to coil longevity. Only the first half of a pressure curve is used for plastic deformation which is causing poor efficiency. Tool coil lifetime is limited due to high thermal and mechanical load.

The comparison between electromagnetic and conventional i.e. mechanical crimping was studied in detail showing how the EM crimping process is advantageous over the conventional technique. The study includes comparing pullout strength, surface roughness, hardness and other parameters

that can explain the quality of the joint manufactured. Rajak and Kore, 2017 found pullout strength which is improved by 50 %, and the average gap was reduced by 70 % in EM crimping compared to the conventional technique. The difficulty in designing and fabricating dies for particular groove profiles, achieving optimum groove filling for maximum mechanical interlock, avoiding early local necking, generating higher deforming pressure, obtaining high processes repeatability and avoiding or minimizing springback which affect interlocking are the major drawbacks commonly faced by conventional crimping processes in which EM crimping can resolve efficiently.

2.8. Theoretical Background of EMF Processes

In the majority of the high-speed forming process, very high pressure is generated when two solid bodies impact each other at significant velocity. One of the critical process parameters is an impact pressure *P* formulated as Eq. 2.7 which is produced when two semi-infinite elastic bodies labeled 1 and 2 collide each other with an impact velocity V_i. Where ρ represents density and *C* is the longitudinal wave speed which can be computed using Eq. 2.8.

$$P = \frac{\rho_1 \rho_2 C_1 C_2}{\rho_1 C_1 + \rho_2 C_2} V_i \tag{2.7}$$

$$C = \sqrt{\frac{3K(1-\upsilon)}{\rho(1+\upsilon)}} \tag{2.8}$$

Where *K* represents bulk modulus and *v* is the Poisson's ratio. The longitudinal wave speeds are on the order of about 7000 m/s for most structural metals (Seth et al., 2005). A source of impact velocity in the case of EM crimping is a magnetic pulse generated from the EMF system which is explained in detail as follows. A schematic representation of the RLC circuit of EM crimping is shown in Fig. 2. 2.

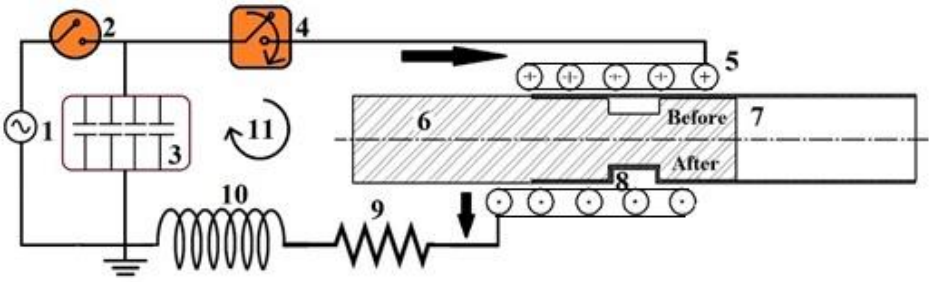

Fig. 2. 2 Schematic representation of EM crimping

where, 1: AC Power supply, 2: Main switch, 3: Capacitor bank, 4: High current switch, 5: Coil, 6: Rod, 7: Tube, 8: Groove, 9: Resistance, 10: inductance, and 11: Direction of current flow.

This process uses a high-velocity electronic pressure pulse to form the workpiece rapidly without mechanical contact. Discharging the electrical energy which is stored in the capacitor bank makes the current to start to flow through the coil and generates a transient magnetic field. Consequently, the generated magnetic field induces a current into the nearby workpiece surface which should be electrically conductive according to Faraday's law. The first wave of the magnetic pulse is the one that plays a key role in tube deformation during electromagnetic forming (Song et al., 2004). The same is true for electromagnetic crimping. Three load transferring mechanisms are considered as the main joining mechanism in joining by EMF (Weddeling, 2015).

1. An interference or force-fit joint is based on a difference in the elastic recovery of the two parts being joined which is leading to an interference pressure P_f between the workpieces after joining process.
2. A form-fit joint is based on additional geometrical features on one of the joining partners, i.e., knurled, threaded or undercut.
3. The impulse-welded joint is a solid-state weld that is generated from high impact velocities V_{imp} up to several hundred m/s and impact pressures up to a few thousand MPa .

The energy stored (E) by the EMF system and the associated current can be calculated using Eq. 2.9 and 2.10 (Rajak and Kore, 2017).

$$E = \tfrac{1}{2} CV^2 \tag{2.9}$$

$$I(t) = \frac{U_0}{\omega L} e^{-\beta t} \operatorname{Sin}(\omega t) \tag{2.10}$$

For the given number of turn and length of the coil, magnetic flux density can be calculated as a function of current using Eq. 2.11. If the number of magnetic field lines diffused is less for lesser skin depth effect, magnetic pressure can be calculated using its simplified form as shown in Eq. 2.12 (Rajak and Kore, 2017).

$$B = \mu(NI/l) \tag{2.11}$$

$$p(t) = \tfrac{1}{2} \mu(H_{gap}(t))^2 \tag{2.12}$$

Two opposing magnetic fields react and generate a radial force called Lorentz's force which is used to deform the workpiece plastically. A rectangular groove of the rod shown in Fig. 2.3 (a) will be filled by the tube as shown in Fig. 2.3 (b) due to deformation which creates permanent mechanical interlock.

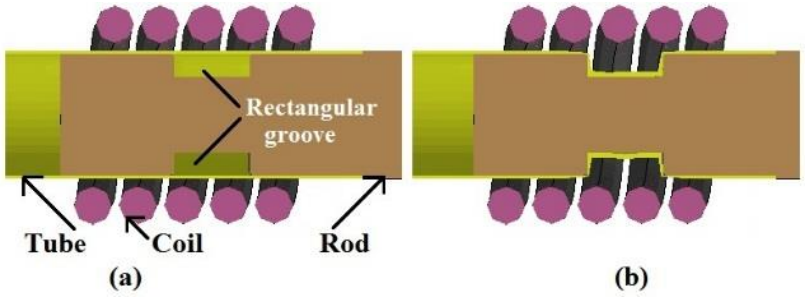

Fig. 2. 3 Workpieces shape (a) before and (b) after deformation

Analyzing EM crimping process using analytical and numerical approach needs to articulate and solve many complex mathematical equations. The physics of an electromagnetic crimping process was explained based on Maxwell's equations. These equations, Eq. (2.13-1.19) underlie all of the electromagnetic field theory (L'Eplattenier et al., 2009).

$$\bar{\nabla} \times \vec{E} = -\frac{\partial \vec{B}_m}{\partial t} \tag{2.13}$$

$$\bar{\nabla} \times \left(\frac{\vec{B}_m}{\mu} \right) = \vec{J} \tag{2.14}$$

$$\nabla \bullet \vec{B}_m = 0 \tag{2.15}$$

$$\nabla \bullet \varepsilon \vec{E} = 0 \tag{2.16}$$

$$\nabla \bullet \vec{J} = 0 \tag{2.17}$$

$$\bar{\nabla} \times \vec{H} = \vec{J} + \varepsilon \frac{\partial \vec{E}}{\partial t} \tag{2.18}$$

$$\vec{J} = \sigma \vec{E} + \vec{J}_s \tag{2.19}$$

$$\vec{B}_m = \mu \vec{H} \tag{2.20}$$

The divergence condition in Eq. 2.15 allows writing the magnetic flux density as Eq. 2.21. Using Eq. 2.17 electric field is given by Eq. 2.22.

$$\vec{B}_m = \bar{\nabla} \times \vec{A} \tag{2.21}$$

$$\bar{E} = -\bar{\nabla} \varnothing - \frac{\partial \vec{A}}{\partial t} \tag{2.22}$$

By using the gauge condition, it allows the separation of vector potential from scalar potential as Eq. 2.23. Using equation (2.17, 2.18, 2.22 and 2.23), Eq. 2.24 is derived.

$$\bar{\nabla} \bullet \partial \vec{A} = 0 \tag{2.23}$$

$$\nabla \bullet \sigma \bar{\nabla} \varnothing = 0 \tag{2.24}$$

Using equations (2.14, 2.18, 2.21, and 2.22) the induced total current density over the workpiece can be expressed as the Maxwell equation in terms of potential as Eq. 2.25.

$$\vec{J} = \bar{\nabla} \times \frac{1}{\mu} (\bar{\nabla} \times \vec{A}) + \sigma \frac{\partial A}{\partial t} + \partial \bar{\nabla} \varnothing \tag{2.25}$$

Where E is the electric field, B_m is the magnetic flux density, V is the voltage, J is the total current density, C is the capacitance, J_s is the current source density, I is current, $\vec{A}$ is the vector potential, ω is the frequency, L is the inductance, $\varnothing$ is the electric scalar potential, β is the damping coefficient, H is the magnetic field intensity, t is the time, σ is the electrical conductivity, F is the Lorentz force, μ is the magnetic permeability, N is the number of turn of the coil, and l is the length of the coil respectively.

A current density is a negative partial derivative of the magnetic field intensity concerning the radius as formulated in Eq. 2.26. The magnetic flux density which is the product of magnetic permeability and the magnetic field strength is shown in Eq. 2.27. Lorentz force (the resultant due

to magnetic and electric force) which is applied radially on the tube is formulated as Eq. 2.28 (Weddeling et al., 2015).

$$\vec{J} = -\frac{\partial H}{\partial r} \tag{2.26}$$

$$\vec{B} = \mu H \tag{2.27}$$

$$\vec{F}_r = \vec{J} \times \vec{B} = -\mu H \frac{\partial H}{\partial r} = -\frac{1}{2}\mu \frac{\partial H^2}{\partial r} \tag{2.28}$$

The magnitude of Lorentz force which is acting on the workpiece is directly affected by the skin effect. In electromagnetic crimping, discharge frequency is a function of circuit inductance and capacitance of the EMF system. Skin depth is a function of frequency, magnetic permeability and electrical conductivity of the workpiece. The empirical formula of skin depth describes this relation as demonstrated in Eq. 2.29 (Weddeling et al., 2011).

$$\delta = \sqrt{\frac{1}{\pi \mu_0 f \sigma}} \tag{2.29}$$

Where E is total stored energy in the capacitor bank, U_0 is voltage, $P(t)$ is acting pressure, H is magnetic field strength, δ denotes skin depth, f is for discharge frequency, and r is radial displacement. Maxwell's equations are a set of partial differential equations used for the general description of electromagnetism in the EMF process. Hence, electrical and magnetic field prediction in the coil or workpieces using the finite element method is based on solutions of these equations. It is often convenient to choose the magnetic vector potential $\vec{A}$ as a system variable in the electromagnetic model such that:

$$\nabla \times \vec{A} = \vec{B} \tag{2.30}$$

$$\nabla \bullet \vec{A} = 0 \tag{2.31}$$

$$\vec{E} = -\frac{\partial \vec{A}}{\partial t} \tag{2.32}$$

Where $\vec{B}$ represents magnetic flux density, *t* represents time and $\vec{E}$ is the electric field intensity, $\vec{J}$ describes the current density in the coil, $-\gamma \partial\vec{A}/\partial t$ is the induced current density in the tube, and γ is the conductance of medium. Substitution of Eqs.2.30-2.32 into Maxwell's equations can give Eq. 2.33 and separately expressed according to different field regions. That means, in the electromagnetic model for free air region around the coil and a tube as Eq. 2.34, for coil region as Eq. 2.35, and a tube region as Eq. 2.36 respectively.

$$\nabla\times\left(\frac{1}{\mu}\nabla\times\vec{A}\right)=\vec{J}-\gamma\frac{\partial\vec{A}}{\partial t} \tag{2.33}$$

$$\nabla\times\left(\frac{1}{\mu}\nabla\times\vec{A}\right)=0 \tag{2.34}$$

$$\nabla\times\left(\frac{1}{\mu}\nabla\times\vec{A}\right)=\vec{J} \tag{2.35}$$

$$\nabla\times\left(\frac{1}{\mu}\nabla\times\vec{A}\right)=\vec{J}-\gamma\frac{\partial\vec{A}}{\partial t} \tag{2.36}$$

The magnetic force $\vec{F}$ which is acting radially can be expressed as Eq. 2.37. Lorenz's force which acts radially is produced due to the interaction of two magnetic fields between a tube and the coil. Workpieces will undergo permanent plastic deformation if acting magnetic pressure is exceeded beyond its yield strength.

$$\vec{F}=\vec{J}\times\vec{B}=\frac{1}{\mu}(\nabla\times\vec{B})\times\vec{B} \tag{2.37}$$

Therefore, the magnetic force acting on the tube expressed using $\vec{A}$ which can be described by substituting Eq. 2.30 and Eq. 2.36 into Eq. 2.37 which is used as an input load in the mechanical model. In addition to that, the transient dynamic equilibrium equation of interest is as shown in Eq. 2.38 (Itoh, 1973).

$$M\ddot{u}+C'\dot{u}+Ku=F^a \tag{2.38}$$

Where M is the structural mass matrix, $C^{'}$ is the structural damping matrix, K is the structural stiffness matrix, $\ddot{u}$ is the nodal acceleration vector, $\dot{u}$ is the nodal velocity, and u is the nodal displacement vector, and F^{a} is the applied load vector.

2.9. Gaps in the Literature

The detailed studies on the literature survey show a limited amount of work had been done on joining by electromagnetic forming for the joining of tubular parts. Moreover, there is still a lot of research needs to be done to industrialize these joining process. The research gaps found in joining by the electromagnetic forming process are summarized as follows.

- Limited research outcomes are available that show how different levels of discharge energies can affect joint quality in electromagnetic crimping.
- 3D strongly coupled simulation with experimental validation that shows how the process and groove parameter affect joint quality needs further study.
- A few researchers are only focused on industrializing of EM crimping process for the applications like joining of electrical, defense, and nuclear parts, etc.
- Optimization of the process and geometrical parameters for different material configuration is still required intensive numerical and experimental studies.
- The effect of field-shaper on joint strength manufactured for torsional load-bearing capacity was not yet covered in detail for industrial application.
- The effect of different material configuration and surface profile on joint strength to support torsional load was not sufficiently studied.
- The effect of rectangular groove parameters on joint strength which can support both axial and torsional load simultaneously was not yet reported.

The research plan implemented in this thesis to fill the research gaps is shown in Fig. 2.4.

Research Plan

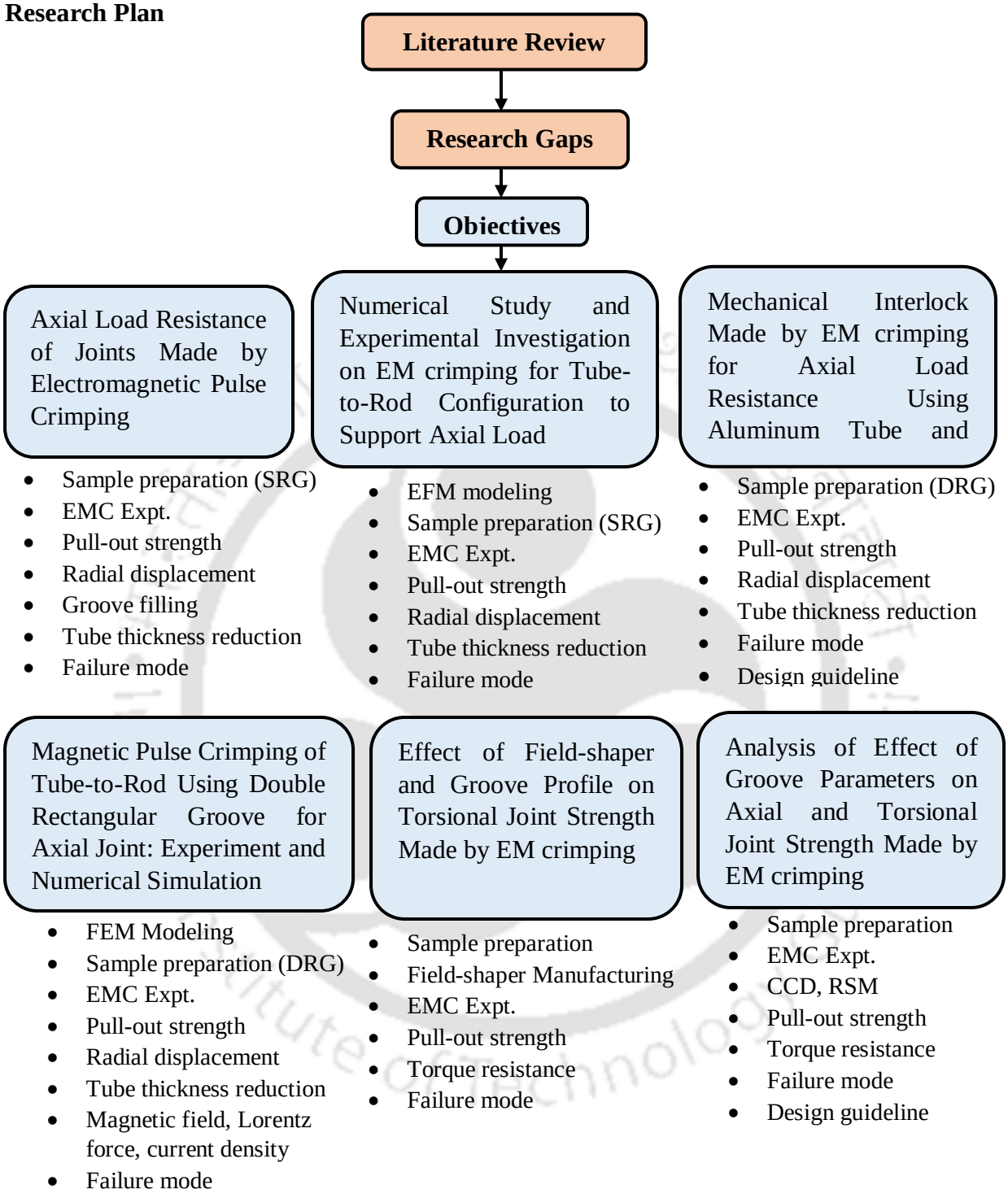

where **EMC**: Electromagnetic crimping, **SRG** & **DRG**: Single and double rectangular groove., **CCD**: Central composite design, **RSM**: Response surface methodology

Fig. 2. 4 The research plan implemented to achieve the objectives

CHAPTER 3

ELECTROMAGNETIC CRIMPING FOR TUBE-TO-ROD CONFIGURATION TO SUPPORT AXIAL LOAD

3 Electromagnetic Crimping for Tube-to-Rod Configuration to Support Axial Load

3.1. Introduction

Using low-density materials like aluminum to reduce the weight of the airframe structure becomes prominent and requires effective joining technology. In this chapter, the effect of discharge energy on joint quality and process parameters was investigated numerically and experimentally. The feasibility of joining aluminum tube with a steel rod to support axial load was primarily studied. The experiment was carried out using seven levels of discharge energies for the same groove parameters. A plastic deformation cause's an aluminum tube to fill a groove machined on a steel rod and create a mechanical interlock. FE modeling, simulation, and analysis were carried out using LS-DYNA^{TM} software of the electromagnetic module. Effects of discharge energies on the effective plastic strain, resultant velocity, displacement, Lorentz force, current densities, magnetic field densities, and maximum shear stress were predicted numerically to determine best energy levels. Three levels of discharge energies were chosen based on the result found from numerical simulations. A tube thickness reduction at groove edge, radial displacement of the tube, and groove filling obtained numerically were compared with experiment. The developed model can be used as a preliminary study to investigate the effect of discharge energies, groove and process parameters on joint quality.

3.2. Methodology

The schematic of the flowchart implemented in this work is shown in Fig. 3.1. FE simulations are carried out initially to found out levels of discharge energy which can give better radial displacement and groove filling before experimenting. The FE model was imported into LS-DYNA^{TM} software after modeling and meshing were done. The experimentally measured currents were imported and used as a load curve in the simulation. Lorentz force in Eq. 2.28 is evaluated at the node and added to a mechanical solver after the magnetic field is computed using electromagnetic solver. The explicit mechanical solver computes the deformation of the tube. Since the workpiece is undergoing plastic deformation, dynamic equilibrium Eq. 2.38 is used to evaluate the exact responses of the workpiece at each time increment.

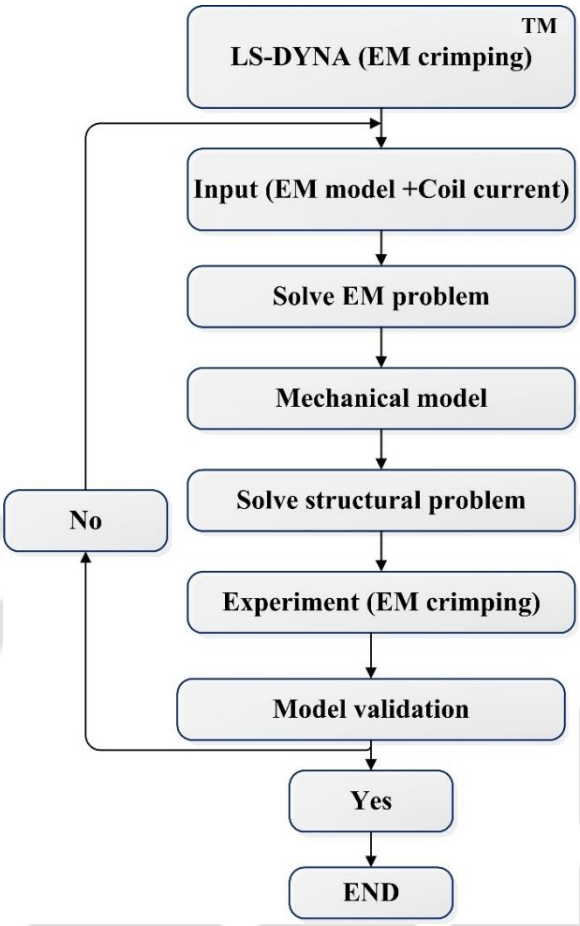

Fig. 3.1 Flow chart of the implemented procedure

After the successive simulation, we found three energy levels that give better groove filling and radial displacement respectively. The rebounding of a tube from a grooved surface was observed using discharge energy more than 4.7 kJ, which reduces radial displacement. Finally, post-processing of output results using LS-DYNA^{TM} was done for model validation. The results obtained in the simulations are compared with the measured experimental results for validation. The effect of energy on process parameters was predicted using a validated model. The displacement found was minimum at discharge energy lower than 3.4 kJ. Therefore, the discharge energy range from 3.4 kJ to 4.7 kJ was found as the best discharge energy levels to get the required deformation and achieve better interlocking. A rectangular groove was machined on a steel rod, and the coil was fabricated which has identical geometry and property to the model used in the simulation. Trials crimping were carried out to confirm levels of discharge energy based on the result of the simulations.

3.2.1. Finite Element Modeling

The shape of a groove and detailed dimension of the rod, tube, and coil are shown in Fig. 3.2. The clearance between the aluminum tube and steel rod was kept very small to avoid an effect of standoff distance on joint strength. Some important groove parameters are determined based on a design guideline that is proposed for better joint strength (Park et al., 2005). Hence, the geometrical shape and overall dimension of the groove on the steel rod were manufactured accordingly.

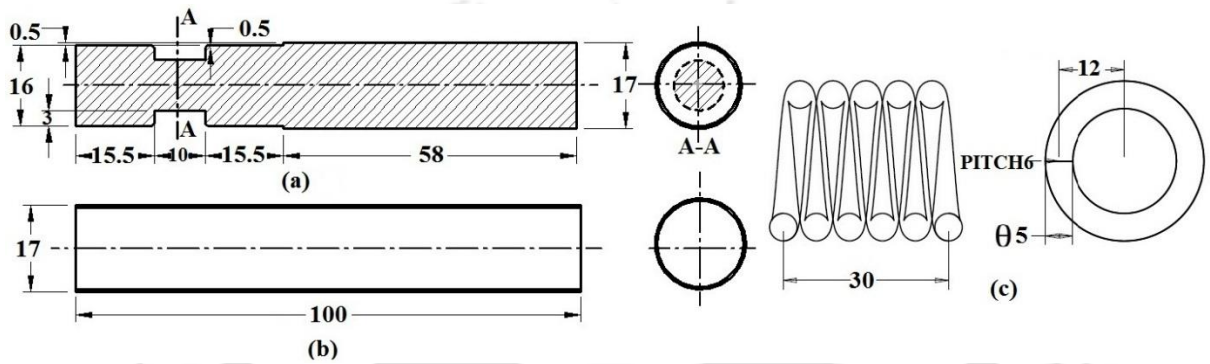

Fig. 3.2 Dimension of (a) rod (b) aluminum tube and (c) coil (All dimensions are in mm)

A model for FE simulation was developed in LS-DYNA^{TM} as shown in Fig. 3.3 (a) and (b). A quadrilateral 3D mesh was built for the coil, tube, and rod respectively. The mesh is composed of 2061 nodes for the coil, 5610 for the aluminum tube, and 24568 for the rod respectively. The boundary conditions are applied to the nodes and the total simulation time is 100 μs and the time step is 0.1 μs. Rectangular groove shape was selected based on literature which suggests as the best profile to provide better interlocking between joining parts (Weddeling et al., 2011).

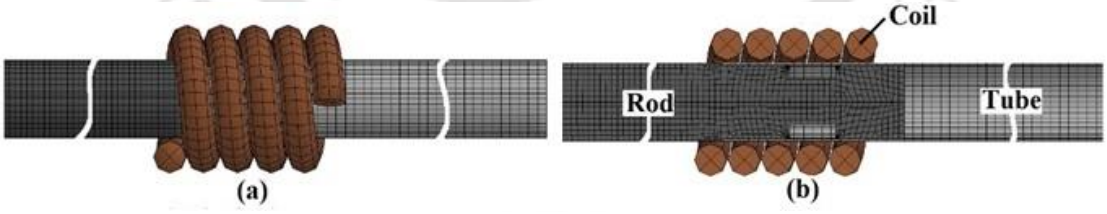

Fig. 3.3 (a) side view and (b) cross-sectional view of assembled models

The coil was modeled as a rigid body to avoid any deformation, and a simplified Johnson-cook material model was selected for modeling tube and rod respectively. Johnson-cook material model which is generally used in an adiabatic transient dynamic analysis and best suited for high strain rate forming process (Johnson and Cook, 1985). The isotropic hardening is a particular type of

hardening in which the yield stress is assumed to be of the form of Eq. 3.1 and used to relate σ, ε, $\dot{\varepsilon}$ and temperatures (Rajak and Kore, 2018).

$$\sigma_y = (A + B(\varepsilon_{eff}^{p})^{n})(1 + C\ln\dot{\varepsilon})\left(1 - \left(\frac{T - T_R}{T_m - T_R}\right)^{m}\right) \tag{3.1}$$

Where A and B are yield strength parameters, C is strain rate sensitivity, ε_{eff}^{p} is equivalent plastic strain, $\dot{\varepsilon}$ is plastic strain rate of the workpiece, n is strain hardening index, m is a thermal softening index, T_R is room temperature, T_m is melting temperature of the workpiece, and T is operating temperature. Johnson-cook constants for Al 1050 and 4340 steel presented in Table 3.1.

Table 3. 1 Johnson-cook constants for Al 1050 and 4340 Steel (Rajak et al., 2018, Johnson, and William, 1983)

Materials	A(MPa)	B(MPa)	n	c	T_m(K)	m
Al 1050	110	150	0.36	0.014	-	-
4340 Steel	792	510	0.26	0.014	-	1.03

The boundary condition considered in the simulation is shown in Fig. 3.4 which illustrates that the coil and rod were entirely fixed/rigid and a portion of the tube in which deformation is not required.

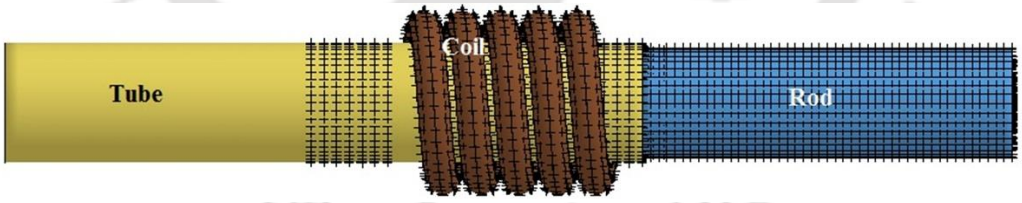

Fig. 3.4 Boundary condition for the tube, rod, and coil

3.2.2. Material and Experimental Setup

A five turn axisymmetric solenoid coil was manufactured from copper wire which has an electrical conductivity of 59.6×10^6 S/m, a density of 8960 (Kg/m^3) and Poisson's ratio of 0.27. Standard materials were used for the samples. For tube Al 1050 and rod Steel 4340 was used. A tube has electrical conductivity of 36.8×10^6 S/m, a density of 2720 (Kg/m^3) and Poisson's ratio of 0.33. The

chemical composition of the materials was also verified by performing EDX test, and the result is tabulated in Table 3.2.

Table 3. 2 Chemical composition of Al 1050 tube and 4340 steel (Dhar et al., 2006)

The weight percentage of the element (%)							
Alloy	**Al**	**Fe**	**Mn**	**Ti**	**Zn**	**Si**	**Cu**
Al 1050	**Balance**	1.1	0.1	0.1	0.1	0.5-0.6	0.1-0.2
	C	**Cr**	**Mn**	**Mo**	**Ni**	**V**	**Fe**
Steel 4340	0.36	1.45	0.92	0.52	2.87	0.20	Rest

The circuit parameters of EMF system used are shown in Table 3.3. Kapton tape was used to insulate the wire before inserting it into the insulation sleeve. The experimental setup consisting of workpieces and a solenoid coil is shown in Fig. 3.5. The process environment in the experimental tests was the same as in numerical simulation. A rigid fixture made of Teflon was used as a reinforcement to perform successive crimping operations without coil bulging. Multiple tests were carried out using energy within the domain found in the simulation.

Fig. 3.5 Experimental setup

A total of 14 samples were prepared with the same geometrical shape and dimensions. Two samples are joined using the same discharging energy, and this had been done for all samples and range of discharge energies. Then half of the sample was used to do a pull-out test, and the remaining was used to measure radial displacement and tube thickness reduction at groove edge. Wire Electrical Discharge Machining (WEDM) was used for cutting samples to see how the groove is filled at different ranges of discharge energy. The electromagnetic forming system utilized in this investigation is shown in Fig. 3.6 which has a capacity of 10 kJ of discharge energy. The voltage level considered was varied from 5.7 kV to 10.2 kV. The circuit parameters of the

EMF system used are shown in Table 3.3. The discharge energy levels varied from a minimum of 1.5 kJ to a maximum of 4.7 kJ as shown in Table 3.4.

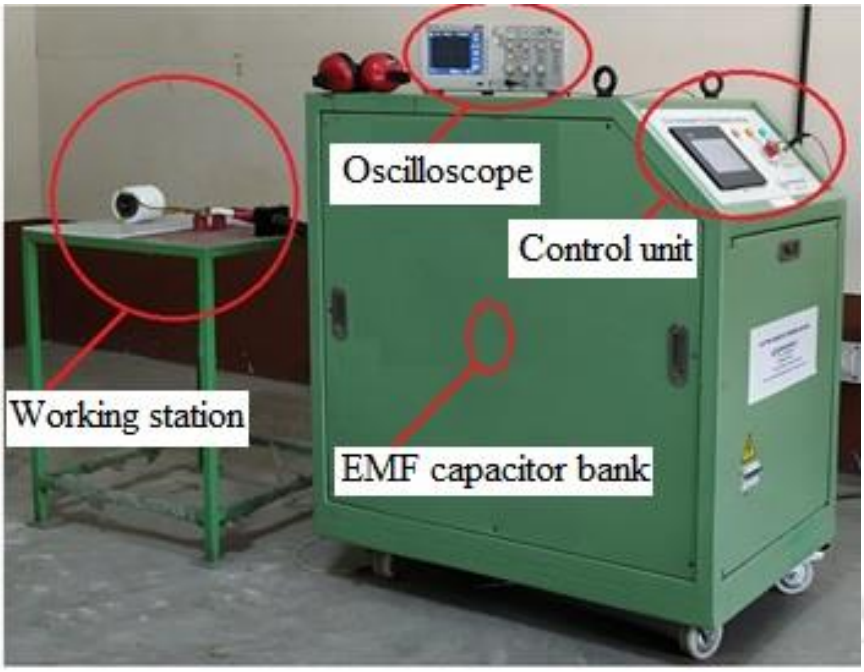

Fig. 3.6 EMF system and experimental setup

Table 3. 3 Circuit parameters of EMF system

Circuit Parameters	Capacitance	Inductance	Resistance	Frequency	Voltage
Values	90 μF	20 μH	23 mΩ	20 kHz	15 kV

Table 3. 4 Sample numbers and process parameters

Sample No	**Energy (kJ)**	**Voltage (kV)**
1	1.5	5.7
2	1.9	6.5
3	2.3	7.2
4	2.9	8.0
5	3.4	8.7
6	4.1	9.5
7	4.7	10.2

3.3. Mechanical Pull-out Test Condition

The quality of the joint manufactured is analyzed by conducting pull-out tests. A comparison between the strength of a crimped sample and the undeformed tube was evaluated. The pull-out testing conditions for crimped sample and tube are shown in Fig. 3.7 (a) and (b). The steel mandrels were inserted into the tube ends while conducting a pull-out test to avoid any failure at the grip of the UTM machine. The crossbar velocity of 0.1 mm/sec was chosen for both crimped sample and tube during the pull-out test.

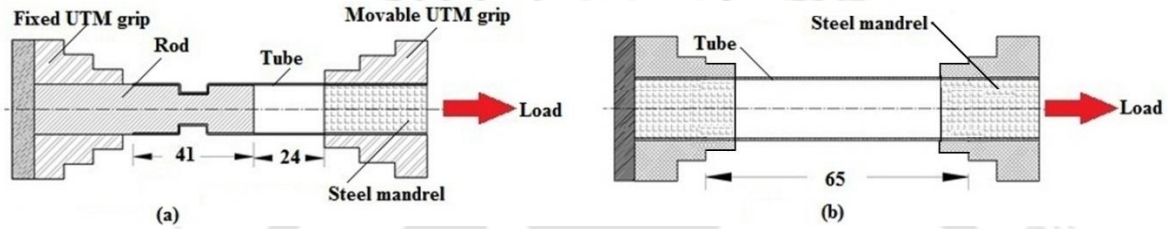

Fig. 3.7 Pull-out testing condition for (a) crimped sample and (b) tube (All dimensions are in mm)

3.4. Results and Discussion

3.4.1. Process Parameters

The range of a current curve measured using a Rogowski coil and oscilloscope that is interfaced with EMF machine during the experiment are shown in Fig. 3.8. Figure 3.8 also demonstrates a coil manufactured which is used to carry out the experiment and crimped sample manufactured at different discharge energy levels. The process parameters used in the experiment are summarized in Table 3.5.

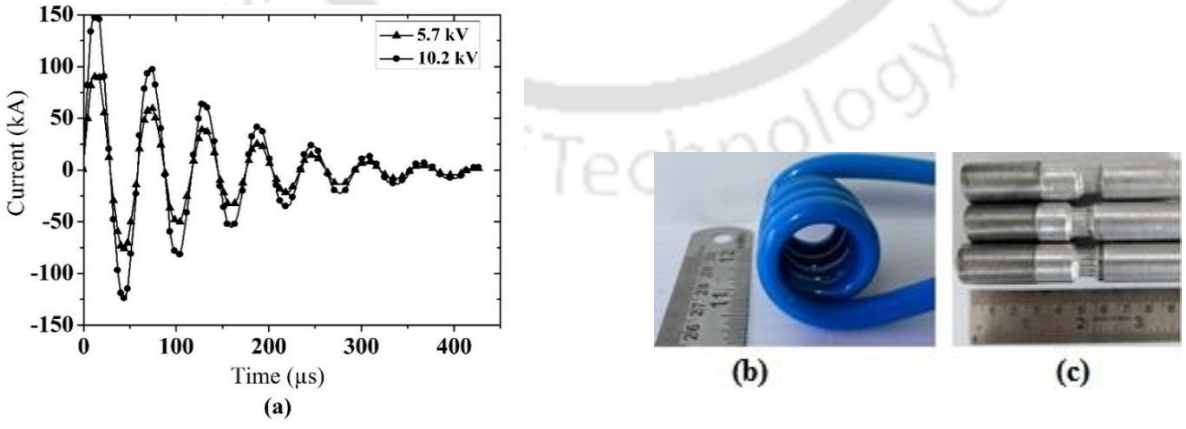

.

Fig. 3.8 (a) The measured current curve for 5.7 kV and 10.2 kV (b) a solenoid copper coil and (c) crimped sample

Table 3. 5 Detail process parameters for best energy levels

S. No	Voltage (kV)	Energy (kJ)	Peak current (kA)	Time period (μs)	Frequency (kHz)
1	8.7	3.4	118	53.4	18.727
2	9.5	4.1	138	53.1	18.832
3	10.2	4.7	148	53.0	18.868

3.4.2. Tube Thickness Reduction at the Groove Edge

The above current curve was imported as a load curve in the simulation. A significant positive and negative effect of groove edge radius on joint strength was studied, and it is recommended to have a minimum of tube thickness size to prevent easy breaking during EM crimping process (Park et al., 2005). If the groove edge radius is zero, it will act as a cutting edge and make the tube sheared-off easily during the impact. This effect makes a tube to separate easily from the groove using a lesser load which is applied axially. The absolute mean percentage of an error in tube thickness reduction at groove edge between experiment and simulation was found 1.93%, 2.17%, and 8.11% for 3.4, 4.1, and 4.7 kJ of discharge energies respectively. The effect of energy on tube thickness reduction obtained from simulation and experiment was found in good agreement as shown in Fig. 3.9.

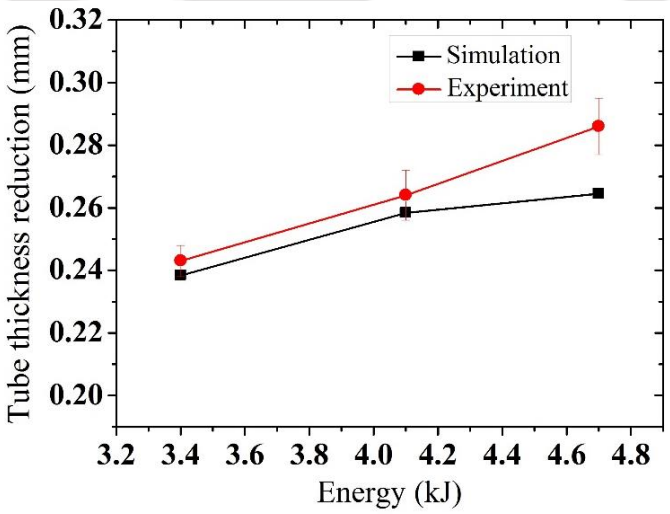

Fig. 3.9 Effects of discharge energy on tube thickness reduction at groove edge

3.4.3. Radial Displacement

The primary goal of simulation in electromagnetic forming is a prediction of workpiece deformation at a high strain rate. The final deformation obtained from the simulation shows good qualitative agreement with the experiments, as shown in Fig. 3.10. As can be seen, the final deformed shape obtained shows good similarity in both cases that were confirmed by comparing the radial displacement of the tube along the joining zone. The fringe values found from the simulation show the radial displacement of the tube which gives the same as the experiment.

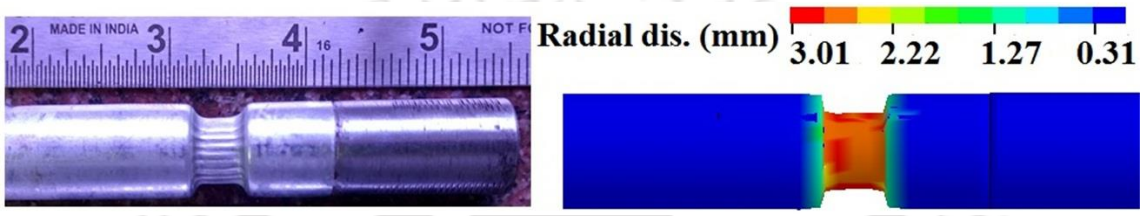

Fig. 3.10 Final shapes obtained in (a) experiment and (b) simulation

The radial displacement between the tube and groove surface along the joining zone was measured as shown in Fig. 3.11. A gap of 1.25 mm is kept between two points, and measurement was taken as shown on the right side of the same figure. Only half section of the joining zone was considered for measuring the displacement in simulation and experiment.

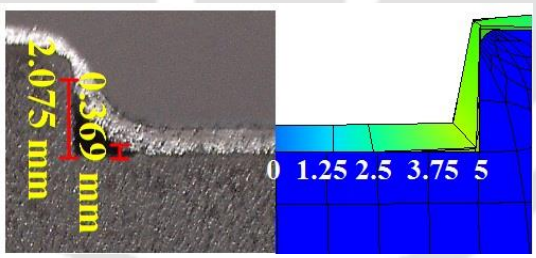

Fig. 3.11 Radial displacement in experiment and simulation

A magnetic pressure which is more at the center of the coil causes maximum radial displacement of the tube in the joining zone. Hence, the radial displacement achieved from different discharge energy levels were found maximum at the center and decreased towards the corner of the groove. The trend of this variation was found identical in both simulation and experiment for respective discharge energies. Radial displacement found from experiment and simulation were plotted and compared for three different discharge energy levels as shown in Fig. 3.12. Average mean absolute percentage error was calculated at each point for 4.1 kJ of discharge energy and found 7.3% which

shows a good agreement between simulation and experiment. The developed model is used to predict and analyses the effect of discharge energy on different process parameters which significantly affects joint quality.

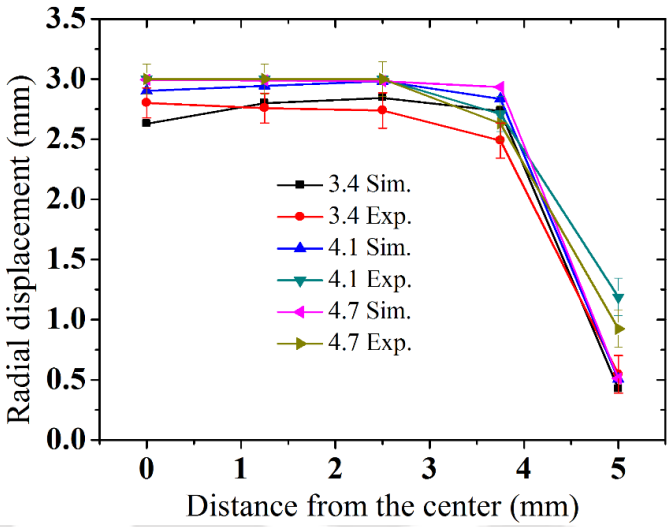

Fig. 3.12 Radial displacement at 3.4 kJ, 4.1 kJ, and 4.7 kJ discharge energy

3.4.4. Groove Filling

A groove filling by the tube at a different time was predicted using 3D simulation and plotted as shown in Fig. 3.13 for 4.1 kJ discharge energy. Maximum radial displacement is obtained after 45 µs approximately.

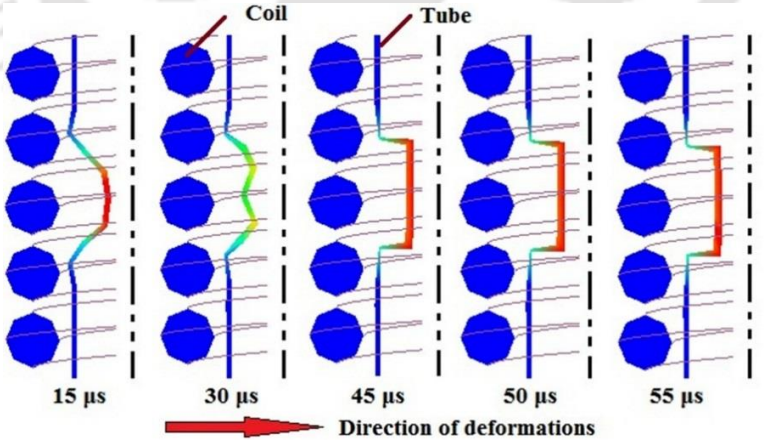

Fig. 3.13 Prediction of groove filling at different time value for 4.1 kJ discharge energy

The clearance at the groove corner which is obtained from simulation using 4.7 kJ and 4.1 kJ found almost nil. The groove was almost getting filled by the tube for discharge energy more than 4.1 kJ

which leads to having better interlocking. The better groove filling or interlock of a tube at groove edge means the better pull-out strength. However, groove filling and joint strength were affected negatively by discharging energy beyond 4.7 kJ due to rebound and severe deformation. The percentage of groove filling will be more if the tube thickness which is considered is more. A lesser groove depth also another option to increase the groove filling keep in mind that tube thickness is not more than the considered depth.

3.4.5. Comparison of Effective Plastic Strain and Resultant Displacement

The minimum required effective plastic strain and resultant displacement should be attended using discharged energies for better joint strength. A variation of effective plastic strain and resultant displacement along the joining zone were analyzed for 4.1 kJ of discharge energy using elements shown in Fig. 3.14.

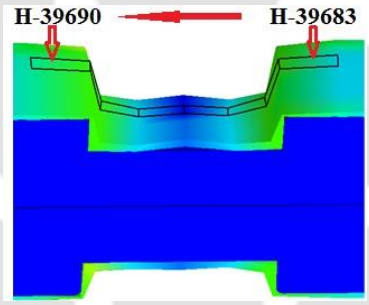

Fig. 3.14 Selected elements along the joining zone

The initial gap between a tube and groove surface allows the tube to accelerate and collide with high velocity. The effective plastic strain and resultant displacement were found higher for the elements (**H-39688, H-39687, H-39686, and H-39685**) which are located at the center of the joining zone. The pressure acting at the center is more for this kind of coil-workpiece arrangement, and that is why we found large deformation in the middle of the joining zone. The change in effective plastic strain and resultant displacement for selected elements obtained using 4.1 kJ discharge energy was demonstrated. The maximum attainable resultant displacement and effective plastic strain along the joining zone for elements chosen are plotted as shown in Fig. 3.15. A change in effective plastic strain and resultant displacement was found symmetric for two elements located on the opposite side of the joining zone. The higher the effective plastic strain, the higher the deformation and resultant displacement. This trend of change in effective plastic strain and resultant displacement along the joining zone was the same for the rest of the energy levels.

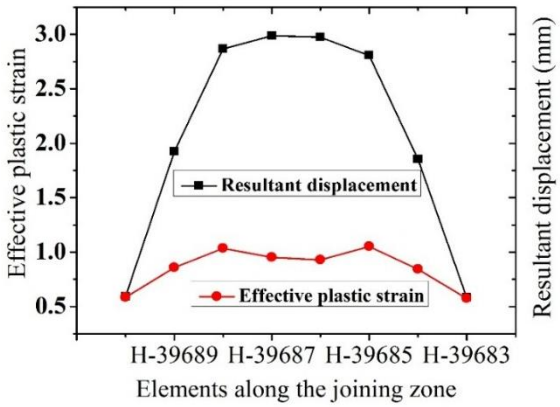

Fig. 3.15 Variations of effective plastic strain and resultant displacement along the joining zone

3.4.6. Resultant Velocity and Effective Plastic Strain

In the majority of a high-speed forming process, high pressure is generated when two solid bodies collide with each other with significant velocity. In electromagnetic crimping, the groove must be filled by the tube for better joint strength without significant thinning at the groove edge. The effect of the energy on the resultant velocity of the flyer tube was predicted using the simulation for 3.4 kJ, 4.1 kJ, and 4.7 kJ as shown in Fig. 3.16. Resultant velocity reached its peak value of 409 m/s, 430 m/s and 480 m/s at 14.8, 15.2, and 17.4 μs, and then it starts to decelerate till the end of the deformation.

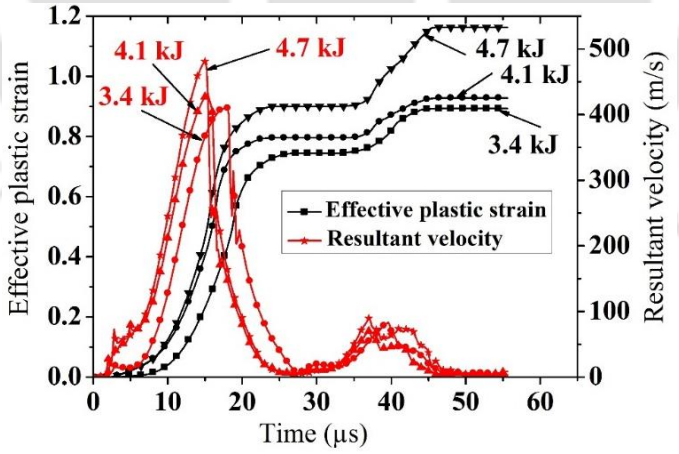

Fig. 3.16 Effect of discharge energies on resultant velocity and effective plastic stain

A 3D simulation can predict the velocity of the flyer tube easily which is challenging to measure using instruments due to the involving speed of the process. Increasing deformation energy by 17% cause the velocity to increase by 4.88%. The resultant velocity increases with discharge

energy. The effective plastic strain increases due to severe deformation caused by a higher discharge energy level. Hence, an effective plastic strain was varied from zero up to a maximum of 1.16 which is obtained using three energy levels as shown in Fig. 3.16. The effective plastic strain is directly proportional to impact velocity which increases as velocity increases and reaches a maximum of 0.89, 0.93, and 1.16 for 3.4 kJ, 4.1 kJ, and 4.7 kJ discharge energies. Maximum effective plastic strain and resultant displacement were achieved at the end of the deformations. Maximum resultant velocity was found at the early stage of deformation with a resultant displacement of 1.5, 2.3, and 2.6 mm and an effective plastic strain of 0.220, 0.389, and 0.442 for the three energy levels.

3.4.7. Resultant Displacement

The effect of energy on resultant displacement was predicted using simulation based on element **H-39686** which is located at the center of the joining zone. A maximum resultant displacement found at 3.4 kJ, 4.1kJ and 4.7 kJ was 2.96 mm, 2.97 mm and 2.99 mm respectively. The maximum displacement was attended within 15 μs to 20 μs from total deformation time, and it remains constant after 45 μs as shown in Fig. 3.17. The maximum radial displacement measured from an experimentally crimped sample was found 3 mm at the center of the joining zone. A mean absolute percentage error of less than 7% was found which shows a good agreement with simulation. Even though the difference at the center is very small, it will become significant for an element located at the end of the joining zone.

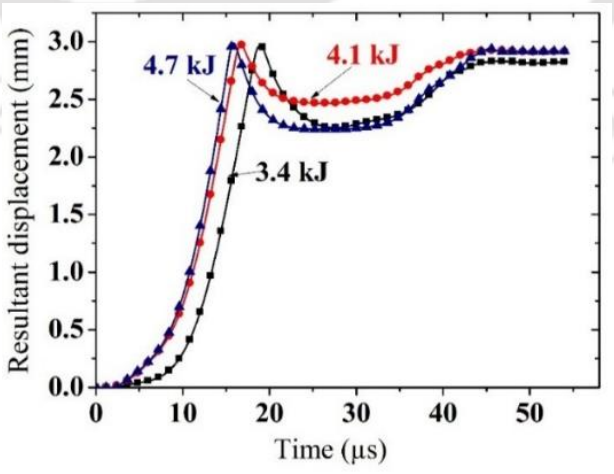

Fig. 3.17 Effect of discharge energies on resultant displacement for different energy levels

3.4.8. Lorentz Force, Current Density and Magnetic Field

A maximum of Lorentz force, current density and magnetic field for different discharge energy levels were found from the simulation are tabulated in Table 3.6. A Lorentz's force which is a volume force acting radially to deform the tube permanently was predicted using simulation. A direct proportionality with discharge energy makes the Lorentz force increases while discharge energy is increasing. Magnetic field density keeps on increasing as discharge energy is rising. The difference in magnetic field density is minimum, but groove filling and joint strength were found better while using 4.1 kJ rather than 4.7 kJ. Hence, 4.1 kJ of discharge energy was considered as a suitable energy level for better strength of the joint manufacturing for the given geometry and material configuration.

Table 3. 6 Maximum Lorentz force, current density and magnetic field

Energies	**Parameters**		
	Lorentz force (kN/m^2)	**Current density (kA/mm^2)**	**Magnetic field (T)**
3.4 kJ	9.53×10^5	75.4	19.46
4.1 kJ	1.326×10^6	90.0	22.89
4.7 kJ	1.538×10^6	96.33	24.62

3.4.9. Mechanical Pull-out Strength

The domain of energy levels, i.e., 3.4 kJ, 4.1 kJ, and 4.7 kJ selected from the simulation was given better joint strength. Pull-out strength for 5.0 kJ was found 3.2 kN which is the weakest, and that is due to tube shearing and cracking at groove edge as shown in Fig. 3.18. Pull-out strength of a joint manufactured using 3.4 kJ, 4.1 kJ, 4.7 kJ was found 4.91 kN, 5.10 kN, and 5.05 kN.

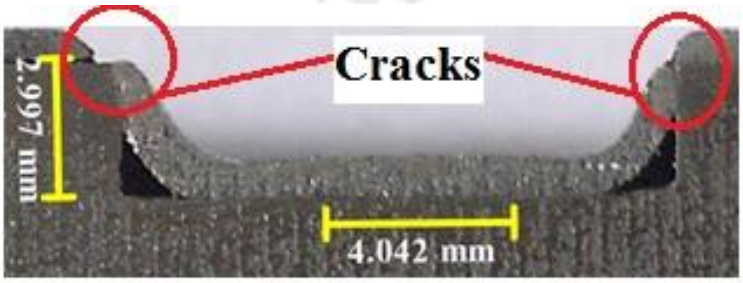

Fig. 3.18 Tube cracking at the groove edge for 5.0 kJ

A maximum pull-out strength was found using 4.1 kJ energy. A groove-edge was acting as a cutting edge while energy increased beyond 4.7 kJ that causes the joint to fail with a lesser applied load. Moreover, energy which is lower than 3.4 kJ affects groove filling and in turn interlocking which gives weaker joint strength. The comparisons of the pull-out load versus extension for tube and crimped sample were plotted as shown in Fig. 3.19. Pull-Out strength of the undeformed tube was found 5.14 kN. The pull-out strength of the joint manufactured using 3.4 kJ was compared and found 95% with the strength of a tube. Failure of the joint due to a thinning effect on the tube takes place at the groove edge of the joining zone while the load is applied. The repetition of samples on the same energy was carried out, and the average value of strength is taken to minimize the error.

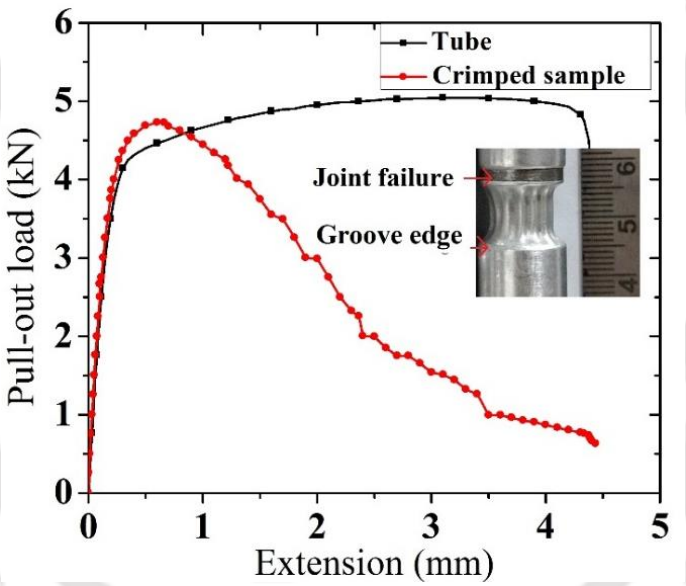

Fig. 3.19 Pull-out strength of crimped sample and tube

The magnitude of pull-out strength was taken at the breaking point of a joint as shown in Fig. 3.20. The load-bearing capacity of such kind of joint will be increasing while applied energy is increasing up to some extent and start decreasing due to failure at the joining zone.

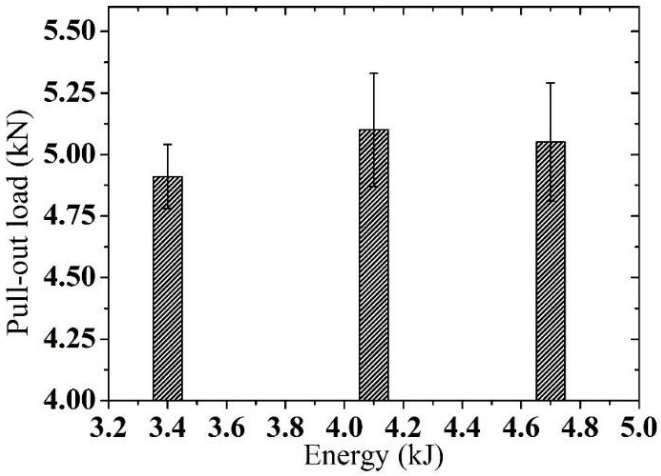

Fig. 3.20 Pull-out loads for 3.4 kJ, 4.1 kJ, and 4.7 kJ discharge energy

A steel rod was inserted at the tube end to avoid any failure due to the grip of UTM while a pull-out load is applied. The tube was started sliding with less than a pull-out load of 2 kN for the first three samples which are joined using discharge energy of 1.5 kJ, 1.9 kJ, and 2.3 kJ, but pull-out curve keeps increasing while plastically deformed portion had contact with groove edge. Load versus extension for all crimped samples is shown in Fig. 3.21. The extensions for all crimped samples at the break were observed wide-ranging due to the strength of the joints.

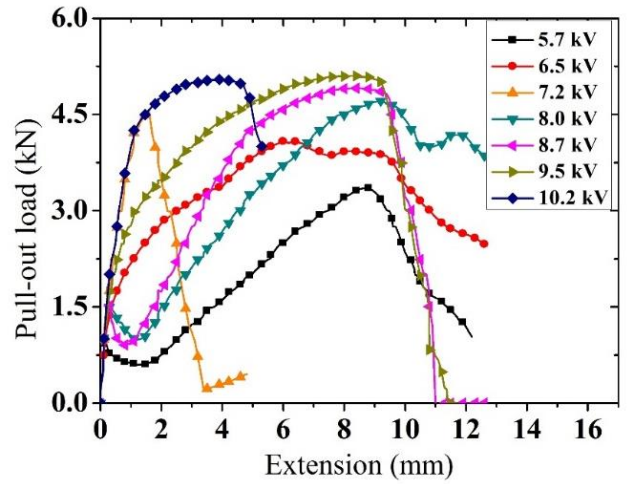

Fig. 3.21 Load versus extension for all samples

A severe plastic deformation causes a tube to interlock at the groove edge mechanically, and this becomes the main joint mechanism in addition to an interference fit. A different mode of joint failures was observed as deforming pressure becomes more due to increasing discharge energy for samples four and five. The tube was kept on sliding until a plastically deformed part touches the

groove edge and fails while increasing the pull-out load further. Wrinkling was observed at the joining zone that was caused mainly due to tube thickness and increasing discharge energies. If groove depth is decreased, wrinkling can be eliminated significantly. Figure 3.22 shows how those wrinkles are produced and failure at the joining zone after the pull-out test.

Fig. 3.22 Crimped sample after the pull-out test

Depending on discharge energy, a tendency of the tube to re-bounce back during impact with a steel rod was seen lesser for sample six compared to the final sample for the same groove parameters. Besides that, pull-out strength for the last sample is not as much as sample six because of a re-bouncing and tube thinning effect which prompts having a less mechanical interlock. A maximum pull-out load transferred by sample number six was found 5.10 kN and failed at a grooved edge which is part of the joining zone. A joint strength of 98 % was achieved using this sample compared to a tube that has a pull-out strength of 5.14 kN. A joint strength achieved from a sample that is crimped using 4.1 kJ of discharge energy can be considered as a promising result for an industrial application.

The load transferring capabilities of the samples are significantly affected by the magnitude of energy used. Applying an excessive amount of discharge energy leads to having tube thinning at the groove edge which leads to weakening joint strength. A maximum radial displacement without tube necking will produce better groove filling which is the function of energy and enhances joint strength. Radial displacement of the tube increases in direct proportionality with discharge energy as shown in Fig. 3.23 (a). The re-bouncing effect of the tube reduces radial displacement while increasing discharge energy beyond 4.1 kJ. Radial displacement for sample seven got reduced comparing to sample six due to the magnitude of applied energy. The magnitude of 4.7 kJ discharge energy causes the tube to rebounded back after impacting the groove surface that leads to reducing radial displacement. Figure 3.23 (b) shows linearity between discharge energy used and the resulted tube thickness reduction at groove edge.

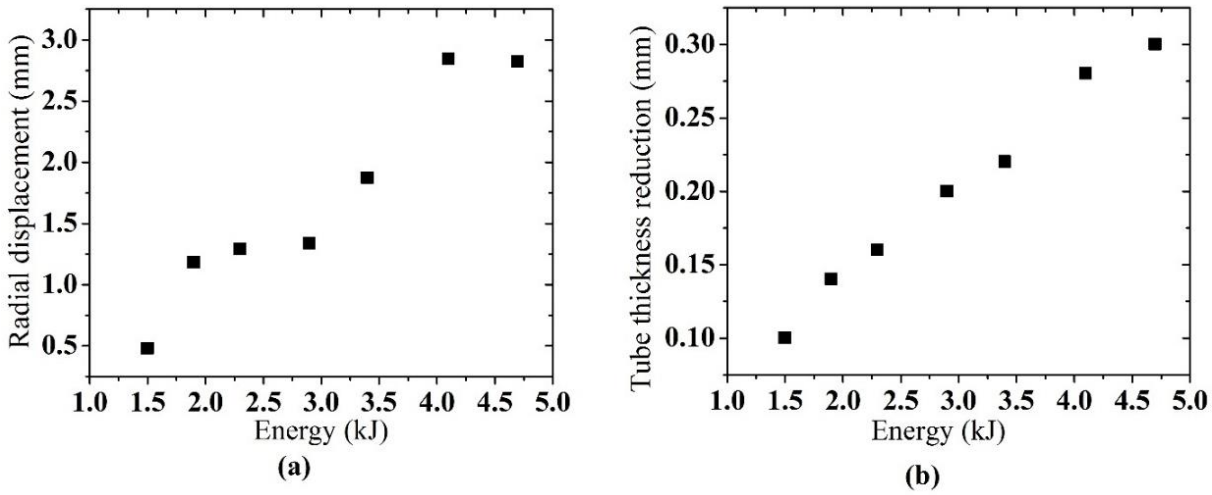

Fig. 3.23 Effect of discharge energy on (a) radial displacement and (b) thickness reduction at groove edge

Pull-out strength will increase by increasing applied discharge energy up to a certain limit as shown in Fig. 3.24 (a). For the given material system and geometrical dimension, it can be concluded that 4.1 kJ is optimal energy. The tube was easily pulled out due to severe plastic deformation at groove edge if discharge energy increased beyond the optimum. Moreover, radial displacement also keeps on decreasing while using excessive energy beyond the requirement. A product of capacitance and voltage gives energy, and graphically these two parameters are plotted as shown in Fig. 3.24 (b).

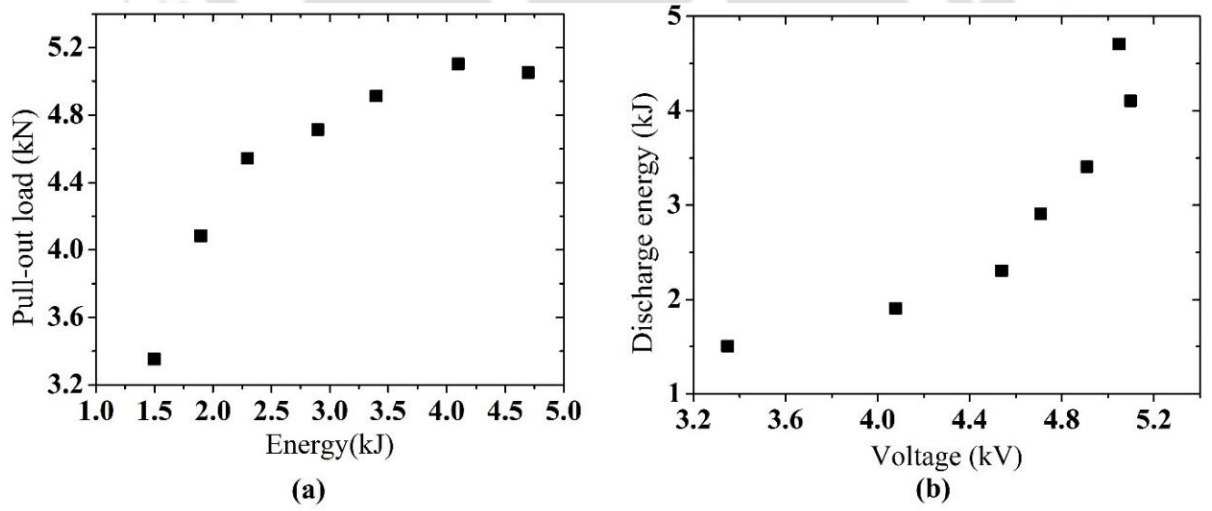

Fig. 3.24 (a) effect of discharge energy on pull-out strength and (b) discharge energy for the respective voltage

The crack at the groove edge was observed for sample seven due to the level of discharge energy used. Hence the joint was failed at groove edge with less pull-out load than sample number six.

Thinning becomes severe at groove edge while using discharge energy more than 4.1 kJ which leads to having a joint failure. High strain rate plastic deformation at groove edge significantly affects the joint strength because of the associated mechanical interlock. The direct proportionality shows the higher radial displacement of the tube which gives the higher pull-out strength as shown in Fig. 3.25.

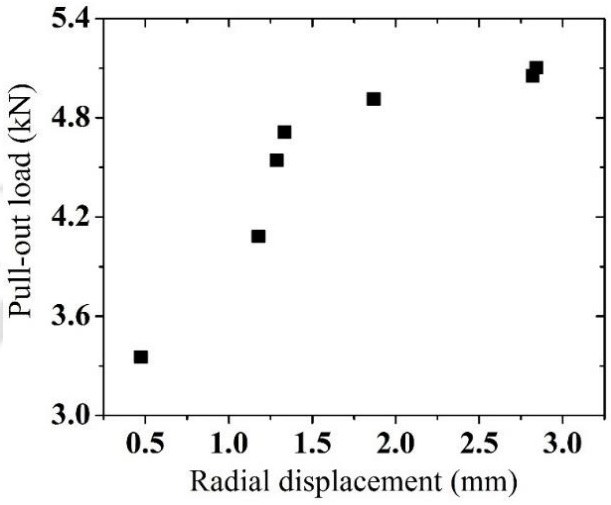

Fig. 3.25 Effect of radial displacement on pull-out strength

Uniformity of tube deformation affected significantly if an axis of helical coil offset from the axis of the workpiece. Therefore, the eccentricity of workpieces and coil was crucial in this regard. Groove filling of lower and upper section has some differences due to the eccentricity problem as shown in Fig. 3.26 (a). Microscopic study at the joining interface of sample seven shows the nonexistence of metallurgical bonding between aluminum tubes and steel rod. Minimum and maximum gap measured as shown in Fig. 3.26 (b). There is no intermetallic compound found at the interface which shows how pure mechanical interlock can be made in this joining technique.

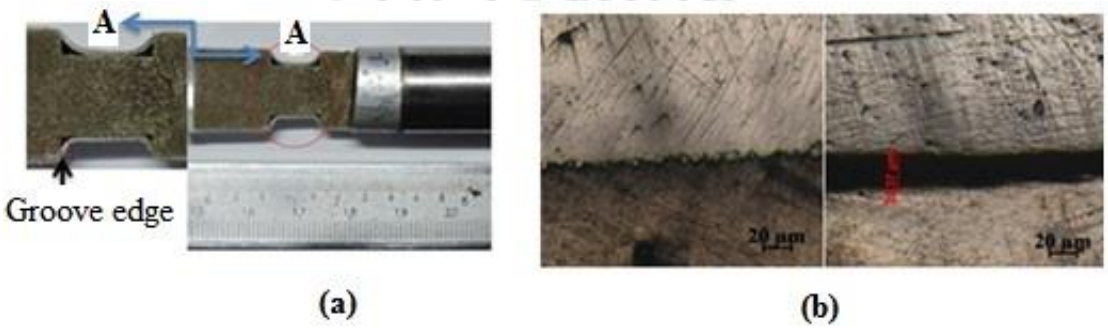

Fig. 3.26 (a) Cross-sectional view of joining zone and (b) metallographic image at the joining zone

3.4.10. Prediction of Possible Failure Region

The possible region of joint failure was predicted using the simulation of maximum shear stress distribution along the joining zone. The distribution was analyzed only for the tube, and maximum achievable shear stress at joining zone for three energy levels at 55.6 µs is shown in Fig. 3.27.

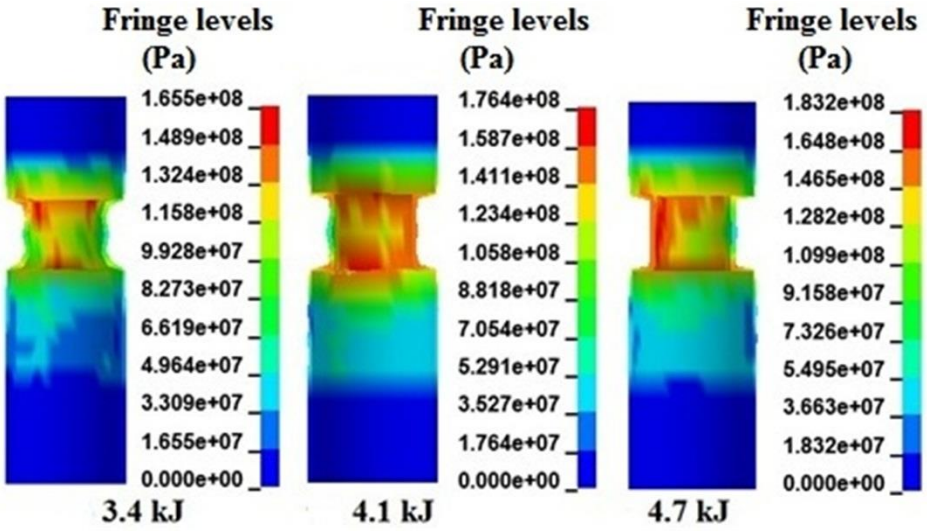

Fig. 3.27 Effect of energy on maximum shear stress distribution along the joining zone

Joint was found failed at the groove edge which is predicted at a region were shear stress is maximum using simulation. Mechanical strength testing clearly shows the region where failure initiated as predicted in the simulation for the applied axial load.

3.4.11. The relation between Resultant Pressure and Displacement

The resultant pressure found at three different discharge energy levels were plotted along with resultant displacement as shown in Fig.3.28. The maximum pressure was considered at each time step to understand the relationship with flyer tube deformation. The maximum resultant pressure values found at 3.4 kJ, 4.1 kJ, and 4.7 kJ are 1948 MPa, 2155 MPa, and 2709 MPa respectively. The first peak pressure generates within 20 µs due to peak current is called critical which causes plastic deformation. Because of exponential decay of current, the second and the remaining peak pressure doesn't have a significant effect in causing severe deformation. The deformation of the tube increases gradually and reaches maximum value depending up on the magnitude of pressure and it remains constant until the end of the process. As the discharge energy increased, the pressure also increased. A discharge energy of 4.1 kJ is optimum in which the pressure obtained was 2155

Mpa."

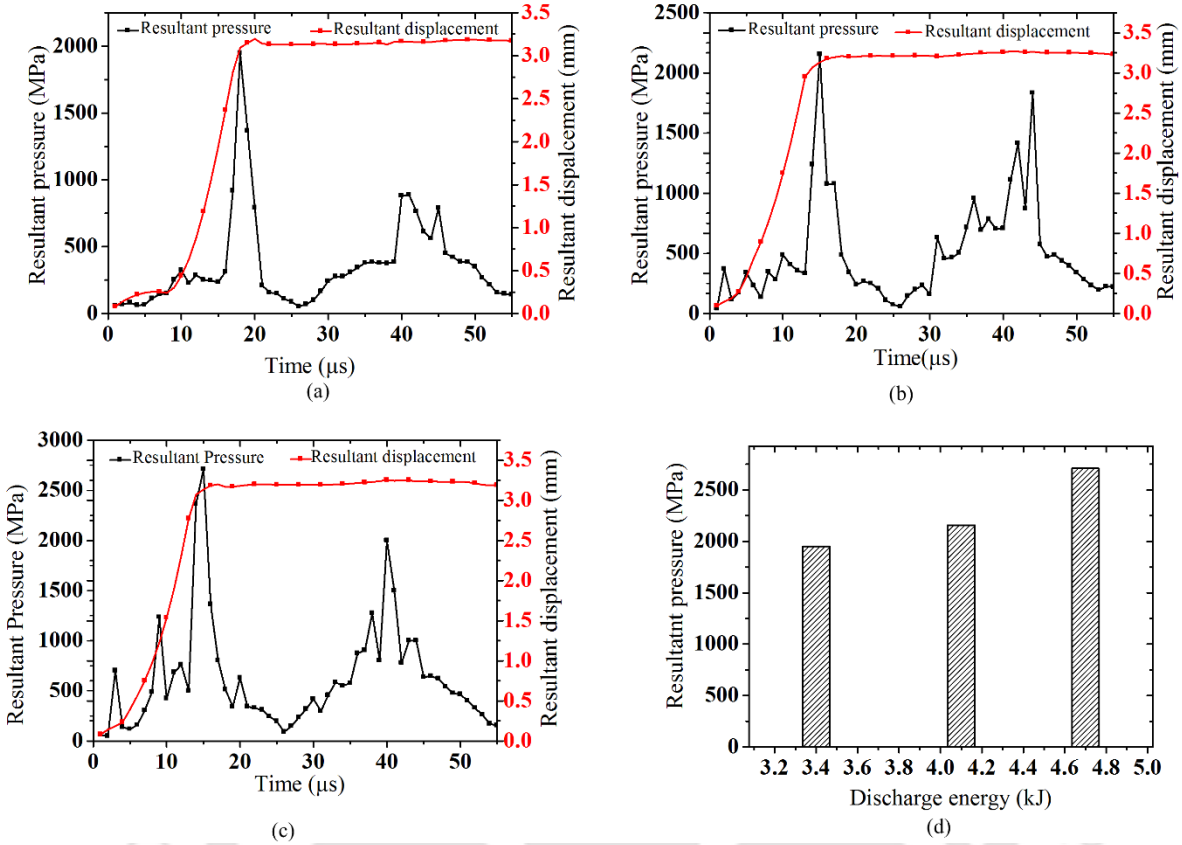

Fig. 3.28 Relation between resultant pressure and displacement at (a) 3.4 kJ (b) 4.1 kJ (c) 4.7 kJ, and (d) comparison

3.5. Summary

A combined FEM/BEM method has been employed for the simulation of the electromagnetic crimping process. The presented analysis is useful for the practical realization of the electromagnetic crimping process to join the tube and the profiled rod and contribute to a better understanding of the working principles. The model was validated with the experimental results and used to predict the effect of energy on joint strength and several process parameters. A comparison of the 3D simulation results with the experiment shows that the model could efficiently predict the effect of energy on parameters. In general, results found from the numerical analysis show how to predict the process parameters of the EM crimping process. Important result found from numerical simulation and experimental investigation is summarized as follows.

- Pull-out strength of the crimped sample was found more than 95% compared to the strength

of the tube.

- A 3D model was developed, and simulation is used to study the effect of energy on joint strength and process parameters which is difficult to address using experimenting only. The domain of energy levels was found out using simulation which gives better joint strength for the given material combinations and groove parameters. Hence, discharge energy of 4.1 kJ is recommended for better joint quality based on the strength of the joint manufactured and a tube thickness reduction at groove edge.
- The 3D model is validated with the experiment by measuring and comparing tube thickness reduction at the groove edge, radial displacement, and groove filling which shows a good agreement.
- Effective plastic strain and radial displacement along the joining zone were found uniform which explains how pressure is uniformly distributed.
- Maximum shear stress distribution along the joining zone leads to identify the region where probably the joint can fail for the applied load.
- The pull-out strength result shows how electromagnetic crimping process can give better joint strength without any defect, unlike thermal welding. Sample six failed at 5.10 kN pull-out force which is almost 98 % of joint strength comparing to the tube which has a pull-out strength of 5.1 kN. Moreover, 4.1 kJ was optimal discharge energy for the given material system and geometrical dimension to obtain higher joint strength.
- A geometrical parameter like groove edge radius considerably affects joint strength either positively or negatively. Discharge energy of 4.1 kJ gave a maximum radial displacement of 2.844 mm, but increasing this energy causes radial displacement to decrease due to the re-bouncing effect. As radial displacement increases up to a certain limit, pull-out strength also increases and found 5.10 kN.
- Reduction in thickness of the tube at groove edge increased while increasing discharge energy. Thinning of the tube at groove edge leads the joint to fail easily.
- This preliminary study shows a promising method for joining the automotive part like drive shaft and space frame specially designed from aluminum which has a different profile. The result shows how qualitative joint strength can be successfully manufactured using this latest green technology.

CHAPTER 4

MECHANICAL INTERLOCK MADE BY ELECTROMAGNETIC CRIMPING FOR AXIAL LOAD RESISTANCE USING DOUBLE RECTANGULAR GROOVE

4 Mechanical Interlock Made by EM crimping for Axial Load Resistance using Double Rectangular Groove

4.1. Introduction

Joining aluminum tube with steel rod using thermal-based welding process like arc welding is challenging due to easy formation of oxide which requires a higher melting temperature than the parent metal. In this chapter, EM crimping process is used to join the aluminum tube and a steel profiled rod mechanically. The circumferential double grooves which have a rectangular shape were machined on the steel rod with different geometrical parameters. Discharge energy of 4.7 kJ and groove edge angle of 0.5 mm was kept constant. Therefore, the primary goal of this study is to investigate the effect of geometrical parameters on joint strength using a double rectangular groove. A mechanical pull-out strength test was carried out to investigate joint strength manufactured and compared with the strength of the aluminum tube. Further, the effect of groove depth on the percentage of gap filling, wrinkling and tube thickness reduction was studied in detail. Moreover, microhardness at the joint interface also investigated. Based on the results obtained, a design guideline that describes the effects of width-to-depth ratio on joint strength is proposed.

4.2. Experimental Detail

4.2.1. Materials and Experimental Method

The chemical composition and mechanical properties of aluminum tube and steel rod used in this experiment are summarized in Table 4.1 and Table 4.2. Energy-dispersive X-ray spectroscopy (EDX) was used for the elemental analysis.

Table 4. 1 The chemical composition of aluminum tube and steel rod (Kumar and Kore, 2017)

	The weight percentage of the element (%)								
Material	Al	Mg	Mn	Ti	Zn	Si	Cu		
Al 1050	99	0.0	0.1	0.1	0.1	0.6	0.1		
	C	Cr	Mn	Cu	Ni	P	Si	S	Fe
1020 Steel	0.16-0.25	0.15-0.25	0.3-0.4	0.1-0.2	≤0.1	≤0.1	0.2-0.3	0.1-0.4	Balance

Table 4. 2 Mechanical properties of the material used (Rajak and Kore, 2018, Kumar and Kore, 2017)

Material	Properties
Al 1050	Conductivity (36.8 X 10^6 S/m)
	Density (2700 Kg/m^3)
	Poisson's ratio (0.33)
1020 Steel	Density (8900 Kg/m^3)
	Young's modulus (500 GPa)
	Poisson's ratio (0.3)
	Ultimate tensile strength (210 MPa)

Initially, grooves were machined using parameters based on the cause and effect matrix that is generated by the central composite design (CCD) method. Six levels of groove depth which is varied from 0.5 mm to 3 mm with an increasing rate of 0.5 mm were considered keeping all other grooves and process parameters constant. Discharge energy of 4.7 kJ was used to carry out the experiment which is determined from the preliminary study. The result achieved from the pull-out test was used as a response for further analysis. The CCD model describes the behavior of the maximum pull-out load. The analysis of variance provides statistical tools to evaluate maximum pull-out load in terms of groove depth for the same width configurations. Further, four different width configuration was considered to study the effect of the width-to-depth ratio on joint strength**.** Detailed dimensions and terminology for the rod, tube, and the coil are illustrated in Fig. 4.1.

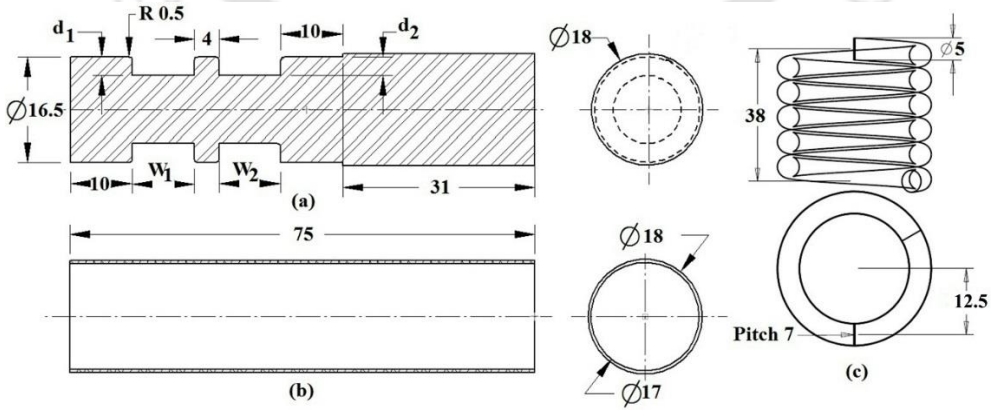

Fig. 4. 1 Dimension and nomenclature of (a) rod (b) tube and (c) coil (All dimensions are in mm)

Experiments were divided into four groups which have different groove width configurations. Each group has six specimens according to CCD with identical groove width configurations but for different groove depth. Detailed dimensions of double rectangular grooves for twenty-four samples are summarized in Table 4.3.

Table 4. 3 Groove geometrical parameters

Sample No.		**S_1-S_6**						**S_7-S_{12}**					
		1	2	3	4	5	6	7	8	9	10	11	12
Groove 1	w_1 (mm)	8						8					
	d_1 (mm)	0.5	1	1.5	2	2.5	3	0.5	1	1.5	2	2.5	3
Groove 2	w_2 (mm)	6						8					
	d_2 (mm)	0.5	1	1.5	2	2.5	3	0.5	1	1.5	2	2.5	3
Sample No.		**S_{13}-S_{18}**						**S_{19}-S_{24}**					
		13	14	15	16	17	18	19	20	21	22	23	24
Groove 1	w_1 (mm)	10						10					
	d_1 (mm)	0.5	1	1.5	2	2.5	3	0.5	1	1.5	2	2.5	3
Groove 2	w_2 (mm)	10						8					
	d_2 (mm)	0.5	1	1.5	2	2.5	3	0.5	1	1.5	2	2.5	3

4.2.2. Experimental Setup

A coil made up of copper wire has five number of turns, 19.625 mm^2 cross-sectional area and 20 mm inside diameter respectively. The experimental setup which consists of a coil and workpieces is shown in Fig. 4.2. An oxide layer was cleaned using "acetone" for moisture free samples, and proper insulation also used before crimping was done. Teflon made fixture was used to support the coil for multiple crimping processes. Hence, successful mechanical crimping was made using this setup.

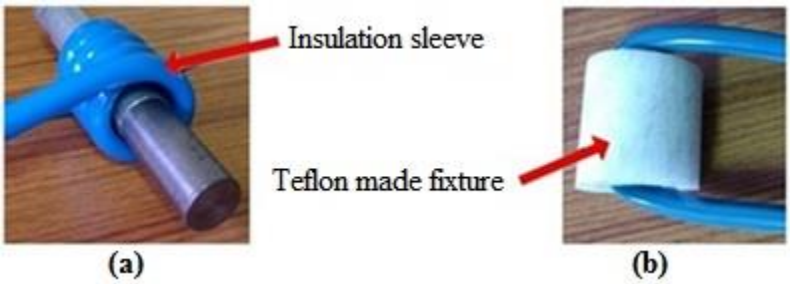

Fig. 4. 2 (a) Experimental setup and (b) coil inside Teflon made a fixture

4.3. Mechanical Pull-out Test

After crimping was done for all samples, pull-out strength tests were performed to evaluate the strength of manufactured joints and aluminum tubes in transferring axial load using a Universal Testing Machine (UTM). The schematic representation of a pull-out test setup for crimped sample is shown in Fig. 4.3. Crossbar velocities of 0.1 mm/s were maintained while testing both tube and crimped specimens.

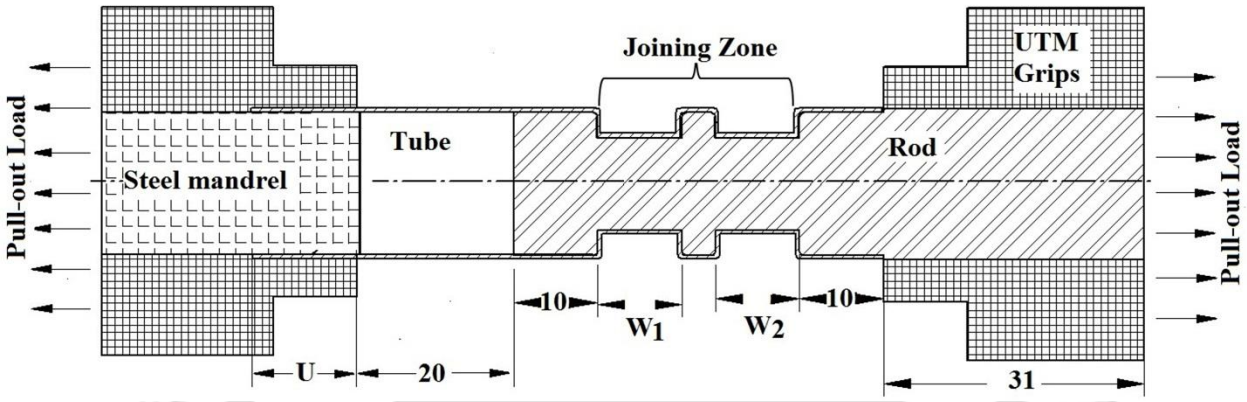

Fig. 4. 3 Schematic representation of pull-out test for a crimped sample (All dimensions are in mm)

Based on the change in width configuration, the values of U will be adjusted. This value of U is identical for each group which has the same groove configurations. Two steel mandrel was inserted at the end of the tube while pull-out is carried out to avoid any deformation where UTM is gripping.

4.4. Results and Discussion

The deformation obtained along the joining zone due to lower discharging energy level was found non-uniform. Few researchers suggest applying higher magnetic pressure to address this problem. (Karimi and Bahmani, 2010). The discharge energy which is more than 4.7 kJ leads to having uniform deformation but weaker joint strength due to failure at groove edge. Moreover, discharge energy which is less than 4.7 kJ also gives weaker joint strength compared to the strength of the aluminum tube. Hence, for the material system and groove configuration considered in this study, the discharge energy of 4.7 kJ was found optimum. Tube thickness reduction due to discharge energy of 4.7 kJ is found less comparing to 5.6 kJ as shown in Fig. 4.4. The tube is getting sheared off entirely at the groove edge after crimping using discharge energy of 5.6 kJ. Pull-out strength for 5.6 kJ was found less than 3 kN which is the weakest due to tube shearing and necking at

groove edge. For this reason, we considered 4.7 kJ as optimum discharge energy level which can give a joint strength up to 5.6 kN without tube necking.

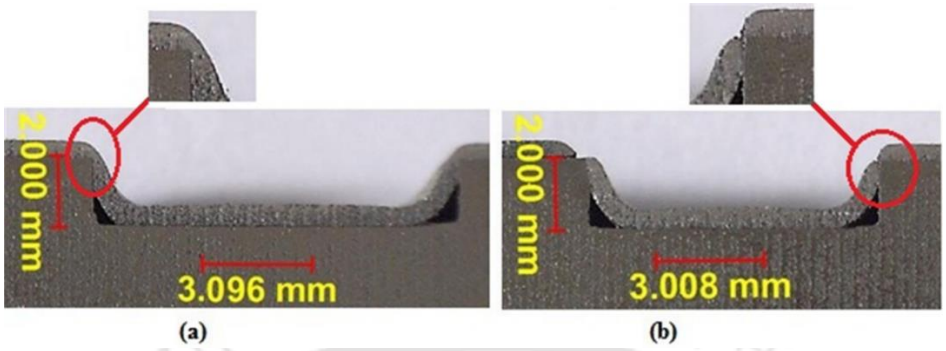

Fig. 4. 4 Tube necking at the groove edge due to discharging (a) 4.7 kJ and (b) 5.6 kJ for groove which has 2 mm depth

The sinusoidal current waveform plotted in Fig. 4.5 was measured using a Rogowski coil which shows an amplitude of 125.8 kA obtained at 4.7 kJ of discharge energy. Using this discharge energy, the effect of groove depth on pull-out strength, groove filling, wrinkling and tube thickness reduction at groove edge were studied in detail. Mechanical pull-out tests were carried out to evaluate joint quality in transferring axial load. Optical microscopic image analysis and hardness tests at the joint interface were also carried out.

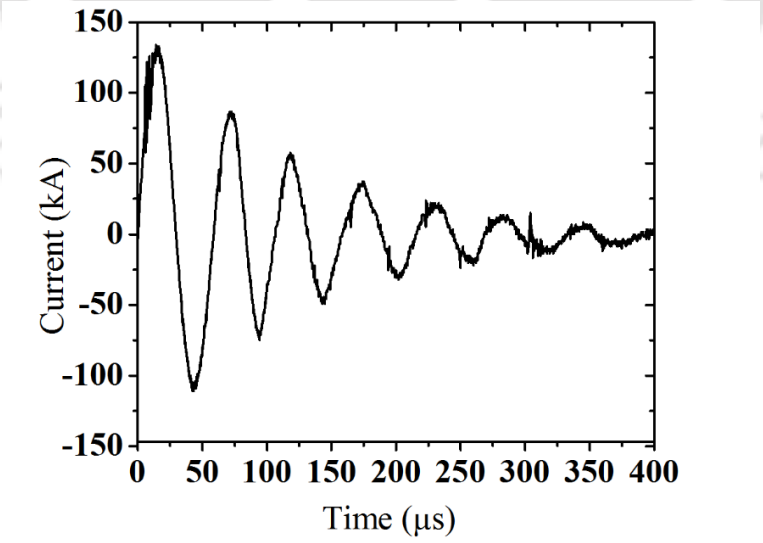

Fig. 4. 5 Measured current waveform obtained at 4.7 kJ of discharge energy

4.4.1. Mechanical Pull-out Strength Analysis

In each of Fig. 4.6, pull-out load versus an extension of six crimped specimens that have identical width configuration but different groove depths were plotted. The maximum pull-out strength of 5.47 kN and 4.16 kN were found for S_4 and S_6 as shown in Fig. 4.6 (a).

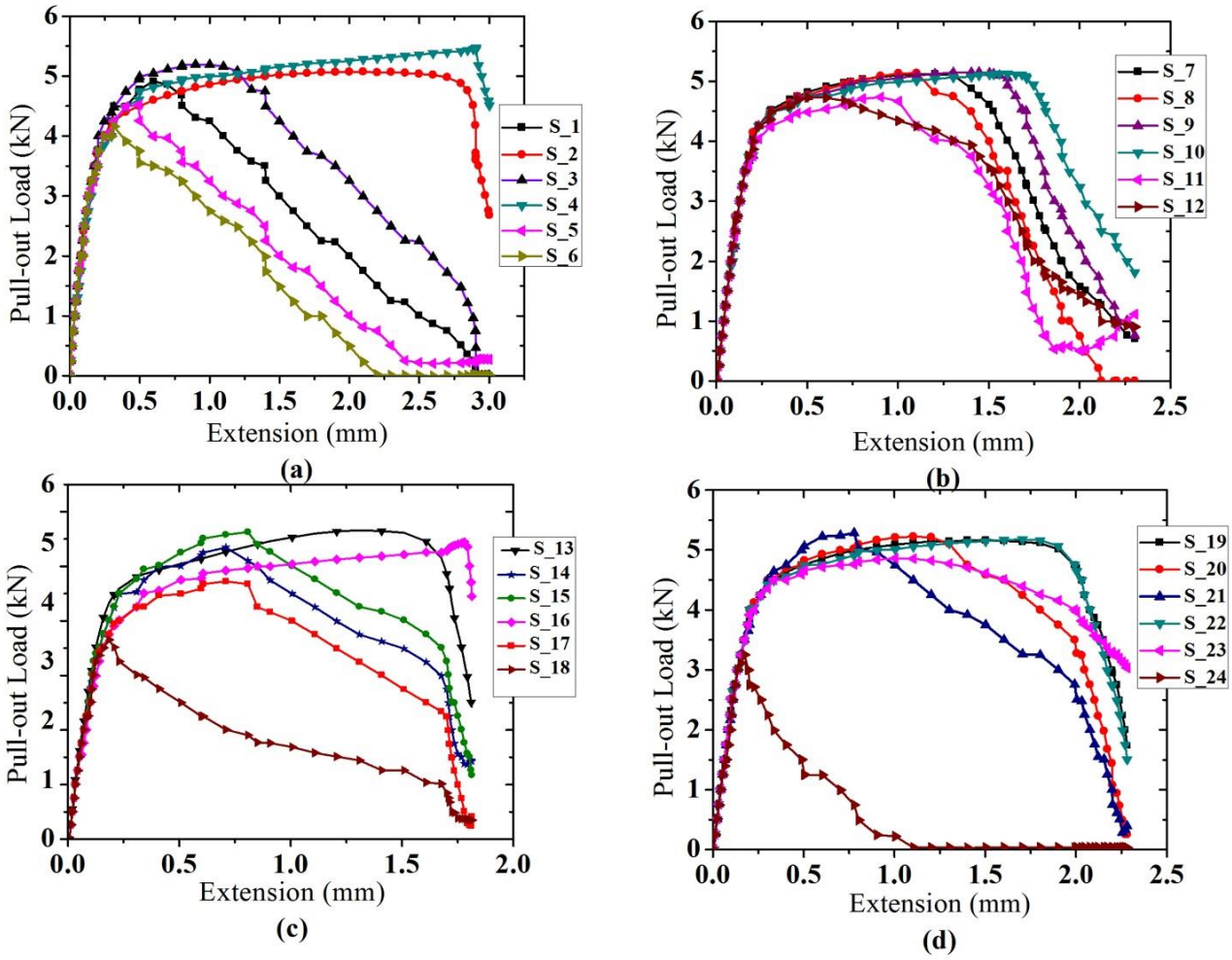

Fig. 4. 6 Pull-out strength vs. extension for (a) S_1-S_6 (b) S_7-S_{12} (c) S_{13}-S_{18} (d) S_{19}-S_{24}

In the current study, a joint strength up to 5.63 kN was found using a discharge energy of 4.7 kJ which is maximum among all groove configurations. As can be seen in Fig. 4.6 (b) maximum pull-out strength of 5.15 kN was found for S_{10}, and 4.73 kN was found for S_{12}. Fig. 4.6 (c) illustrates the maximum pull-out strength of 5.63 kN which was found from S_{16} and 3.65 kN from S_{18}. A maximum pull-out strength of 5.28 kN and 3.25 kN was found from S_{22} and S_{24} as shown in Fig. 4.6 (d) respectively. The samples which have 2 mm and 3 mm groove depth in each group were

compared for a maximum pull-out load that can be transferred. The maximum load was taken at the point where the joint was broken using a pull-out load versus extension plot.

The response variable, i.e., pull-out load *P* (kN) and the examined factors, i.e., groove depth *D* (mm) were related by Eq. 4.1 and 4.2 which is the polynomial equation of second-and-third order by applying multiple regression analysis on the data. Analysis of variance calculated the determination coefficient (R^2) as 0.9735 for Eq. 4.1 and 0.9988 for Eq. 4.2 which represents the pull-out load as a function of groove depth.

$$P = 4.97032 + 0.34127 \times D - 0.13968 \times D^2 \quad (4.1)$$

$$P = 5.72643 - 1.88502 \times D + 1.76314 \times D^2 - 0.47002 \times D^3 \quad (4.2)$$

where *P* is pull-out load and *D* is groove depth.

The results indicate that the model can efficiently predict 97.35 % and 99.88 % of the pull-out strength for the given levels of groove depth. Therefore, the models were found to be highly significant. Figure 4.7 demonstrated predicted analytical values and the actual result of maximum pull-out strength that shows how the model is significant.

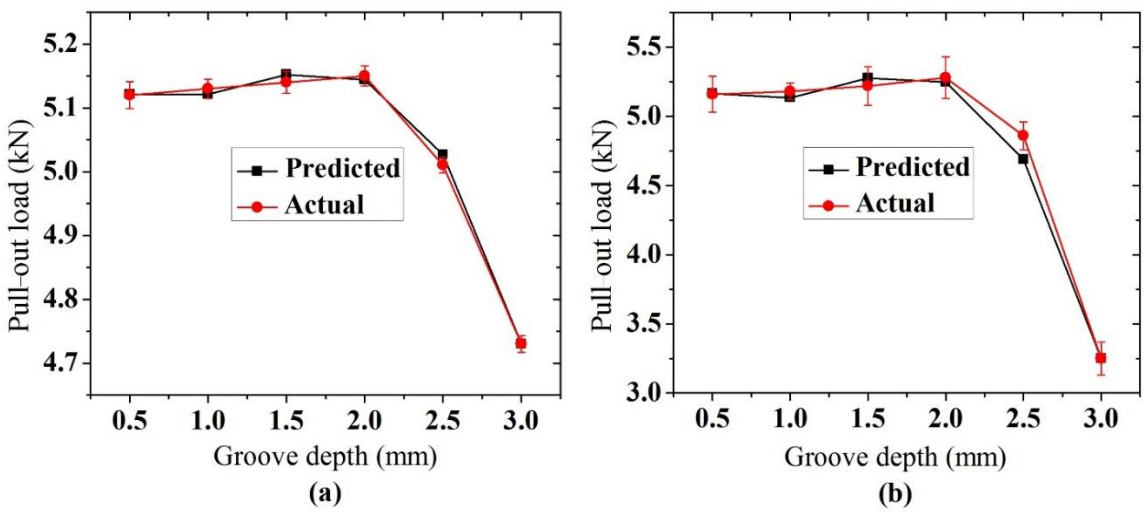

Fig. 4. 7 Predicted and actual pull-out load for (a) S_7-S_{12} and (b) S_{19}-S_{24}

Specimens number S_5, S_6, S_{11}, S_{12}, S_{17}, S_{18}, S_{23}, and S_{24} (see table 5. 3) have failed at joining zone as shown in Fig. 4.8 (a) due to increased groove depth. Hence, pull-out strength analysis relies on these samples to show how strong joint can be manufactured in EM crimping process. It is observed that joint strength keeps increasing as groove depth increases for all groove

configurations up to 2 mm and start declining after breaking takes place. Pull-out load versus extension for comparison of those specimens failed at joining zone with the aluminum tube is shown in Fig. 4.8 (b). The tube is failed at 5.1 kN of pull-out load which is higher than the maximum pull-out strength of crimped specimens failed at joining zone. Specimen S_{23} which is failed at 4.86 kN was found better compared to the strength aluminum tube. Specimens that have the wider width of the first groove (in the tube side) and a smaller width of a second groove provided the highest joint strength. A minimum of 72% and a maximum of 95% joint strength was achieved compared to the strength of the undeformed aluminum tube. Specimen S_{24} is failed at 3.25 kN pull-out load which gave weaker axial load resistance.

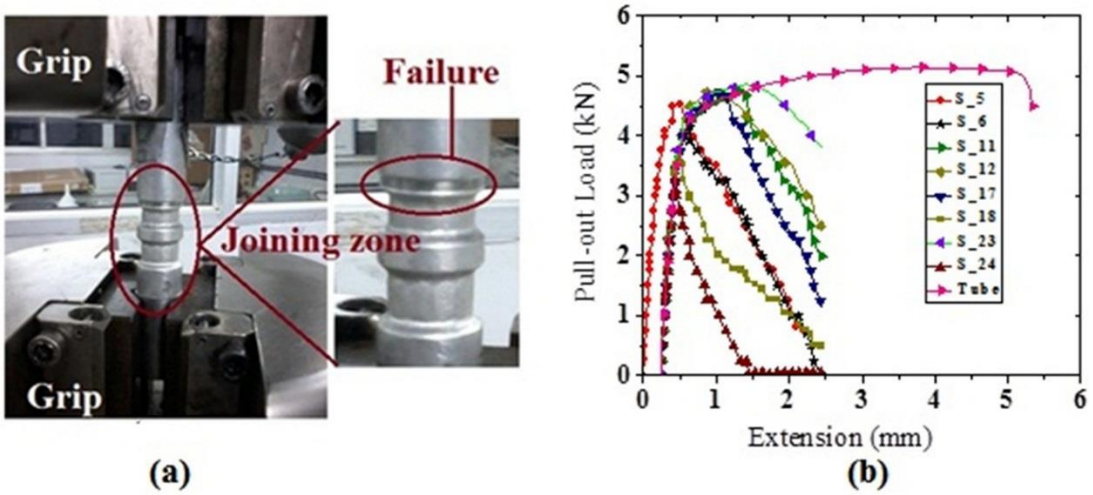

Fig. 4. 8 (a) UTM pull-out test setup for a crimped sample and (b) pull-out strength of tube and samples failed at the joining zone

Increasing groove depth has a significant effect on reducing tube thickness and joint strength respectively. Hence, a tube fracture at the groove edge as shown in Fig. 4.9 (f) leads to weakening a joint strength. A groove depth has a significant effect on gap-filling which influences the quality of load transferring capability of the joints. Measurements were taken to investigate how increased groove depth affects the gap between joint parts at the corner of the groove surface. For the joint manufactured using a groove depth of 0.5 mm, 1.0 mm and 2.0 mm, the percentage of groove filling is declining for the same discharge energy and tube thickness. A better groove filling was found for 0.5 mm groove depth, but the tube can come out easily during the pull-out strength test.

The gap fillings were investigated for the last set of the specimens (S_{19}-S_{24}). Figure 4.9 (a-f) shows the measured values of a gap at the corner of the groove surface that was taken from the collar section of the joining zone. A minimum of 0.151 mm gap was found for the specimen which has 0.5 mm groove depth as shown in Fig.4.9 (a), and the maximum gap of 0.987 mm obtained from the specimen which has a 3 mm groove depth as shown in Fig. 4.9 (f).

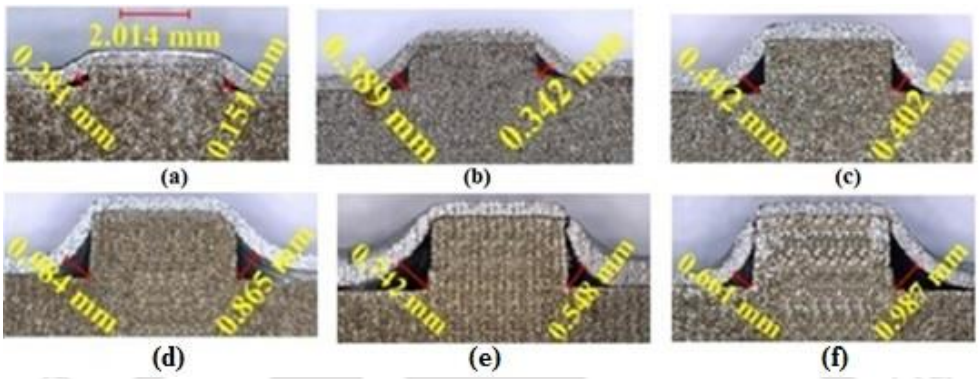

Fig. 4. 9 Gap measured for (a) 0.5 mm (b) 1 mm (c) 1.5 mm (d) 2 mm (e) 2.5 mm and (f) 3 mm groove depth

Percentages of gap fillings based on measured values were calculated and plotted as shown in Fig. 4.10 that describes gap filling on the left and right (GF_L and GF_R) side of the collar respectively.

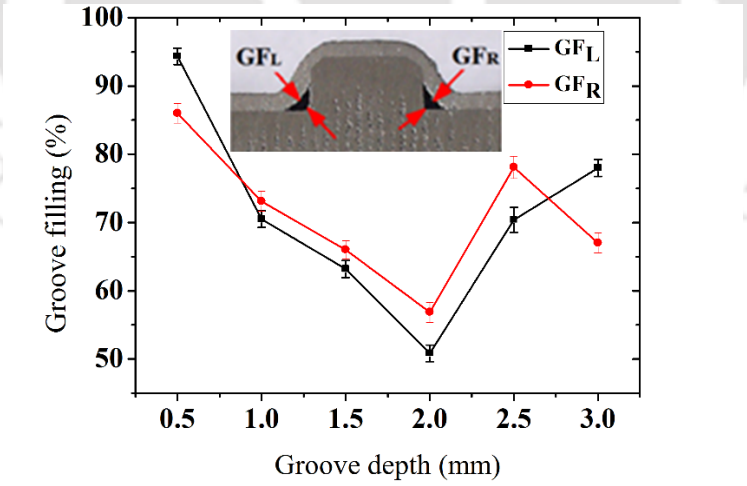

Fig. 4. 10 Effect of groove depth on percentage gap filling

Above 94% of the gap was filled for the sample which has 0.5 mm groove depth, and more than 60% of the gap was found filled for the specimen with the groove depth of 2.5 mm and 3 mm. Gap filling percentage keeps decreasing while groove depth increases up to 2 mm and begins rising due

to tube fracture at groove edge. Tube thickness reduction at the groove edge was found maximum for joints manufactured using more than 2 mm groove depth. A connection or joint strength obtained from electromagnetic crimping process is affected significantly by groove depth. Tube cracking and shearing at groove edge become severe due to the increment of groove depth more than 2 mm. Hence, pull-out strength increases for increasing groove depth up to 2 mm then it begins decreasing as shown in Fig. 4.11. The joints manufactured using a groove depth of more than 2 mm were failed in the joining zone with a minimum pull-out load.

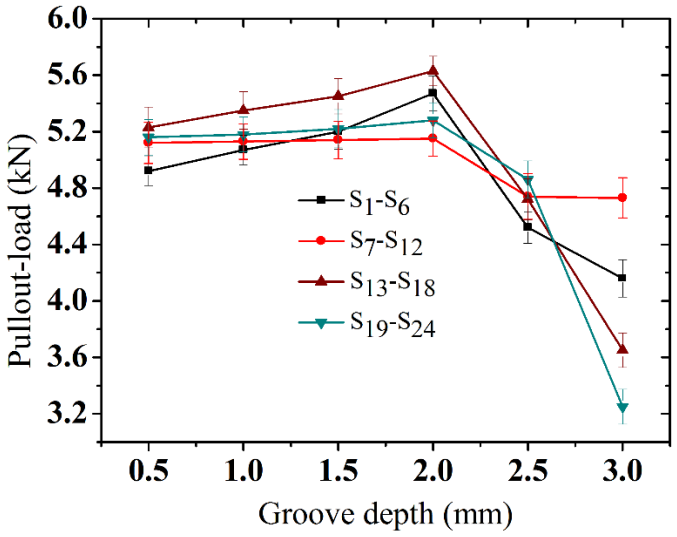

Fig. 4. 11 Effect of groove depth on joint strength for all samples

4.4.2. Effects of Width-to-Depth Ratio on Joint Strength

The effects of width-to-depth ratio on joint strength for all specimens were plotted as shown in Fig. 4.12. A range of width and depth for the highest joint strength for the given material system and process parameters were investigated.

If the ratio of $Q_1=W_1/d_1$ and $Q_2=W_2/d_2$ are selected in the range of four to six and two to four ($4d_1<W_1<6d_1$ and $2d_2<W_2<4d_2$), joint strength becomes higher as shown in Fig. 4.12 (a). Similarly, if Q_1 and Q_2 are equal to four ($4d_1=W_1$ and $W_2=4d_2$), joint strength becomes highest for similar groove configuration as shown in Fig. 4.12 (b). Joint strength will increase as contact area increases as shown in Fig. 4.12 (c) for increased Q_1 and Q_2 compared to Fig. 4.12 (b). If the ratio of Q_1 selected in the range of four to six and Q_2 in the range of two to four ($4d_1<W_1<6d_1$ and

$2d_2<W_2<4d_2$), joint strength becomes higher as shown in Fig. 4.12 (d) for different groove configurations.

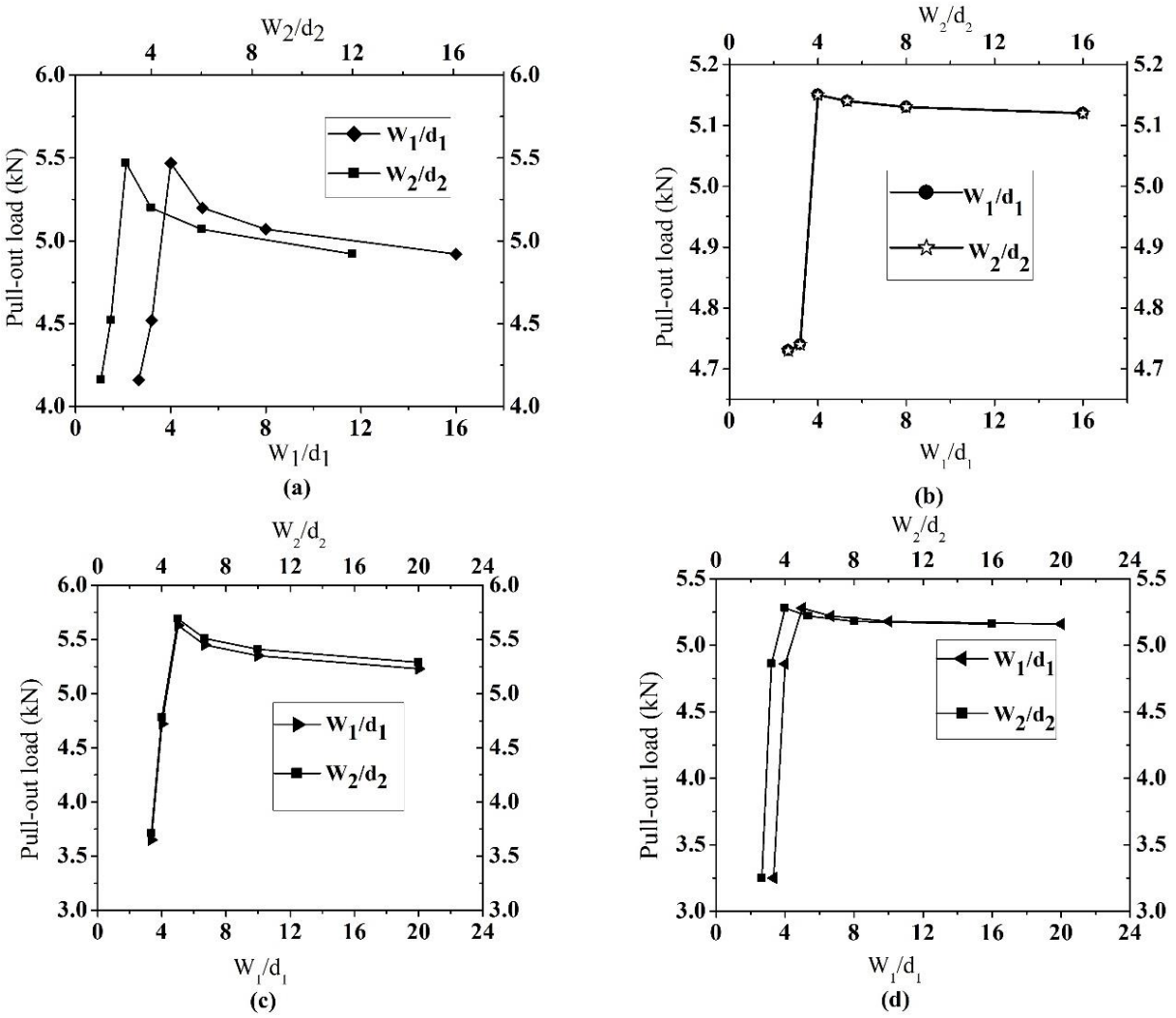

Fig. 4. 12 Effect of width-to-depth ratio on joint strength (a) S_1-S_6 (b) S_7-S_{12} (c) S_{13}-S_{18} (d) S_{19}-S_{24}

If the width-to-depth ratio increases, the joint strength will decrease for all groove configurations. The main reason for this effect is the change in the joint mechanism in which interference-fit becomes dominant over form-fit. Besides that, the increasing width-to-depth ratio will increase weight at the joining zone which is undesirable from a lightweight design point of view.

4.4.3. Failure Mode

In the current study, three modes of failure were observed while conducting the pull-out strength test. Among 24 samples, the tube is sliding for samples which has 0.5 mm groove depth and 12 of

them are failed in the tube section whereas 8 of them are failed at the joining zone as shown in Fig. 4.13 (a) and (b). Those samples having a depth of more than 2 mm and different width configuration were failed at groove edge at lowest pull-out load. However, the rest of specimens failed on the tube at a higher pull-out load compared to aluminum tube. Increasing the residual stress on surfaces of aluminum sheet metal with holes was found during electromagnetic peening process (Li and Cheng, 2009). The residual stress produced on joining-zone leads to an increasing joint strength between workpieces. A similar conclusion was reported about the tube failing for the same kind of groove geometry (Weddeling et al., 2015). Three modes of failure were found from an experimental study of crimping aluminum tube with tubular aluminum mandrel using a single rectangular groove (Marré et al., 2009). The hardness of the joining zone was enhanced due to strain hardening. Hence, the crimped samples failed on the tube which was exposed to a magnetic field gave the highest connection strength.

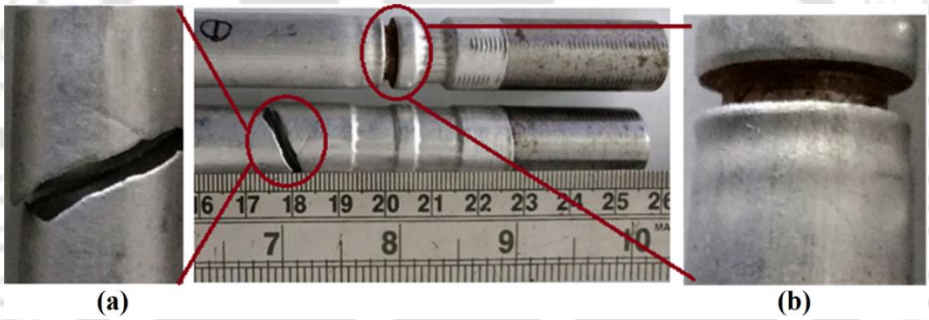

Fig. 4. 13 Failed sample (a) on Al tube and (b) on groove edge (joining zone)

4.4.4. Effect of Groove Depth on Wrinkling and Tube Thickness Reduction

The imperfections of the material trigger buckling which causes wrinkles under radial compression (Demir et al., 2010). The clearance between a tube and a rod keeps on increasing while groove depth is rising which leads to creating wrinkles. Increasing groove width also reduces the number of wrinkles, but it will add the weight of a joining zone that is undesirable from the lightweight design point of view. Hence, numbers of wrinkles were found more for the specimens which have 3 mm groove depth comparing to the specimen which has 0.5 mm as shown in Fig. 4.14 (a-b). Wrinkling/buckling can be reduced by increasing flyer velocity, which can be done by increasing input energy or by using a capacitor bank with higher discharge frequency, and the rapid imposition of the pressure pulse also reduce wrinkling (Vivek et al., 2011). Furthermore, there will be wrinkling if the groove depth is not proportional to tube thickness even though flyer velocity

increases. Hence, using energy more than 4.7 kJ for 2 mm groove depth and 1 mm tube thickness was expected to give less number of wrinkles. Both strain hardening and increasing wrinkling effects were achieved by a higher pressure impulse (Kleiner et al., 2005). However, groove depth proportional to a tube thickness gives less number of wrinkles or no wrinkles.

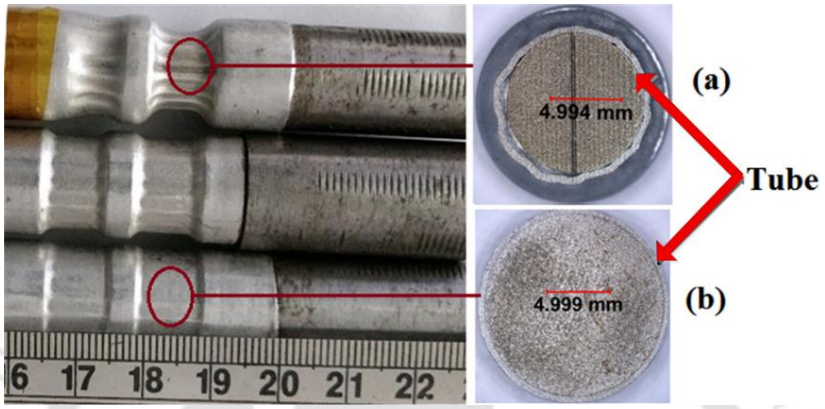

Fig. 4. 14 Wrinkles for a sample which has (a) 3 mm and (b) 0.5 mm groove depth

The tube thickness got reduced for different depths at the collar section of the joining zone located between two grooves. Tube thickness reduction was investigated for the last set of samples (S_{19}-S_{24}) and plotted as shown in Fig. 4.15.

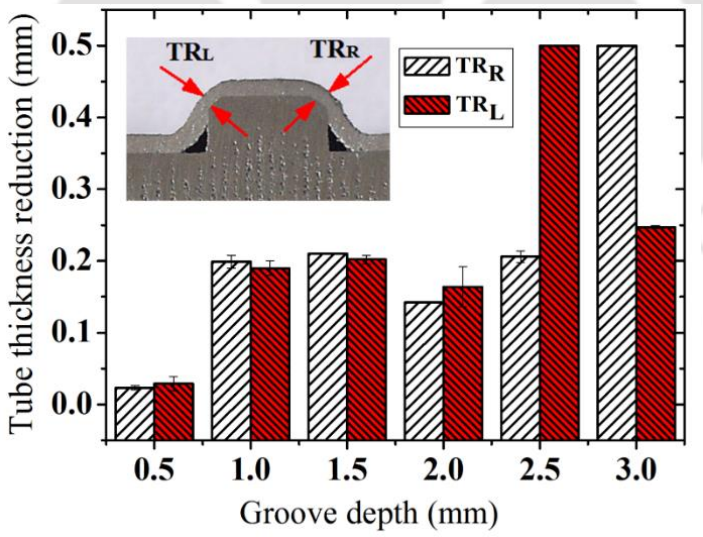

Fig. 4. 15 Tube thickness reduction at groove edge for various depths

Magnetic field density on the coil center is more which can intensify the radial force (Patel et al., 2017). Hence, deformation becomes more at the center of the joining zone. TR_L and TR_R stand for thickness reduction on the left and the right side of a collar. Further, the trend for tube thickness

reduction was found identical for each set of samples. Minimum tube thickness reduction of 0.02 mm was achieved from S_{19} which has 0.5 mm groove depth, and a maximum of 0.5 mm was found from S_{23} and S_{24} which have a groove depth of 2.5 mm and 3 mm. Hence, minimum groove depth gives minimum tube thickness reduction and vice versa.

4.4.5. Hardness Analysis

The intention of carrying out a microhardness test in our investigation is to see how hardness is varied along the joining zone. Vickers microhardness test result at the interface of the joining zone is shown in Fig. 4.16. Test results revealed that the hardness was changed at the interface and found more compared to aluminum tube due to strain hardening effect. Further, magnetic field density and Lorentz force are more at the center which increases hardness at point C refereeing Fig. 4.16, but hardness decline to the point far from the center. These tests were carried out using sample S_{23} which has 2.5 mm groove depth. Since energy was kept constant, the distribution of hardness at the collar section for the remaining samples was expected equal with a small variation.

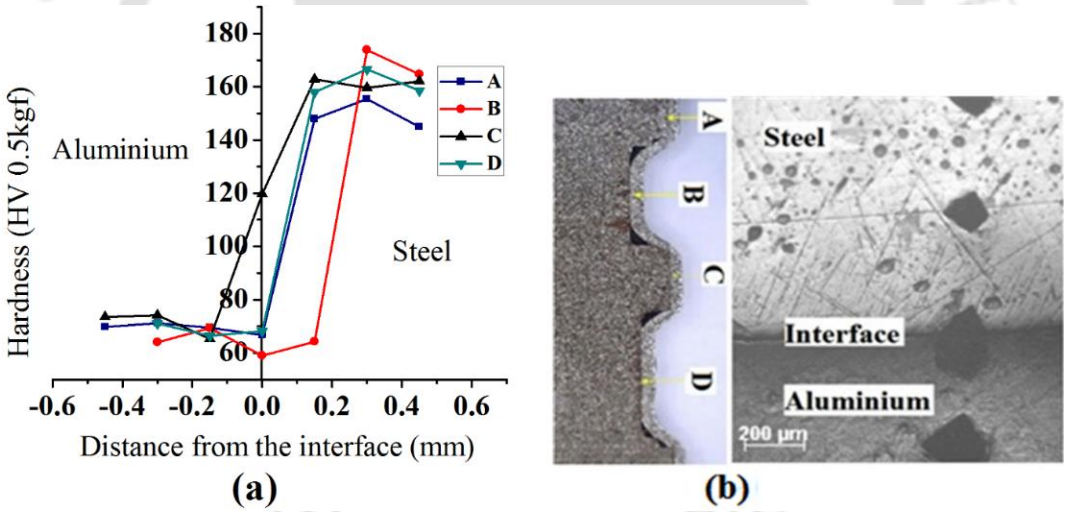

Fig. 4. 16 (a) Hardness distributions across the interface of the crimped sample and (b) indentation locations

4.5. Summary

In this chapter, EM crimping process for joining the aluminum tube on steel rod was investigated experimentally using a double rectangular groove. Studies on EM crimping are mainly focused on evaluating joint strength that can be obtained using different energy levels. However, the effect of

geometrical parameters like groove depth on groove filling, wrinkling and tube thickness reduction at the joining zone was not studied in detail. The pull-out test result was analyzed to evaluate the load transferring quality of joints manufactured. Based on results found, the effect of the width-to-depth ratio on joint strength was studied and proposed as a design guideline. The microhardness study at the joint interface is also carried out. From the result analyzed, it can be concluded that the joint strength obtained in this process mainly relies on a mechanical interlocking between a tube and the edge of a groove.

A joint manufactured in this investigation were dominated by a mechanical interlock at the groove edge. The predicted and actual maximum pull-out load found in a good agreement. A maximum of 95 % joint strength was found based on samples failed at joining zone compared to the strength of the aluminum tube. Most of the joints failed in the tube shows high strength due to mechanical interlock without cracking at the groove edge. However, the joints manufactured using groove depths more than 2 mm were failed at groove edge with lesser pull-out load due to severe plastic deformation and tube thinning effect. Hence, increasing groove depth shows two opposite effects on joint strength. Increasing groove depth beyond optimum leads to an increase in tube thickness reduction, groove filling, and wrinkling respectively which significantly affect joint strength. In EM crimping, data related to crimping for multiple material systems are not sufficiently available. The effect of the width-to-depth ratio on joint strength is proposed as a design guideline.

CHAPTER 5

MAGNETIC PULSE CRIMPING USING DOUBLE RECTANGULAR GROOVE FOR AXIAL JOINT: EXPERIMENT AND NUMERICAL SIMULATION

5 Electromagnetic Crimping Using Double Rectangular Groove for Axial Joint: Experiment and Numerical Simulation

5.1. Introduction

In this chapter, EM crimping process is used to join aluminum tube to a steel rod. The simulation was carried out using the EM module of LS-DYNA^{TM} to find suitable coil dimension and discharge energy. The radial displacement of a tube found from the experiment was compared with simulation for model validation. A failure mode was predicted using simulation and compared with an experiment. Pull-out strength for a crimped sample was performed to investigate the load transferring capability of the joint manufactured. The microscopic image was studied to make sure that joining is due to mechanical interlock rather than metallic bonding. Finally, a simulation is used to predict resultant displacement, effective plastic strain, Lorentz's force, magnetic field density, and resultant velocity respectively. A model is developed that is useful for manufacturing industries encompasses EM crimping as a joining method.

5.2. Material and Method

Copper coil and aluminum tube used in the current study have property shown in Tabe 5.1. Multiple simulations were carried out using a coil that has a different pitch to determine its optimum dimension which can give better deformation.

Table 5. 1 Property of coil and tube material

Parameters	Coil (Copper)	Tube (Al 1050)
Conductivity (S/m)	59.6×10^{6}	38.6×10^{6}
Density (Kg/m3)	8960	2700
Poisson's ratio	0.27	0.33

The workflow chart implemented in this procedure is illustrated in Fig. 5.1.

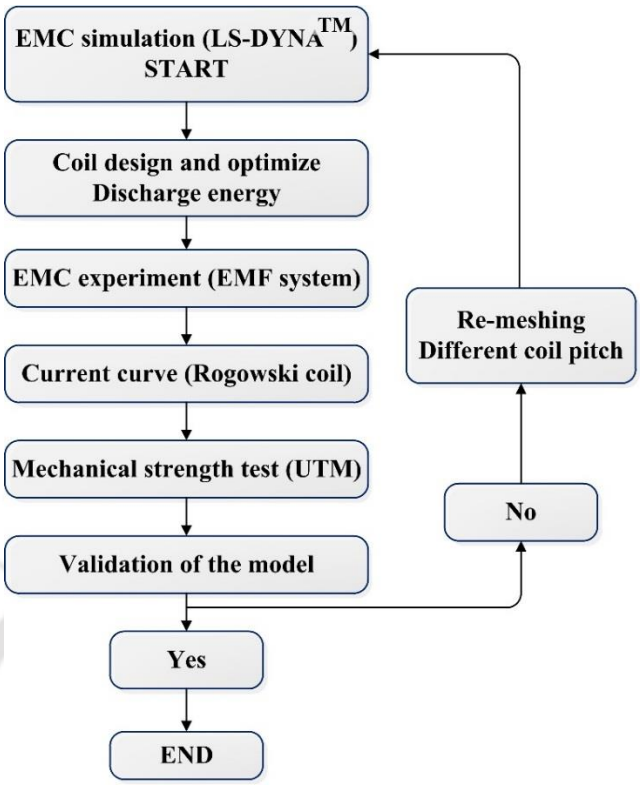

Fig. 5. 1 Workflow chart implemented in this procedure

5.3. Numerical Modeling

Since EM crimping is a high-speed joining process, a material model which takes care of high strain, strain rate hardening and softening due to temperature has to be chosen. The hardening is a particular type of isotropic hardening in which the yield stress σ_y is assumed to be of the form of Eq.3.1. Johnson-cook material constants for Al1050 and DP Steel is presented in Table 5.2.

Table 5. 2 Johnson-cook constants for Al1050 and DP steel (Melby and Eide, 2013, and Vedantam et al., 2006)

Materials	An (MPa)	B(MPa)	n	c	T_m(K)	m
Al 1050	110	150	0.36	0.014	918	1
DP Steel	430	823.6	0.5	0.08	1048	0.6

The coil was modeled as a rigid body to avoid any deformation and Johnson-cook was selected as a material model for the tube and the rod respectively. Johnson cook material model is generally used in an adiabatic transient dynamic analysis and best suited for the high-speed forming process. A quadrilateral 3D mesh was built for the coil, tube, and rod. The mesh is composed of 9061 nodes

for the coil, 6120 for the tube, and 14196 for the rod respectively. The numerical model developed is shown in Fig. 5.2. A detail dimension of a tube, rod, and the coil are shown in Fig. 5.3 (c).

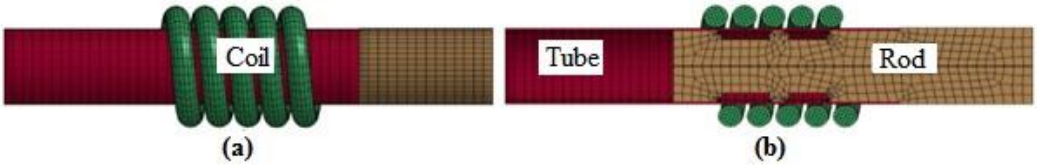

Fig. 5. 2 (a) Side view and (b) cross-sectional view of assembled parts

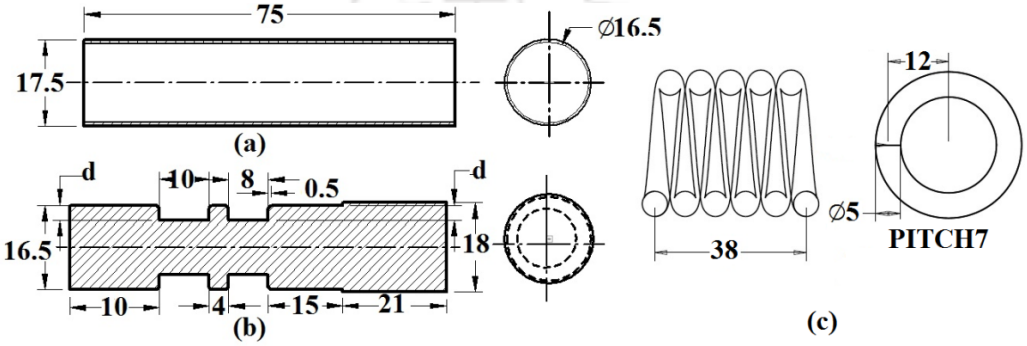

Fig. 5. 3 Detail dimension of (a) tube (b) rod and (c) coil (All dimensions are in mm)

5.4. Analysis and Discussion

The current was measured using a Rogowski coil while conducting an experiment and imported into LS-DYNA^{TM} software for simulation. A waveform of the current curve that is obtained at a discharge energy of 4.7 kJ is shown in Fig. 5.4 and used as a load for all groove parameters.

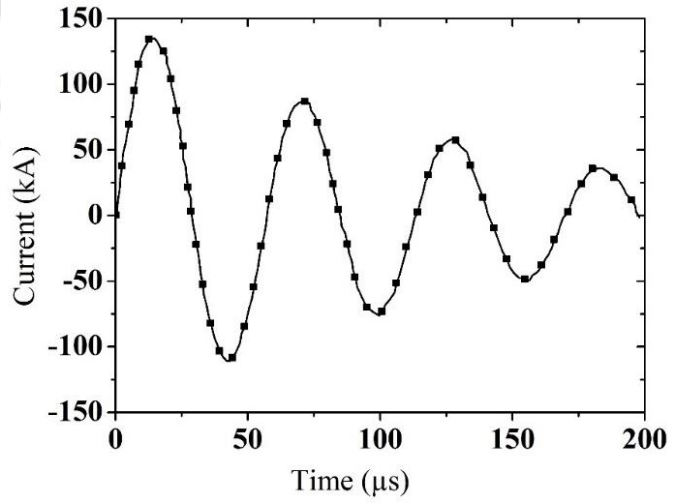

Fig. 5. 4 The waveform of the current curve obtained from the experiment

The maximum displacement is achieved after 45 µs for the sample that has 1 mm, 2 mm and 3 mm groove depth and only 10 µs was found enough for the sample which has 0.5 mm groove depth. A resultant displacement for different groove depth obtained from simulation is shown in Fig. 5.5. A mean absolute percentage error of 7% was found compared to the experiment that shows how the model can efficiently predict the parameter.

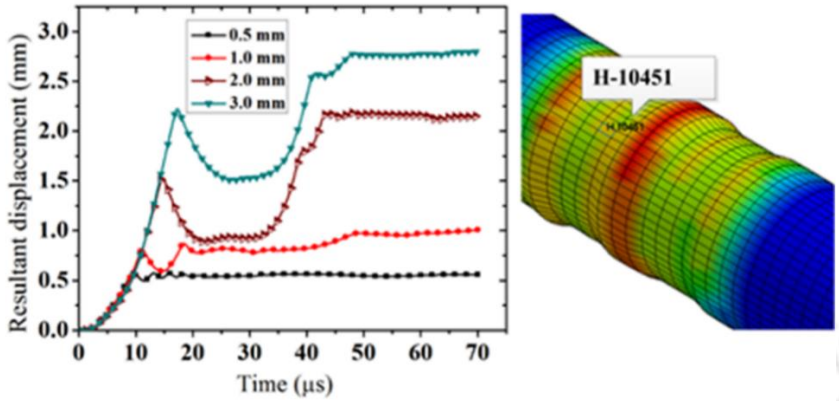

Fig. 5. 5 Resultant displacements for different groove depth

5.5. Experimental Work

The experimental setup used and a crimped sample that is joined using 4.7 kJ of discharge energy is demonstrated in Fig. 5.6. A Kapton tape was wrapped-on the copper wire before inserted into the insulation sleeve. A Teflon made fixture was used as reinforcement to support and avoid bulging of the coil due to repetitive crimping process. Moreover, acetone was applied to clean the workpiece surface from dirt and oil for better conductivity. A coil is designed and manufactured based on geometrical parameters found from the simulation that gives better crimping quality. A rectangular double groove was machined on the steel rod with different groove configuration. Four different groove depth, i.e., 0.5 mm, 1 mm, 2 mm and 3 mm were considered, and the groove width was kept constant.

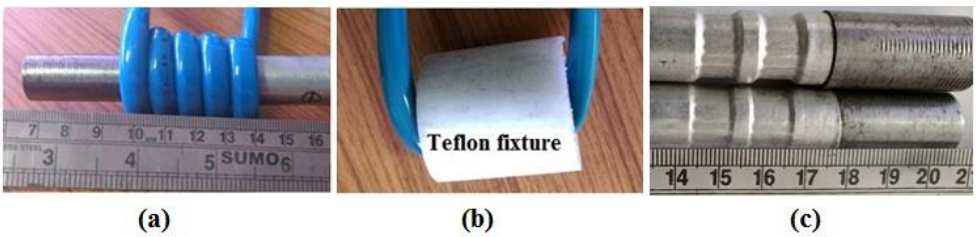

Fig. 5. 6 (a) Experimental setup (b) coil with Teflon fixture and (c) crimped sample

The experiment was carried out using electromagnetic forming system which has a specification described in Table 3.3. The deformation on a joining zone leads the tube to make mechanical interlock on the groove of the rod. The crimped sample that is obtained from simulation and experiment is depicted in Fig. 5.7 which shows how qualitatively agreed to each other for different groove depth.

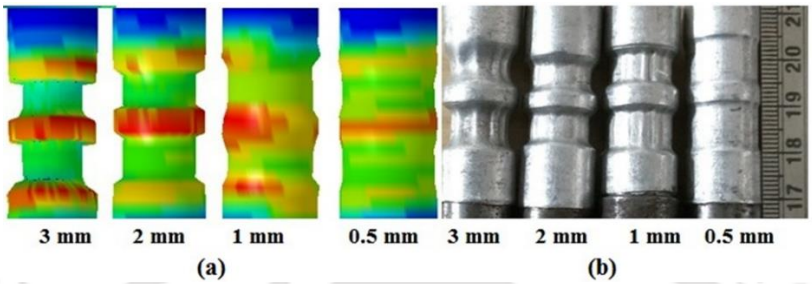

Fig. 5. 7 Crimping in (a) simulation and (b) experiment for the different groove depth

The radial displacement of a tube along the joining zone is investigated based on numerical simulation and experiment that was found in a good agreement. Points are taken from center to center of the grooves with 2 mm separation. Figure 5.8 shows a **r**adial displacement comparison for 0.5 mm groove depth. The radial displacement of a tube for a sample that has a groove depth of 0.5 mm and 2 mm is compared as shown in Fig. 5.8 and 5.9 and found in a good agreement with simulation. The absolute percentage error of 5.13% and less than 1% were found for considered groove depth. The trend of variation of radial displacement in both sides of the center shows similarity in experiment and simulation, and this is because of uniform pressure distribution along the joining zone.

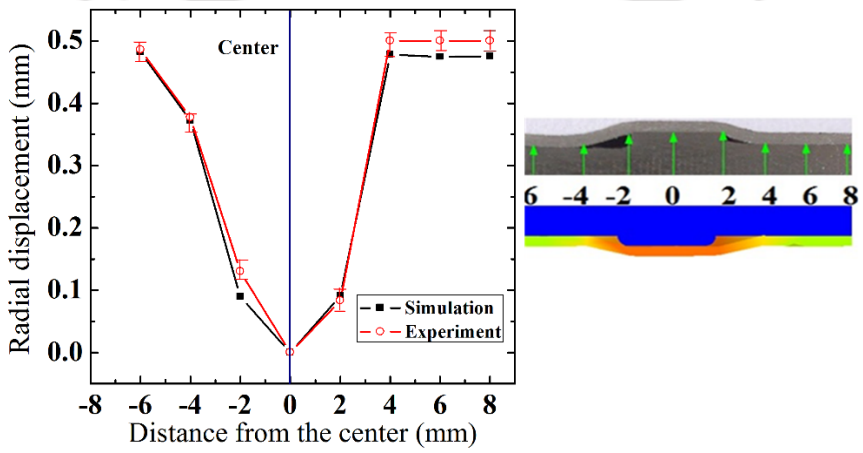

Fig. 5. 8 Radial displacement comparison using simulation and experiment for 0.5 mm groove depth.

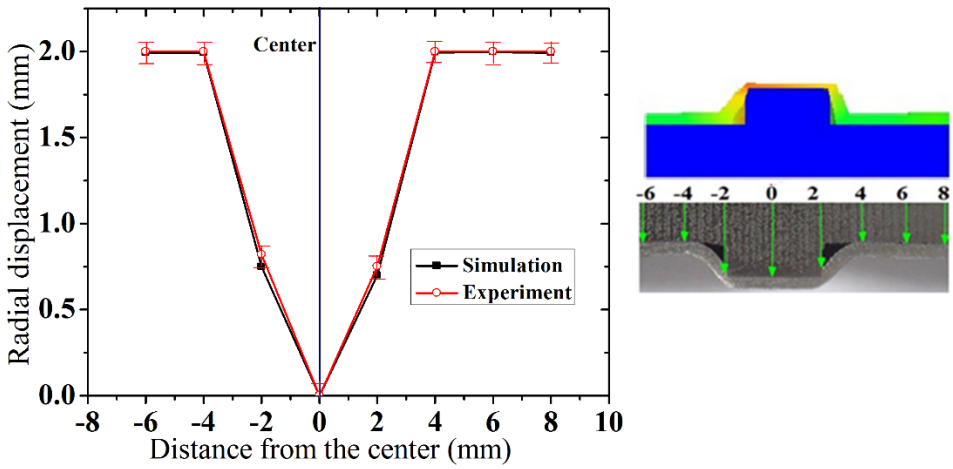

Fig. 5. 9 Radial displacement comparison using simulation and experiment for 2 mm groove depth

The effect of groove depth and groove edge radius on the deformation of a tube in EM crimping process was predicted using FEM simulation. The magnetic pressure is higher at the center which leads to having maximum Lorenz's force. Figure 5.10 shows contours of maximum shear strain at a different time in the joining zone which can successfully predict the location where failure is possible.

The groove edge radius was chosen 0.5 mm for all width and groove configuration that plays a significant role in affecting joint strength. It is observed that there is no chance for the tube to get sheared-off at the edge of the groove which has groove depth less than 2 mm. Failure of the tube has possibly occurred at the groove edge when groove depth is increased beyond 2 mm, and that weakens the joint strength.

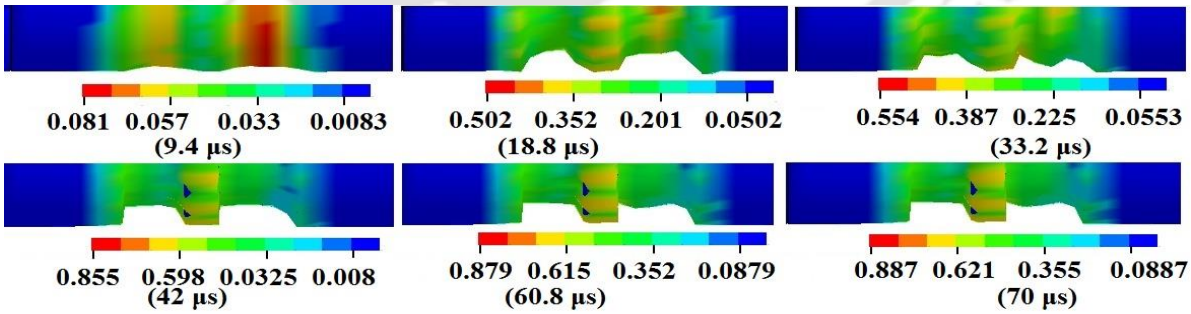

Fig. 5. 10 Contours of maximum shear strain at a different time value

Necking and shearing of the tube at the joining zone for a sample that has a groove depth of 3 mm are easily identified using physical inspection. Necking has occurred at a region where shear strain is maximum which significantly affects pull-out strength of the joint. Fig. 5.11 shows the location

where the failure occurred in simulation and experiment and found in a good agreement. Digital Microscope was used to capture the failure of the experimental sample.

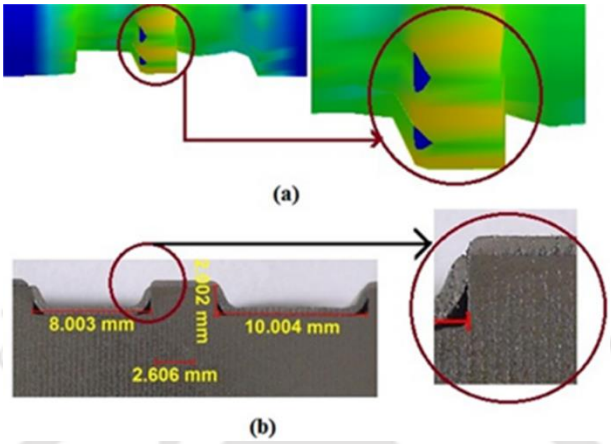

Fig. 5. 11 A contour of (a) magnetic pressure maximum at different time value and joining zone failure in (b) simulation and (c) experiment

Figure 5.12 shows the comparison of pull-out strength between the undeformed tube and crimped sample which has a different groove depth. As can be seen from Fig. 5.12 (a) the joint strength obtained using a sample with 0.5 mm, 1 mm and 2 mm groove depth has comparatively more than a tube strength due to strain hardening effect. The necking of a tube at the groove edge can be seen with the necked eye for sample that has 3 mm groove depth which leads to having minimum load transferring capacity.

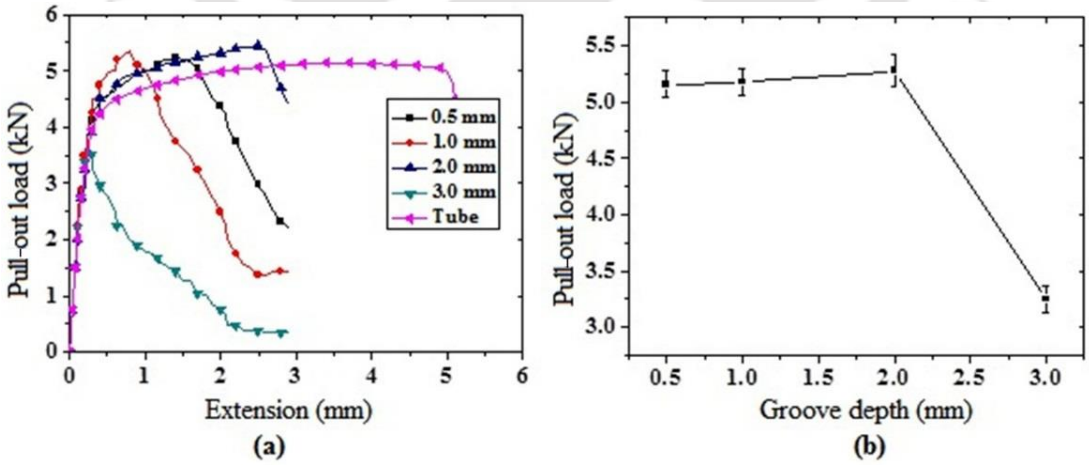

Fig. 5. 12 (a) pull-out strength of tube and crimped sample with different groove depth and (b) effect of groove depth on pull-out load

The maximum load transferred by the joint manufactured using 0.5 mm, 1 mm and 2 mm groove depth is by far more than a strength achieved by a sample that has 3 mm depth. Pull-out load keeps rising while groove depth is increasing up to 2 mm and drastically dropped due to failure at groove edge as shown in Fig. 5.12 (b). Maximum pull-out strength was found 5.45 kN for a sample that has 2 mm groove depth, and a minimum of 3.65 was found from a sample that has 3 mm groove depth. A load of 5.14 kN, 5.34 kN, and 5.23 kN were transferred by a tube and a sample that has a depth of 0.5 mm, and 1 mm respectively.

The integral of a plastic component of the rate of deformation is effective plastic strain that was predicted using simulation at a different groove depth. An element (H-10451) is selected to predict the effect of depth on the effective plastic strain and resultant velocity respectively. The Lorentz force is a function of magnetic field strength which is directly affected by its density. The acting pressure becomes higher and depends on the strength of the magnetic field at the joining zone. The maximum deformation occurs during the first 10 to 20 μs in which the velocity of the tube reaches highest due to the increasing density of the magnetic field.

The associated result for the sample that has 0.5 mm, 1 mm, 2 mm and 3 mm groove depth is shown in Table 5.3. Effective plastic strain and resultant velocity are rising while groove depth is increasing. The discharged energy which is applied to accelerate the flyer tube increases the velocity before touching a grooved surface. Measurement of velocity of the flyer tube in EM crimping is challenging, but it is possible to predict using simulation. A magnetic field is maximum at 15.6 μs which are 18.84 T comparing to 12.47 T, and 14.77 T found at 59.4 μs and 70 μs respectively.

Table 5. 3 Predicted parameters

Groove depth (mm)	Effective plastic strain	Resultant velocity (m/s)
0.5	0.19	129
1	0.62	162
2	1.17	235
3	1.22	259

5.6. Summary

In this chapter, electromagnetic crimping of tube and rod is investigated numerically and experimentally. Simulation is carried out to determine optimum discharge energy level before experimental investigation for the given material system and groove geometry. The model is validated by comparing numerically predicted radial displacement with the experiment. The developed model in this study is potentially useful to predict failure region and process parameters respectively.

The prediction of the failure zone using simulation is giving an insight on what will be the level of discharge energy and what should be the maximum depth so that the manufactured joint strength becomes best in its quality. Radial displacement measured numerically for different groove depth along the joining zone is compared with the experiment and found in a good agreement with a percentage error of 5.13%. The pull-out test result revealed that the joint strength manufactured was found better compared to the strength of the un-deformed tube. A joint strength obtained from the sample which has 3 mm groove depth was found 71% of tube strength. Parameters challenging to measure while experimenting like shear strain, resultant velocity, effective plastic strain, magnetic field, resultant velocity, and Lorentz force are easily predicted using 3D strongly coupled simulation.

CHAPTER 6

EFFECT OF FIELD-SHAPER AND GROOVE PROFILE ON TORSIONAL AND AXIAL JOINT STRENGTH

6 Effect of Field-shaper and Groove Profile on Torsional and Axial Joint Strength

6.1. Introduction

In this chapter, the effect of a single-stepped and tapered field-shaper on joint strength is investigated. Four rectangular grooves were machined on aluminum and steel rod to enhance the torsional and axial load-bearing capacity of the joint. For the same groove parameter and discharge energy, the effect of conductivity of a rod material and groove profile on joint strength was also studied. Geometrical parameters of the groove were kept constant, and discharge energy in the range of 1.9 kJ to 3.5 kJ and 1.2 kJ to 2.1 kJ was used for crimping an aluminum tube to aluminum and steel rod. A new testing approach to measure the mechanical strength of a manufactured joint was applied. Effect of discharge energy on torsional strength, pull-out strength, tube thickness reduction at groove edge, contact-length, and failure modes were analyzed and discussed in detail.

6.2. Experimental Methods

6.2.1. Materials and Profile

Standard materials were used for the samples. For tube Al 1050, Al 6061 and rod Steel 1020 was used. The chemical composition of the materials were also verified by performing EDX test, and the result is tabulated in Table 6.1.

Table 6. 1 Chemical composition of Al1050 and Al 6061 tube

The weight percentage of the element (%)							
Alloy	**Al**	**Fe**	**Mn**	**Ti**	**Zn**	**Si**	**Cu**
Al 1050	**Balance**	1.1	0.1	0.1	0.1	0.5-0.6	0.1-0.2
	Al	**Fe**	**Si**	**Cu**	**Cr**	**Mg**	
Al 6061	**Balance**	0.7	0.4	0.2	0.1	0.7	

Detail dimension and geometry of single-stepped field-shaper, tapered field-shaper and workpieces are demonstrated in Fig. 6.1. Schematic diagram and pictorial representation of field-shaper, tube and rod are shown in Fig. 6.1 and in Fig. 6.2 respectively. Figure 6.2 shows the joining zone with plain and knurled profile which has a medium and diamond pattern with a 1 mm

pitch between two adjacent grooves. Knurled profiles between adjacent grooves were made only on steel rod for the enhancement of joint strength.

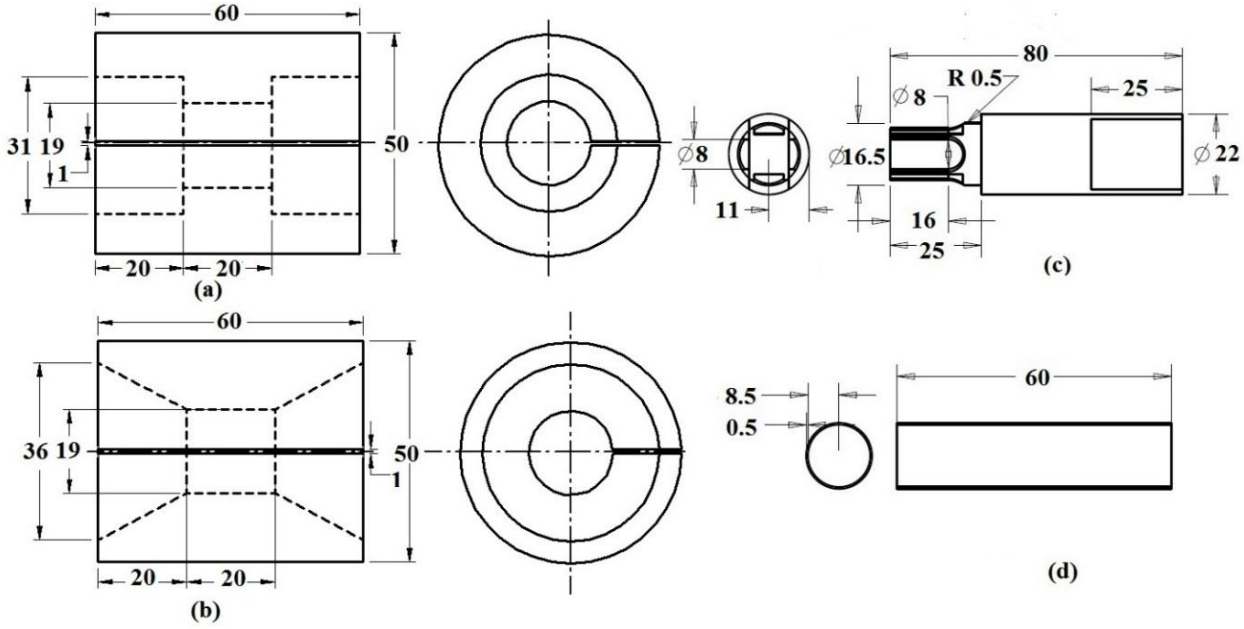

Fig. 6. 1 Geometry and dimensions of (a) single-stepped field-shaper (b) tapered field-shaper (c) rod and (d) tube (All dimensions are in mm)

Fig. 6. 2 Steel rod with (a) plain and (b) knurled profile

6.2.2. Experimental Procedure and Setup

The effect of field-shaper on deformation at the joining zone was investigated using four levels of discharge energy chosen based on the preliminary study. Initially, crimping was carried out to investigate the performance of single-stepped and tapered field-shaper using an aluminum-to-aluminum configuration. Based on its performance, crimping of aluminum tube to a steel rod that has different profile was carried out using a single-stepped field-shaper. The range of discharge energy was varied from 1.6 kJ to 2.7 kJ. The geometrical parameter of coils are shown in Table

6.2. The coil C_1 was used to carry out crimping without field-shaper, and the same discharge energy was applied to crimp using C_2 along with a single-stepped field-shaper.

Table 6. 2 Coils parameters

Coils	Wire diameter (mm)	Length (mm)	Pitch (mm)	Internal Dia. (mm)	Number of turns
C_1	5	40	7	17.5	5
C_2	5	60	7	50.5	8

Figure 6.3 shows an experimental procedure implemented in this study. The coil which has an equal number of turns were used to understand the effects of the field-shaper on joint strength clearly.

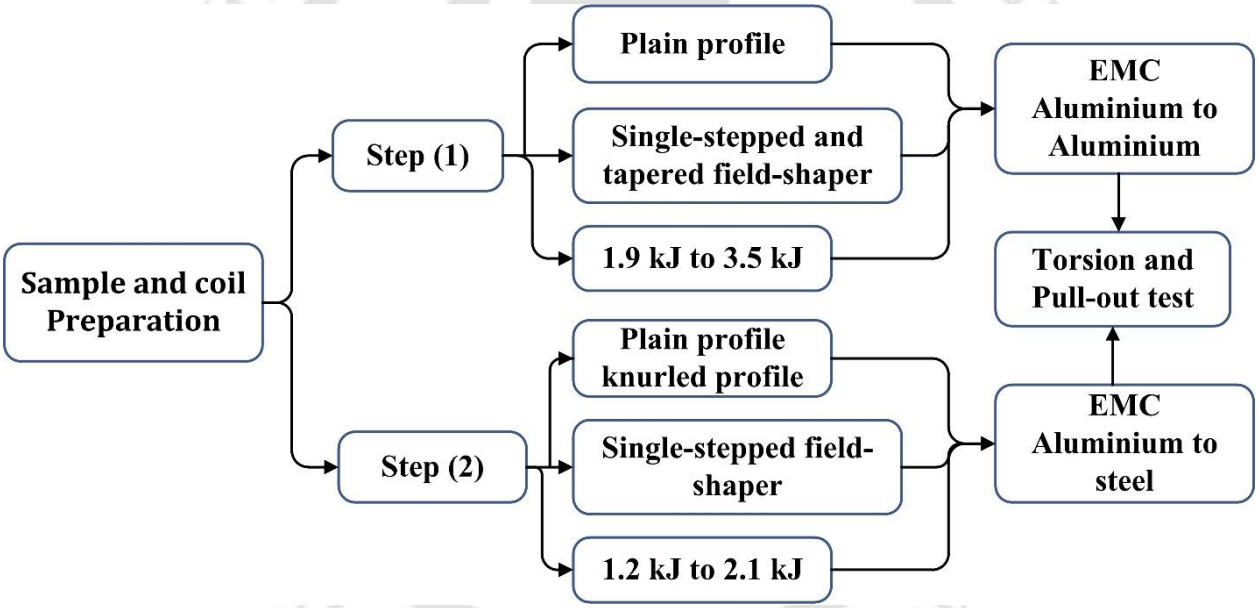

Fig. 6. 3 Experimental procedure implemented

The experimental setup which is demonstrated in Fig. 6.4 consists of two copper made field-shaper, i.e., tapered field-shaper and single-stepped field-shaper. Nylon rod was used to made fixtures for reinforcement of the coil and alignment of the workpiece joining zone with the interior section of the field-shaper. The distribution of the magnetic field in the solenoid coil is not uniform throughout its length. A tool called field-shaper is used for improving the uniformity of pressure distribution at the joining zone. The two field-shaper which are manufactured and used in this investigation are shown in Fig. 6.5.

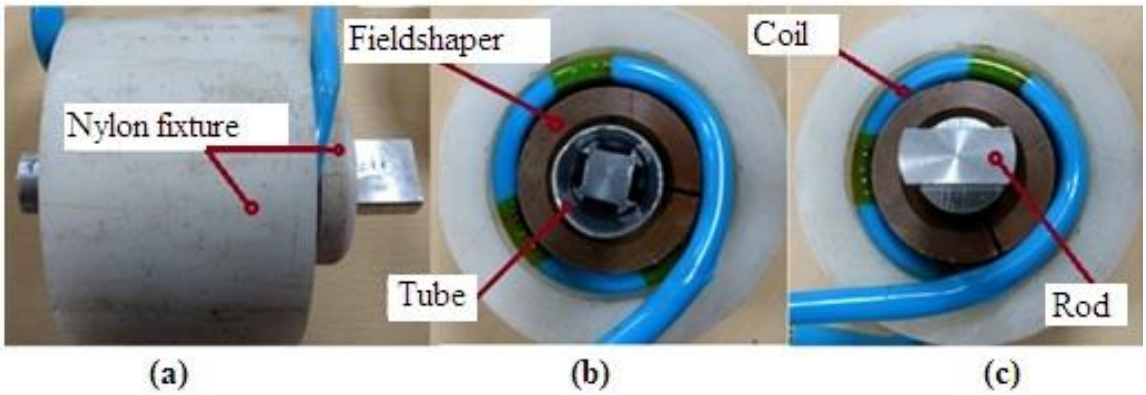

Fig. 6. 4 Experimental setup (a) a top (b) left side and (c) right side view

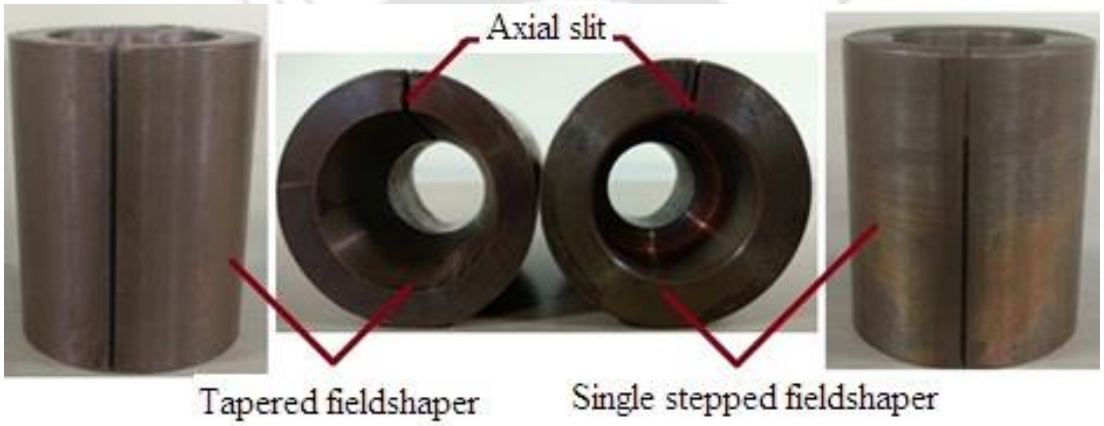

Fig. 6. 5 Tapered and single-stepped field-shaper

6.3. Mechanical Strength Testing Conditions and Setup

The two significant mechanical strength tests, i.e., torsion and pull-out tests were carried out to evaluate the quality of the manufactured joint. Figure 6.6 demonstrates the schematic representation of testing conditions used for torsion and pull-out test respectively.

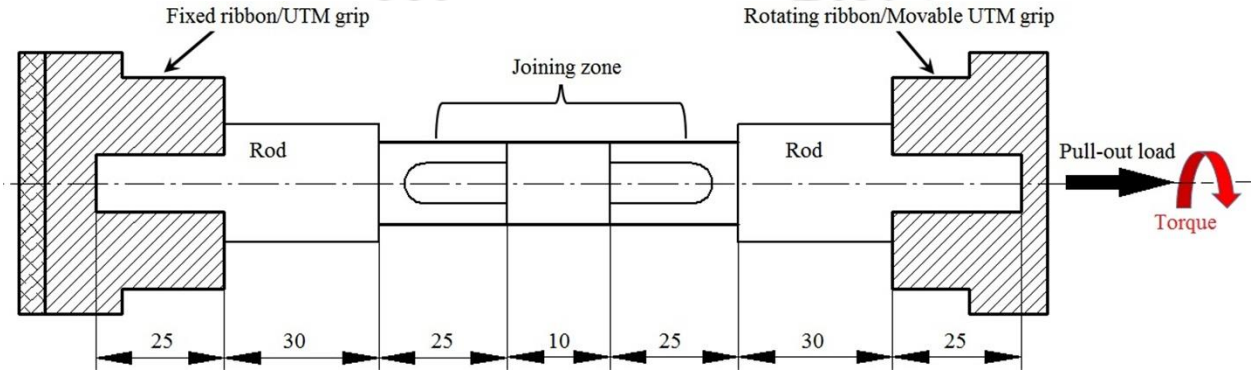

Fig. 6. 6 Testing condition for torsion and pull-out test (All dimensions are in mm)

A rotational and crossbar speed of 0.5 RPM and 0.1 mm/s were chosen for the torsion and pull-out test. A crimped sample for torsion and pull-out test was fixed in Digital Torsion Testing Machine and UTM as shown in Fig.6.7.

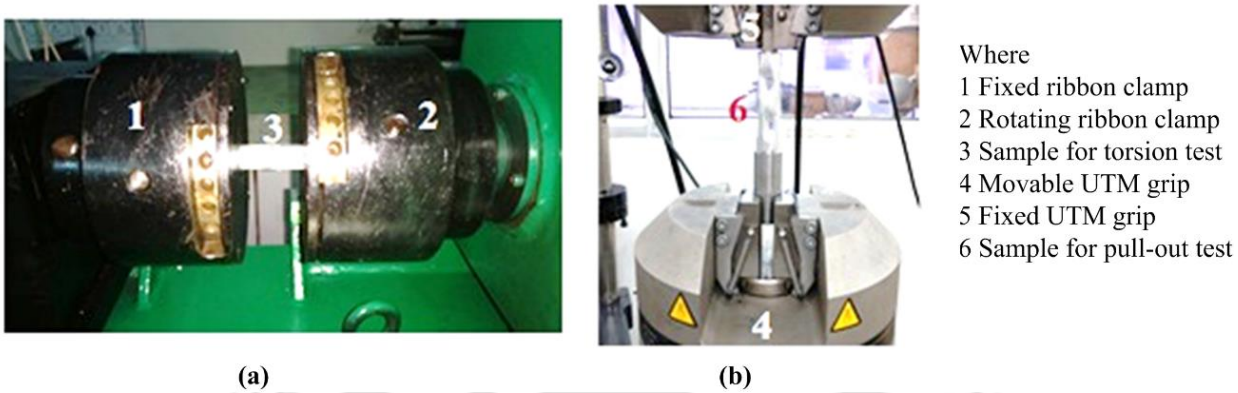

Fig. 6. 7 (a) Torsion and (b) pull-out test set up

6.4. Results and Discussion

6.4.1. Deformation with and without Field-shaper

The peak current measured using a Rogowski coil for the same discharge energy was found different for C_1 and C_2. The peak current found in C_1 is more than in C_2 with field-shaper for the same discharge energies due to size differences (see Table 6.2). Figure 6.8 shows how a peak current is varying in C_1 without field-shaper and in C_2 with single-stepped field-shaper for different discharge energy levels.

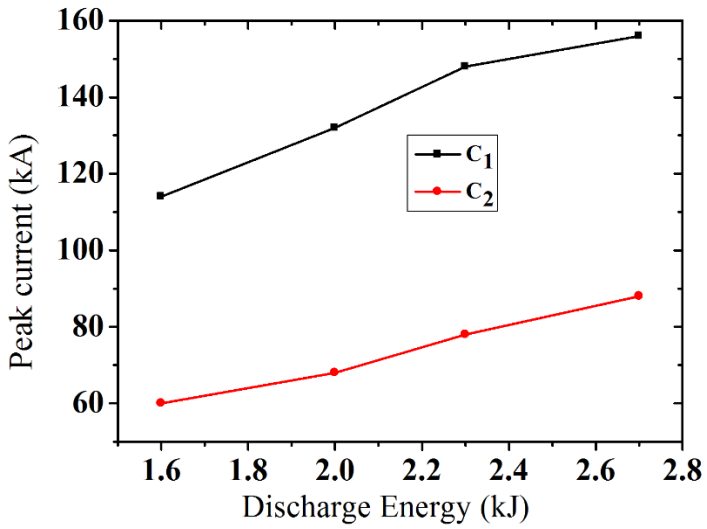

Fig. 6. 8 Peak current for C_1 without and C_2 with single-stepped field-shaper

In general, Fig 6.8 shows how the peak current in the coil is reduced due to a field-shaper at different discharge energy levels. Based on equation 2.10, it is clear that the current and the equivalent inductance are inversely proportional to each other. As the equivalent inductance is more in the system, the current is getting reduced keeping all other parameters constant. Using a field-shaper in the system causes the equivalent inductance to increase which leads to having lower peak current. In addition to that, the coil considered for the comparison has a different dimension as shown in Table (6.2) which affects the peak current significantly. The coil labeled as C_2 encloses a field-shaper. The density of a magnetic field for the smaller coil is more which causes the peak current to become higher. The deformation of the tube using C_1 without and C_2 with field-shaper is shown in Fig. 6.9. A tube is getting deformed none uniformly while crimping using C_1 without field-shaper. However, crimping using C_2 with field-shaper shows uniform deformation of a tube at the joining zone regardless of discharge energies. The coil end effect in the case of crimping without field-shaper is significant as shown in Fig. 6.9. Based on this effect and for high repeatability of the result, C_2 with field-shaper is used for the rest of the experiment.

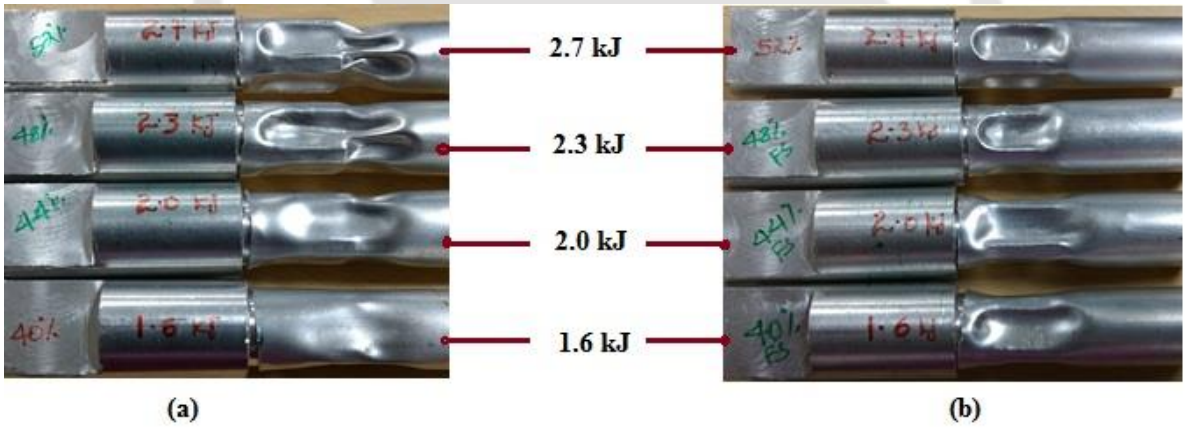

Fig. 6. 9 Deformation using (a) C_1 without field-shaper and (b) C_2 with field-shaper

6.4.2. Effect of Voltage on Current

Figure 6.10 shows a waveform of the discharged current which is measured using a Rogowski coil for voltage levels used in crimping aluminum-to-aluminum and aluminum-to-steel configurations. The electrical conductivity of aluminum and steel which are used as the rod materials causes a significant difference in the levels of discharge energy required for successful crimping. A minimum of 1.2 kJ and a maximum of 2.1 kJ was found as the effective range of discharge energy for joining of aluminum tube and steel rod successfully. The magnetic field generated due to the

current induced in the aluminum rod cause a repelling force against the tube and weaken the joint strength. Hence, 1.9 kJ to 3.5 kJ was found an effective range of discharge energy to crimp aluminum tube on the aluminum rod which is more compared to the level of discharge energy required for aluminium-to-steel configuration.

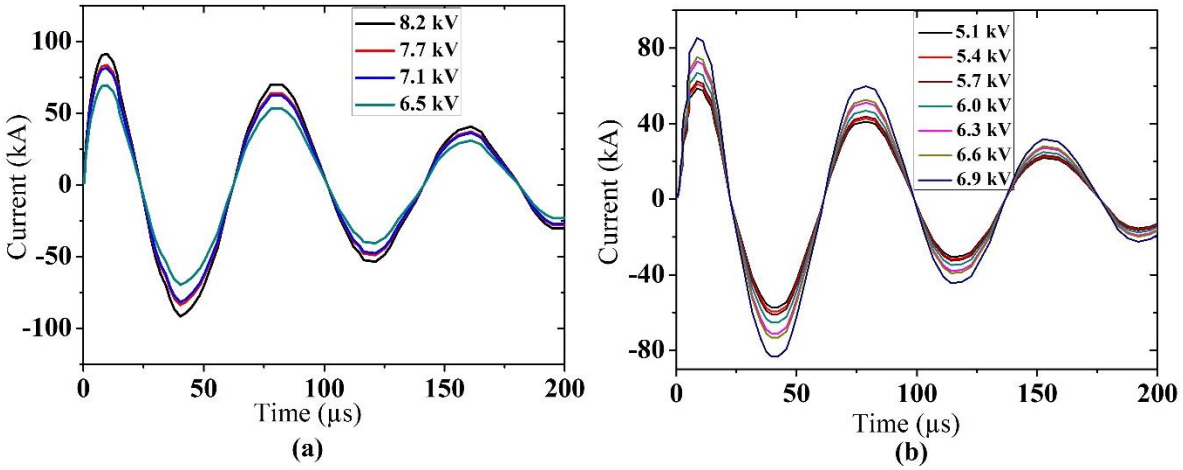

Fig. 6. 10 Typical waveform of the current for various voltages used in (a) aluminum-to-aluminum and (b) aluminum-to-steel configuration

In the case of Aluminium-to-aluminium configurations, the magnetic field which induces current on the rod creates force acting opposite to the main crimping force due to its conductivity. To compensate for the reduced magnetic pressure due to the diffused magnetic field, increasing discharge energy is required for creating better mechanical interlock. But, the magnetic field induces an insignificant current on the rod in a case of Aluminium-to-steel configuration which leads to having a negligible reacting force against the main crimping force. In addition to that, the strength and rigidity of steel rod are better than aluminum which assists easy interlocking.

6.4.3. Effect of Field-shaper on Torsional strength

6.4.3.1. For Aluminium-to-Aluminium Configurations

As reported by Rajak et al. (2018), the current density induced in a single stepped field-shaper was found more comparing to tapered one for the same discharge voltage. Figure 6.11 shows the effect of single-stepped and tapered field-shaper on torsional strength at different levels of discharge energies. As shown in Fig. 6.11 (a), the maximum and minimum torque that is obtained using single stepped field-shaper at 2.7 kJ and 3.5 kJ were found as 44.21 Nm and 11.79 Nm respectively.

Tube necking and thinning at the groove edge were observed without magnification for the joint manufactured using discharge energy more than 3.0 kJ which leads to having weaker strength in case of single-stepped field-shaper.

A significant deformation and joint strength were achieved using discharge energy starting from 1.9 kJ in case of a single-stepped field-shaper. However, a minimum of 2.3 kJ of discharge energy was required to have significant deformation in the case of tapered field-shaper. The torque resistance keeps on increasing while discharge energy is increasing up to 3.0 kJ and start declining as shown in Fig. 6.11 (b). This result reveals how single-stepped field-shaper is efficient than tapered field-shaper in concentrating magnetic fields at the point of interest.

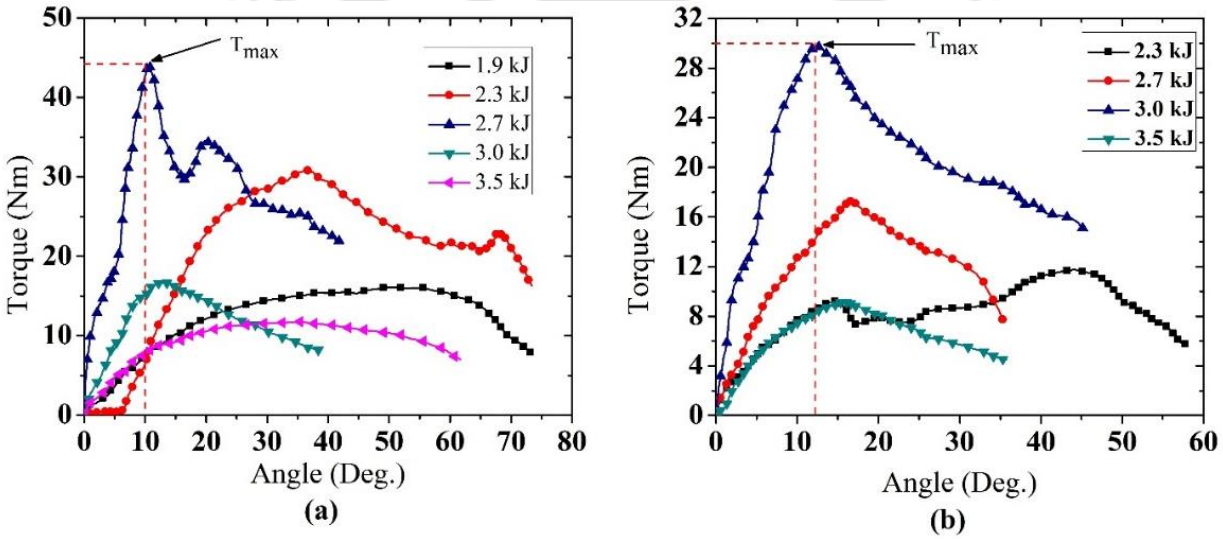

Fig. 6. 11 Effect of discharge energy on torque using (a) single-stepped and (b) tapered field-shaper

Figure 6.12 shows maximum torque found at different energies using single-stepped and tapered field-shaper. All measurement was taken at the breaking point of the joint during torsion test. The torque resistance of the joint made using a single-stepped field-shaper was found better than the tapered field-shaper. The trends of variation of torque using four levels of energies were found similar regardless of their shape and length. The torque resistance becomes weaker for samples crimped using discharge energy more than 2.7 kJ and 3 kJ in case of single-stepped and tapered field-shaper. Hence, the efficiency in concentrating energies at the joining zone was found better in the case of single-stepped field-shaper than in tapered field-shaper.

From the previous analysis, it is clear how a single stepped field-shaper is better than tapered one for any configuration. Hence, a single stepped field-shaper was used to crimp Al 6061 and steel rod with a discharge energy of 2.5 kJ, 5.0 kJ, 5.6 kJ, and 6.5 kJ respectively.

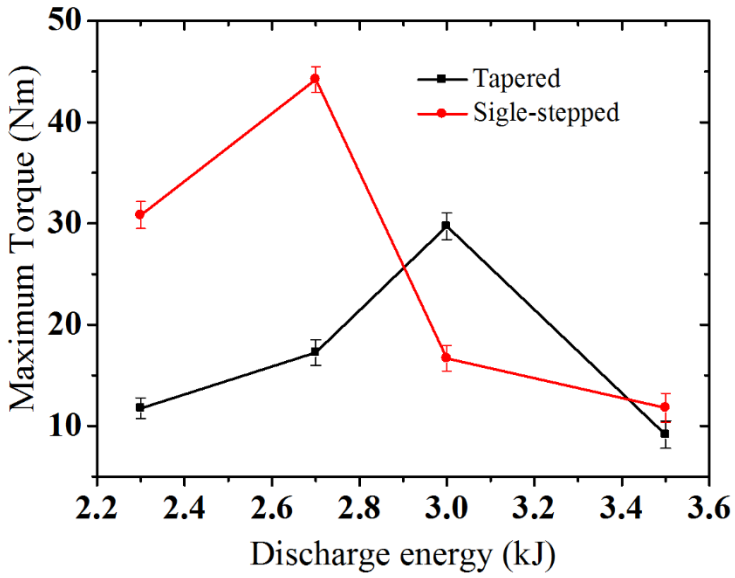

Fig. 6. 12 Effect of field-shaper geometry on torque resistance (Aluminium-to-aluminium)

The torsional strength found at different discharge energy is shown in Fig. 6.13. The maximum torque of 16.68 Nm was achieved by a joint manufactured using 2.5 kJ as shown in Fig. 6.13 (a). Torque is increased from zero to maximum as shown in the region one. A tube at the joining zone was reinforced by the rod and start separation in region two by twisting in the range of 60^0 -100^0 angle. The interference joint is mainly dominated in this case due to less discharge energy. The tube was completely separated from the rod in region three with a maximum angle of 101^0. For discharge energy of 5.0 kJ, the maximum torque of 54.3 Nm was found at 22^0 angles as shown in Fig. 6.13 (b). The tube was getting buckling at the center which leads to the tube to fail without cracking in the region one and two. The tube starts cracking at the region of buckling in region three.

A similar phenomenon was investigated for a joint manufactured using 5.6 kJ of discharge energy which gives a maximum torque resistance of 54.5 Nm at 71^0 as shown in Fig. 6.13 (c). Figure 6.13 (d) shows the weakest joint strength which is manufactured at discharge energy of 6.5 kJ which shows a torsional strength of 6.45 Nm achieved at 53^0. The crack at the groove edge due to severe deformation was seen without magnification even before conducting a torsional test. The tube

starts cracks at the groove edge as soon as a torsional load is applied and reinforced by the rod at the same time as shown in region two. Then the joint completely failed and the tube getting separated from the rod entirely. Based on the results found, discharge energy in the range of 5.0 kJ to 5.6 kJ can be the best level to give better joint quality in terms of torsional load resistance.

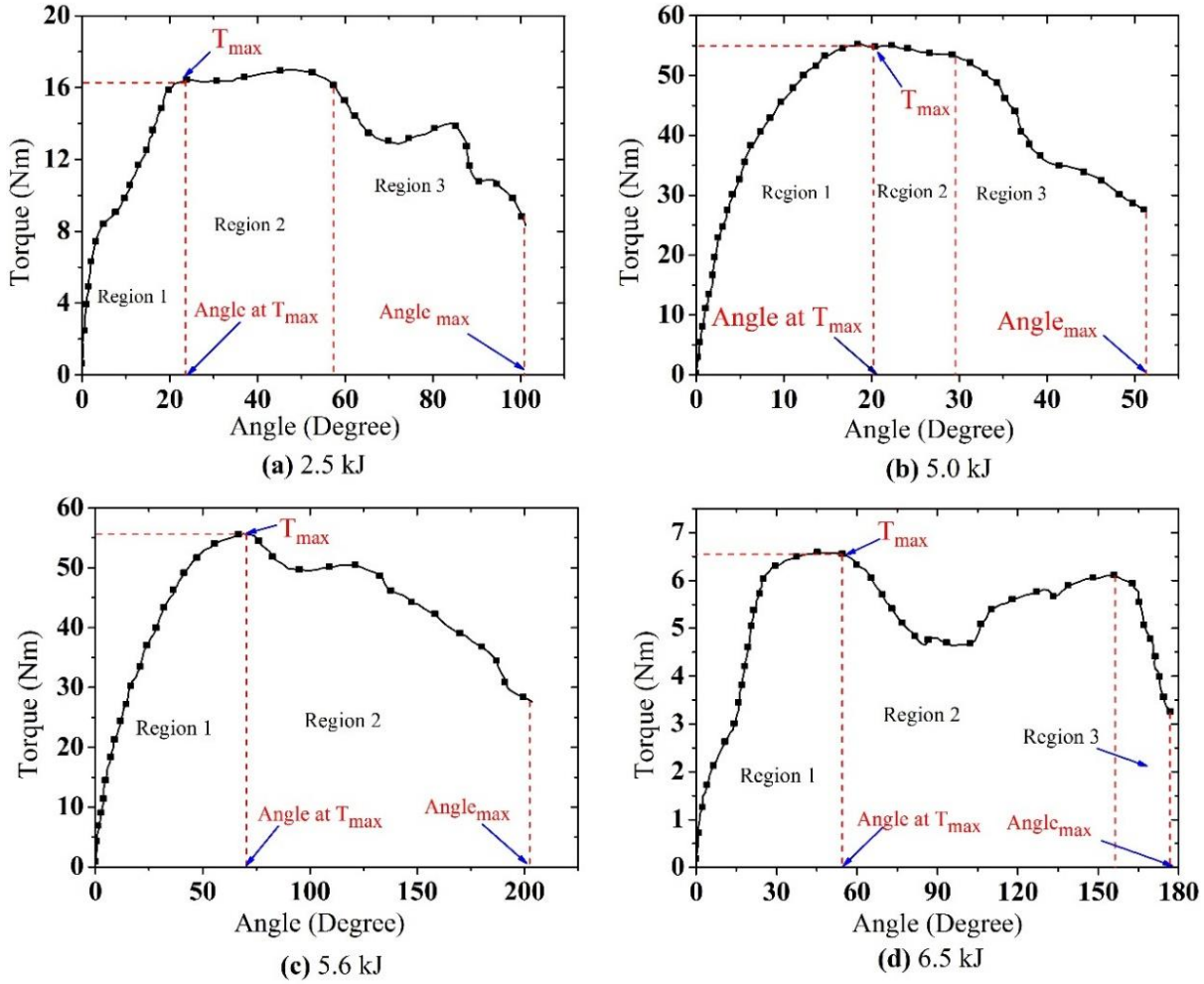

Fig. 6. 13 Effect of discharge energy on torsional strength

6.4.3.2. For Aluminium-to-Steel Configuration

A single stepped field-shaper was found efficient than tapered field-shaper in crimping even using lower discharge energy. Based on this fact, the experiment to investigate the effect of groove profile on joint strength was carried out using a single stepped field-shaper. A crimped sample with a plain and knurled profile is shown in Fig. 6.14.

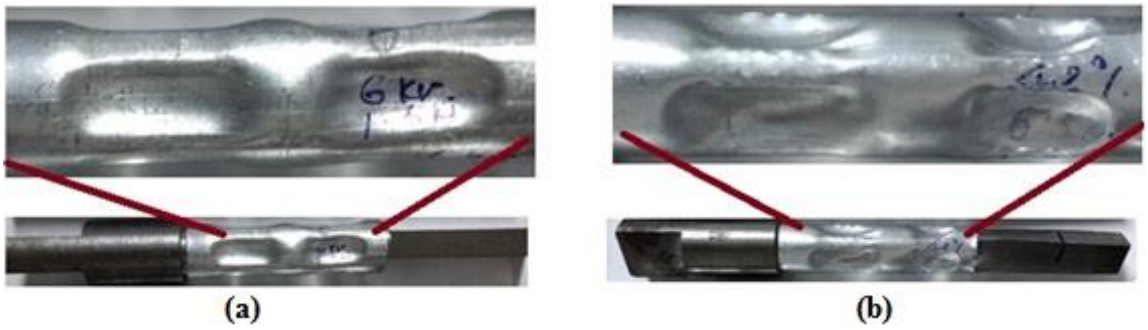

Fig. 6. 14 Crimped sample with (b) plain and (c) knurled profile

Figure 6.15 shows the effect of knurled and plain profiles on maximum joint strength which was found using seven levels of discharge energies. In both cases, joint strength keeps on increasing up to 1.8 kJ and starts declining due to severe deformation at groove edge. The maximum torque of 41.89 Nm and 43.32 Nm was found from the sample with a plain and knurled profile. A sample with the knurled profile at the joining zone shows better torsional strength due to its roughness. Hence, the maximum achievable torque resistance in case of a knurled profile was found better than plain profile, but joint strength is mainly dominated by the interlocking of the tube at the groove.

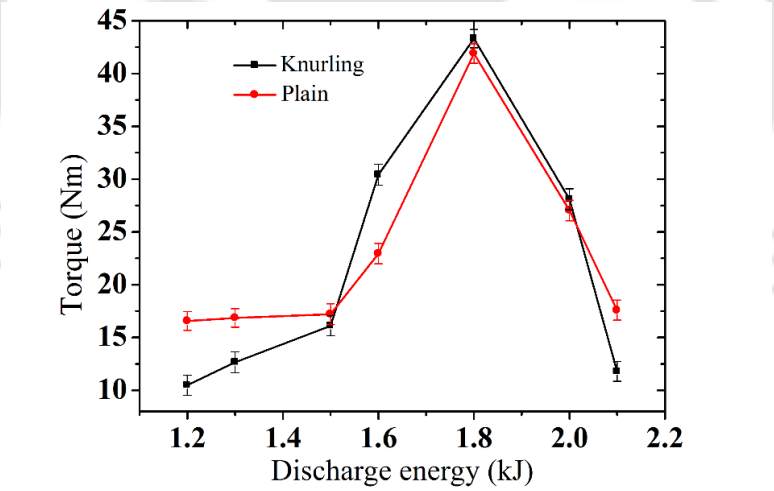

Fig. 6. 15 Effect of knurled and plain profile on torque resistance (Aluminium-to-steel)

6.4.4. Effect of Field-shaper and profile on Pull-out Strength

6.4.4.1. For Aluminium-to-aluminium Configuration

Figure 6.16 shows the effect of energy and field-shaper geometry on pull-out strength. The pull-out strength achieved using a single-stepped field-shaper and tapered field-shaper at discharge

energy of 2.3 kJ, 2.7 kJ, 3.1 and 3.3 kJ were plotted. Measurements are taken at a breaking point of the joint from load versus extension plot. Maximum pull-out strength is achieved using 3.1 kJ of discharge energy in case of single-stepped field-shaper and start decline while applying 3.3 kJ due to severe deformation at groove edge. The pull-out strength was found increasing even discharge energy increased beyond 2.7 kJ in case of both field-shapers. The groove edge was acting like cutting edge during discharging 3.3 kJ that leads to having weaker joint strength. From this result, it can be concluded that a single step field-shaper is better than tapered for the same discharge energy and groove geometry.

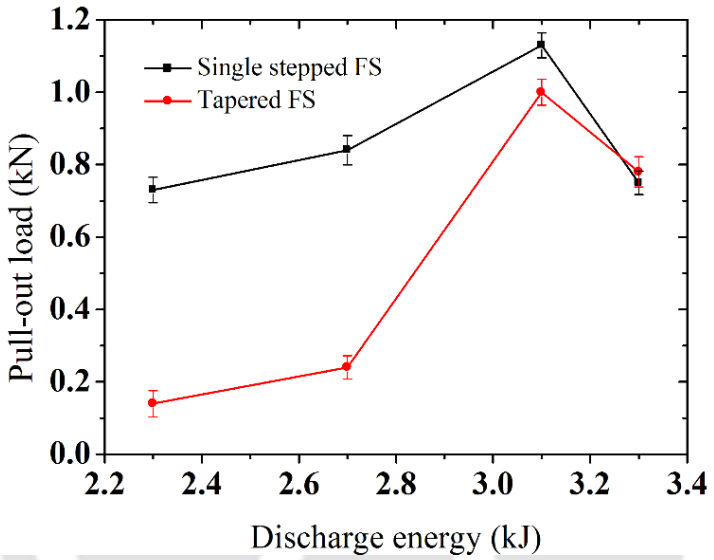

Fig. 6. 16 Effect of field-shaper geometry on pull-out strength

6.4.4.2. For Aluminium-to-steel Configuration

Effects of knurled and plain profile on pull-out strength were investigated and found weaker in case of plain as shown in Fig. 6.17. The formation of micro forming due to the knurled profile on the steel rod improves the joint strength. The knurled profile enhances the pull-out strength compared to plain profile using the same discharge energy. Therefore, a knurled surface profile is proposed for better joint strength in transferring axial load over the plain profile. The electrical conductivity of the aluminum rod can significantly reduce the acting pressure due to the magnetic cushion effect. Hence, it is recommended to increase discharge energy for better joint strength.

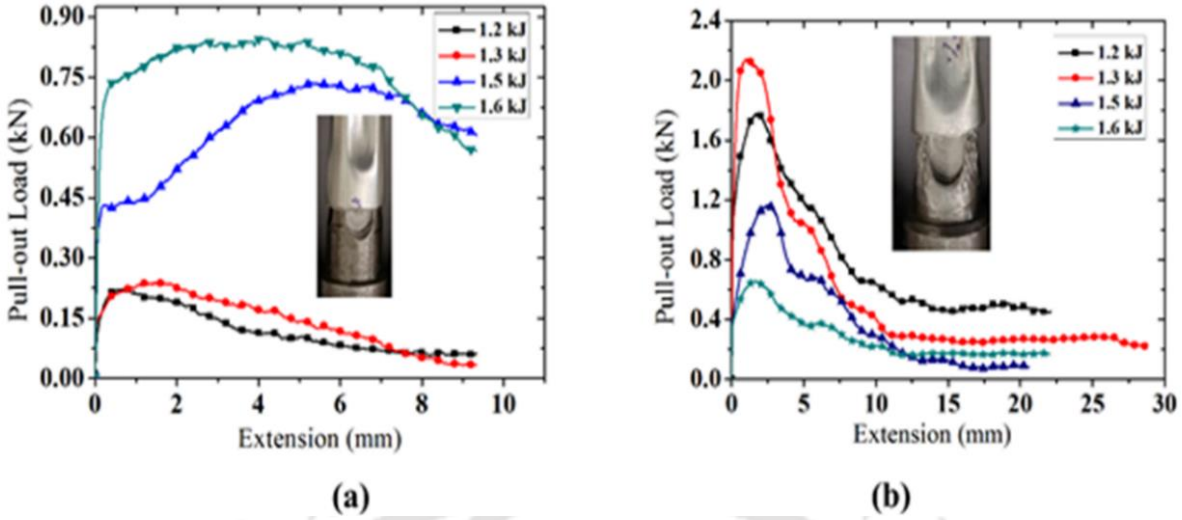

Fig. 6. 17 Pull-out strength for (a) plain and (b) knurled profiles

6.4.5. Tube Thickness Reduction and Contact Length

Figure 6.18 shows how tube thickness reduction and contact length are affected by discharge energy for aluminum-to-aluminum configuration using a single-stepped field-shaper.

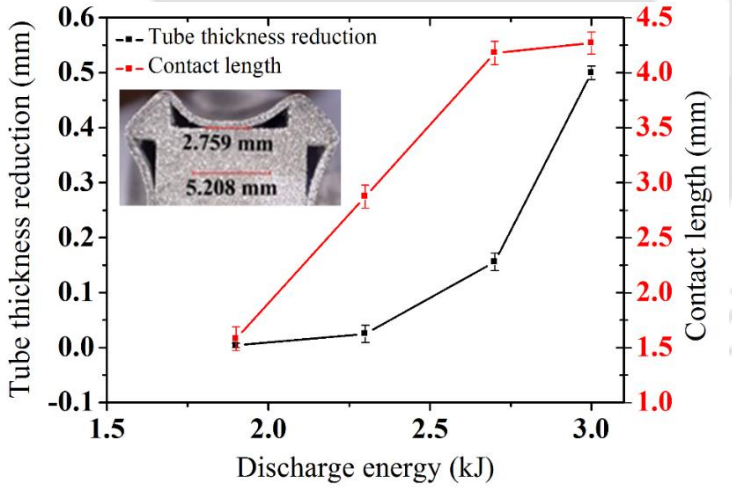

Fig. 6. 18 Tube thickness reduction and contact length

The joint strength obtained using 2.7 kJ of energy was found better due to a strong mechanical interlocking without tube necking at the groove edge. Discharge energies more than 3.0 kJ cause tube thinning which leads to breaking of joints with a lower load. Hence, joint strength either to resists torsional or axial load becomes weaker as tube thickness reduction becomes maximum due to severe deformation.

6.4.6. Effects of Energies on Deformations

Figure 6.19 shows the effect of increasing discharge energies on the uniformity of tube deformation into the groove. Wire-electro discharge machines and digital microscopic cameras were used to cut the crimped sample and investigate deformation. The contact length between tube and groove surface becomes uniform as energies rising from 2.3 kJ to 3.0 kJ respectively. The density of the magnetic field at a joining zone becomes higher as discharge energies increases which leads to having uniform deformation. Mechanical interlocking between tube and rod significantly affects the joint strength. Hence, better joint strength obtained using discharge energy which provides strong interlocking without tube thinning or necking at groove edge like what we found at 2.7 kJ in the current study.

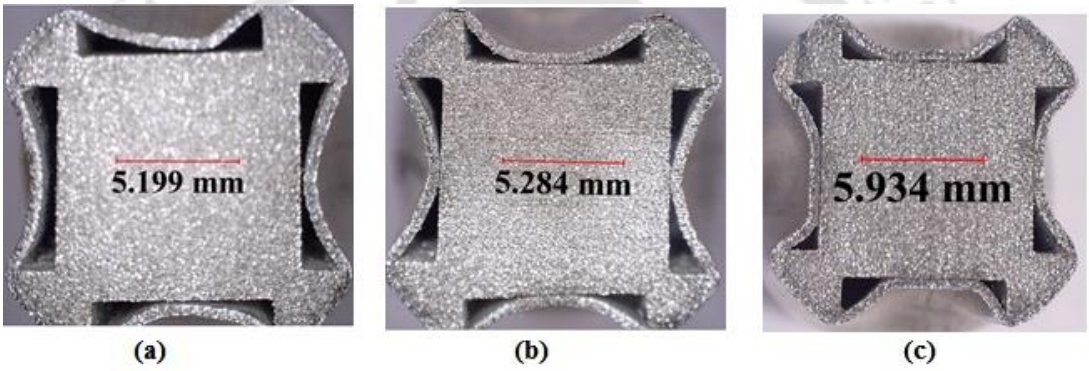

Fig. 6. 19 Deformation at (a) 2.3 kJ (b) 2.7 kJ and (c) 3.0 kJ

6.4.7. Failure Mode in a Torsion and Pull-out Test

Figure 6.20 shows aluminum-to-aluminum crimped samples before and after the torsion and pull-out test. In general, three modes of failure were observed during the torsion test. The rod was kept on rotating relative to a tube while the torsional load was applied for a sample manufactured using 1.9 kJ which shows weaker joint strength. The tube shows buckling at the center of the tube base material for samples that are manufactured using 2.3 kJ and 2.7 kJ with the higher torsional load resistance. For sample crimped using 3.0 kJ, the tube was sheared off at the joining zone with the lesser torsional load. Hence, failure at groove edge with weaker joint strength was found as discharge energy increases beyond 2.7 kJ in this configuration. Finally, the rod was sliding and come out while the pull-out load is applied to all samples regardless of joint strength.

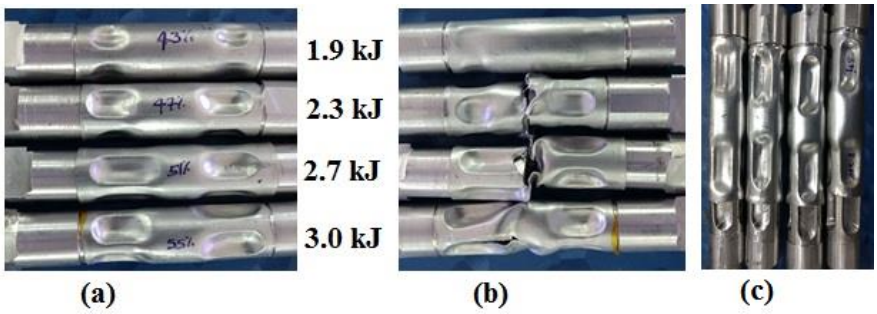

Fig. 6. 20 Samples (a) before the test (b) after torsion test and (c) after pull-out test

Three modes of failure were observed during torsion test in the joint manufactured using different rod profile and energy levels. Figure 6.21 demonstrates failed samples after the torsion test for aluminium-to-steel configuration using plain profile. The rod was kept on rotating relative to the tube for a sample that was crimped using 1.0 kJ and 1.2 kJ due to less deformation. The joint strength found at discharge energy of 1.6 kJ and 1.8 kJ was more and considered as best discharge energy levels. Hence, the tube base material is buckling at the center for samples crimped using 1.3 kJ, 1.5 kJ, 1.6 kJ, and 1.8 kJ of discharge energies. Further, a joint manufactured using 2.0 and 2.1 kJ for both types of the profile shows shearing off the tube at a joining zone with the weakest torsional strength. Figure 6.21 (c) shows the failure of the joint which is manufactured using a knurled profile. The rod is sliding and coming out while pull-out load is applied to all sample regardless of surface profile and discharge energies.

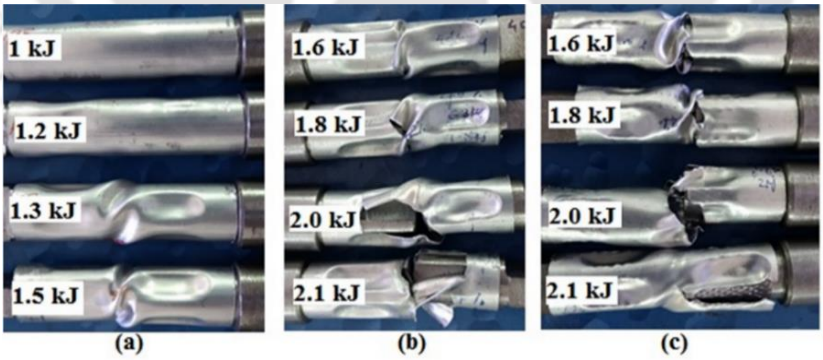

Fig. 6. 21 Joint failure (a, b) using plain groove surface and (c) knurled groove surface

6.5. Summary

The aluminum tube is successfully crimped over an aluminum and steel rod which has four longitudinal and symmetrical grooves. A study on joint manufactured using field-shaper and different profiles in EM crimping to support torsional load were found limited which is addressed

in this chapter. This chapter investigates the effects of a field-shaper, conductivity of rod materials and groove profile on joint strength manufactured using different levels of energies. Tube thickness reduction, contact length and failure mode of the joints manufactured were also investigated. This study has great importance for an industrial application that encompasses the joining of a tube and the rod using EM crimping. The following conclusion has been made based on the result found from different tests.

- The deformation of the tube was found uniform at the joining zone while using field-shaper regardless of a groove profile. Based on joint quality obtained for the same effective joining zone and discharge energies, a single-stepped field-shaper was found better than tapered field-shaper.
- The torque resistance achieved between aluminum tubes and a steel rod was found higher even for lower discharge energies as compared to aluminum to the aluminum joint. Torsion and pull-out test result reveals the knurled profile enhances the joint strength compared to plain profile. The contact length should be higher for better joint strength without significant tube thickness reduction.
- Three modes of failure were observed during the torsion test, i.e., rod rotating, tube buckling of the tube at the center and tube sheared off at the joining zone respectively. At its best discharge energy level and groove profile, failure occurred on the base tube. Besides that, the rod is sliding and keeps coming out during the pull-out test with different load-bearing capacity regardless of material configuration and groove profile. Hence, the circumferential groove is generally advisable in supporting the axial load.

CHAPTER 7

ANALYSIS OF EFFECT OF GROOVE PARAMETERS ON AXIAL AND TORSIONAL JOINT STRENGTH

7 Analysis of Effect of Groove Parameters on Axial and Torsional Joint Strength

7.1. Introduction

In this chapter, EM crimping is used to join aluminum tube and a steel profiled rod mechanically to support torsional and axial load simultaneously. The effects of three geometrical parameters of a rectangular groove, i.e., length, width, and depth on joint quality were investigated using experiment and central composite design (CCD) method. Discharge energy of 1.8 kJ and the groove edge angle of 0.5 mm was kept constant for all samples. A new technique in mechanical strength testing is introduced for the crimped sample which can resolve challenges faced so far in this regard. The torsional and pull-out strength predicted using response surface methodology (RSM) was compared with the actual strength obtained from the test. The optimum groove parameters found using RSM and predicted values are also compared with measured parameters. A failure mode observed during each type of strength test was investigated. The developed method has great importance to identify parameters that significantly affect joint strength in the manufacturing of airframe structure using EM crimping. Finally, a guideline is proposed to design a rectangular groove to transfer maximum torsional and axial load respectively.

7.2. Experimental Methodology

7.2.1. Experimental Procedure

The experimental procedure implemented is depicted in Fig. 7.1. Initially, the manufacturing of four symmetrical axial grooves was completed based on cause and effect matrix generated by CCD before EM crimping experiment was carried out. The CCD model describes the behavior of the maximum torque and pull-out load. The ANOVA provides statistical tools to evaluate statistical hypotheses. Discharge energy of 1.8 kJ or 6.3 kV was used to carry out the investigation which is determined from the preliminary study. The results achieved from mechanical strength tests like torsion and pull-out load were used as a response for further analysis. The effect of each groove parameters on joint strength was investigated in detail. Finally, optimum groove parameters were determined and evaluated using RSM and analysis of variance (ANOVA).

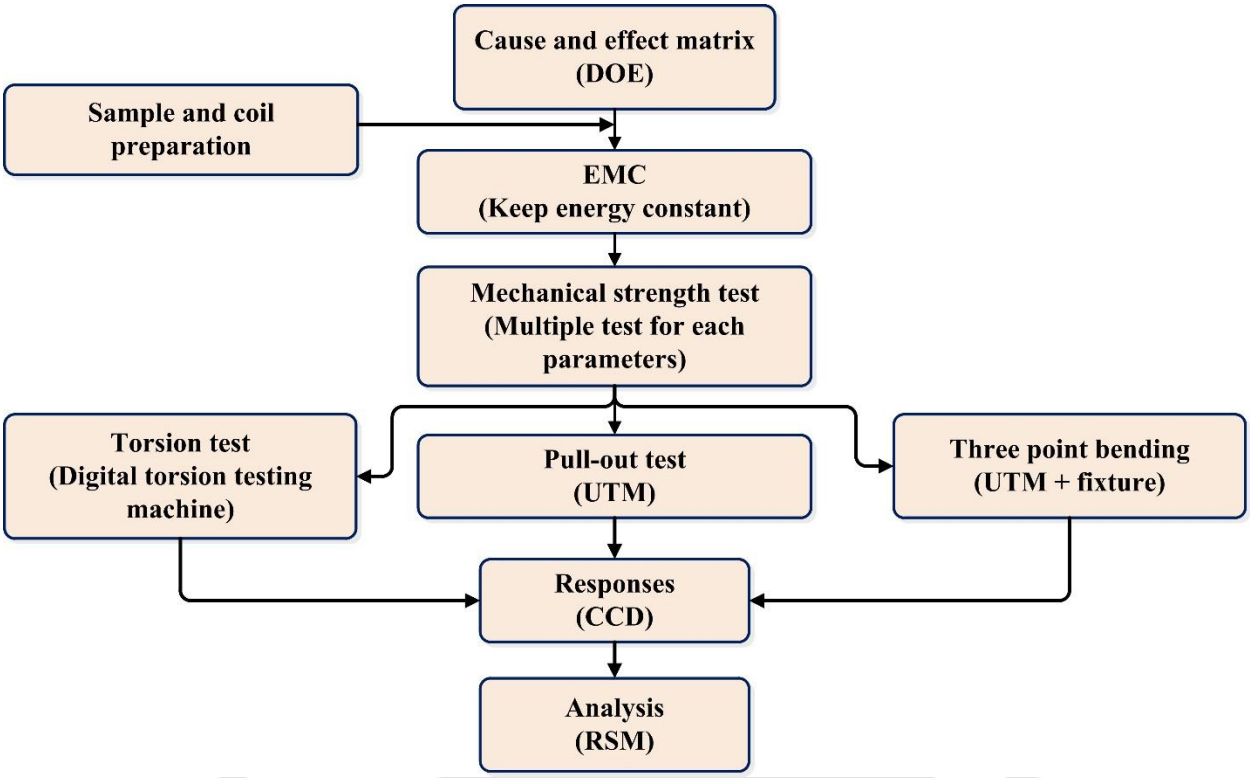

Fig. 7. 1 Implemented procedure for an experiment and analysis

7.2.2. Material and Experimental Setup

Standard materials were used for the samples. For tube Al 1050 and rod 1020 steel was used. The chemical composition of materials was also verified by performing the EDX test, and the result is tabulated in Table 4.1. A solenoid copper coil which has 5 mm wire diameter, 60 mm length, 7 mm pitch and 8 number of turn were used as a joining tool. The geometrical shape and dimension of the tube, rod, and single-stepped field-shaper are shown in Fig. 7.2. The value of "X" as shown in Fig. 7.2 (b) is 5, 10, and 15 mm for a sample that has 20, 15, and 10 mm groove length respectively.

The flat end of a steel rod was designed and machined for simplicity in griping during mechanical strength test. The surface of grips in UTM and torsional testing machine was found flat which force us to do the same profile on every single sample. This design helps to firmly grip the sample to measure the strength of the joint manufactured effectively.

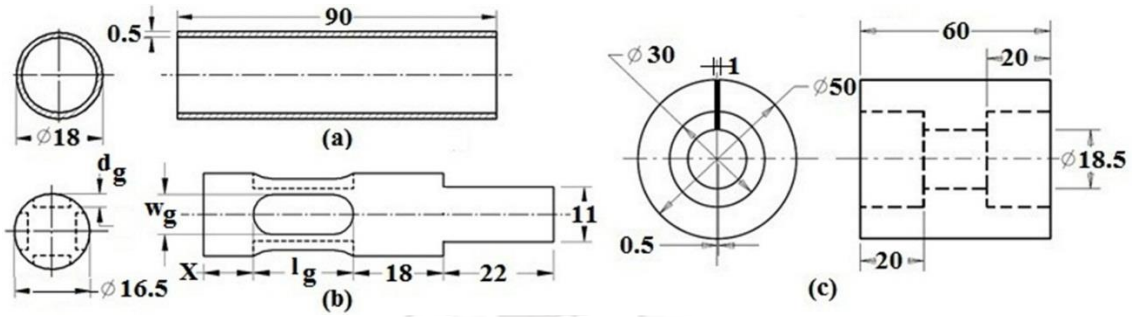

Fig. 7. 2 Geometrical shape and dimensions of (a) tube (b) rod and (c) single-stepped field-shaper (All dimensions are in mm)

Figure 7.3 shows the experimental set up used in the current study. Nylon made fixture is manufactured and used as reinforcement to protect the coil from bulging due to continuous crimping process. Fig. 7.4 demonstrates the waveform of a current curve measured experimentally using Rogowski coils with a peak value of 70 kA, a time-period of 68 µs, and a frequency of 14.71 kHz.

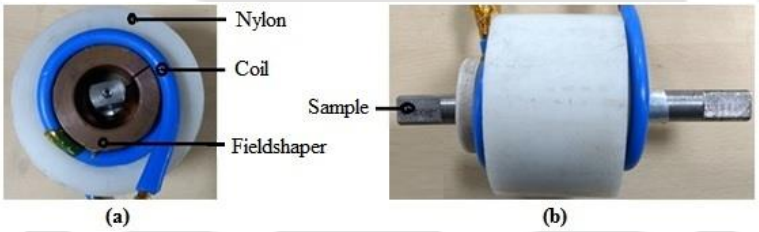

Fig. 7. 3 Experimental setup (a) side and (b) top view

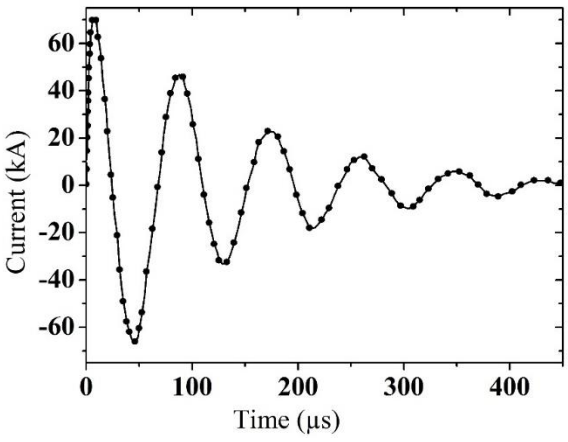

Fig. 7. 4 Current waveforms measured from the experiment

7.3. Testing Condition

EM crimping was carried out at both ends of the tube using two profiled rods which have identical groove parameters to simplify the testing procedure. A flat end of a rod makes the sample to be gripped firmly during testing. The two most crucial mechanical strength testing, i.e., torsion and pull-out that is represented schematically in Fig. 7.5 (a) was carried out successfully. Digital Torsion Testing Machine and UTM are used to perform strength testing. The three-point bending test also carried out using a testing condition which is shown in Fig. 7.5 (b). For torsional, pull-out and three-point bending test, a revolution and crossbar speed selected was 0.5 rpm, 0.1 mm/s and 1 mm/s respectively.

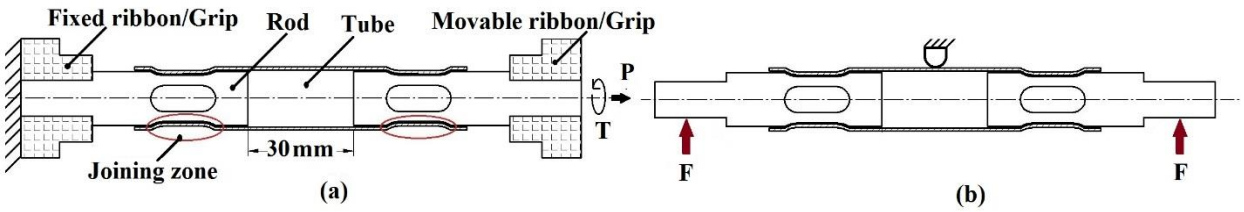

Fig. 7. 5 Test condition for (a) torsion, pull-out and (b) three-point bending

7.4. Result and Discussions

The effect of groove parameters in transferring transverse load was found insignificant. The decision was made to focus on the result achieved from the torsion test and pull-out test which is significantly affected by groove parameters. Hence, the overall analysis of this study is based on the effect of groove parameters on joint strength to resist the torsional and axial load. However, a three-point bending test was carried out to investigate only failure mode during transverse loading.

7.4.1. Cause and Effect Matrix

The CCD comprises a total of 20 experiments for each response (result from strength test): a full factorial design (8 experiments), six axial points which turned to the nearest, and six central points. The three groove parameters which significantly affect joint quality in EM crimping are depicted schematically in Fig. 7.6. The cause and effect matrix are tabulated in Table 7.1.

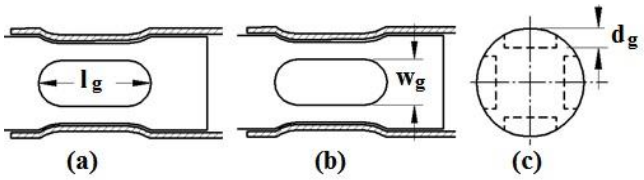

Fig. 7. 6 Groove parameters (a) length (b) width and (c) depth

Table 7. 1 Cause and effect matrix

Run number	Input data (Groove parameter)			Output data (Response)	
	Length (l_g) (mm)	Width (w_g) (mm)	Depth (d_g) (mm)	Torque (Nm)	Pull-out Load (kN)
1	15.00	8.00	2.00	41.054	3.932
2	10.00	10.00	1.00	20.454	3.495
3	15.00	8.00	2.00	38.366	4.301
4	20.00	6.00	3.00	12.909	2.517
5	15.00	8.00	2.00	34.913	4.022
6	15.00	8.00	2.00	37.051	4.205
7	15.00	6.00	2.00	26.468	3.911
8	15.00	10.00	2.00	25.416	4.431
9	10.00	8.00	2.00	31.157	3.648
10	20.00	10.00	1.00	22.122	3.923
11	10.00	10.00	3.00	10.526	3.342
12	15.00	8.00	3.00	15.548	3.025
13	20.00	6.00	1.00	32.167	3.649
14	20.00	10.00	3.00	12.115	3.719
15	15.00	8.00	2.00	37.767	4.221
16	15.00	8.00	2.00	38.964	3.989
17	10.00	6.00	1.00	21.425	3.335
18	20.00	8.00	2.00	36.788	4.691
19	15.00	8.00	1.00	25.681	3.679
20	10.00	6.00	3.00	11.772	2.301

7.4.2. Model Validation

The response variable, i.e., torque (T) and pull-out load (P) and the examined factors l_g, w_g, and d_g were related as Eq. 7.1 and 7.2 by applying multiple regression analysis on the data. These equations are second-order polynomial.

$$T = -121.431 + 0.751l_g + 28.541w_g + 43.310d_g - 0.117l_g w_g - 0.242l_g d_g + 0.561w_g d_g + 0.034{l_g}^2 - 1.797{w_g}^2 - 12.515{d_g}^2 \quad (7.1)$$

$$P = 1.382 + 0.038l_g - 0.087w_g + 2.14d_g + 0.0034l_g w_g - 0.0037l_g d_g + 0.113w_g d_g - 0.00036{l_d}^2 - 0.0019{w_g}^2 - 0.826{d_g}^2 \quad (7.2)$$

Figure 7.7 demonstrates the distribution of predicted values and the actual result of maximum torque and pull-out strength that shows how the model is significant.

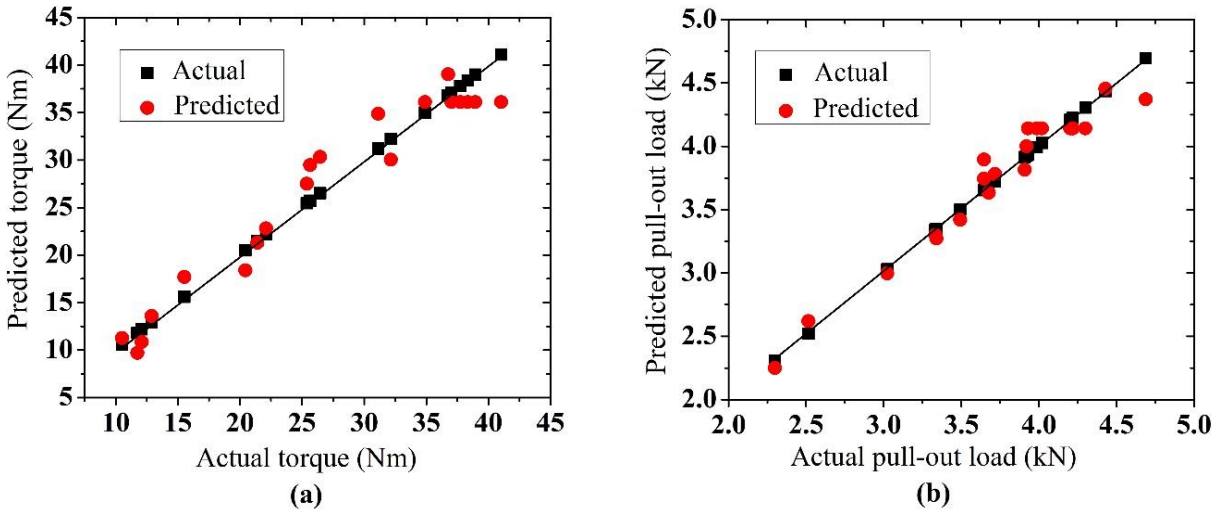

Fig. 7. 7 Predicted versus actual (a) torque and (b) pull-out strength

ANOVA calculated the determination coefficient (R^2) as 0.9432 for Eq. 7.1 and 0.9508 for Eq. 7.2 which formulate torque and pull-out load as a function of groove depth, width, and length. The results indicate that the model can efficiently predict 94.32 % for torque and 95.08 % for the pull-out strength. Therefore, the developed models were found to be highly significant. The experimental result was taken at five trial conditions, and the results were compared with predicted

values from the fitted equations. For torque and pull-out load, comparisons between actual and predicted results with associated absolute percentage error are provided in Fig. 7.8 and 7.9.

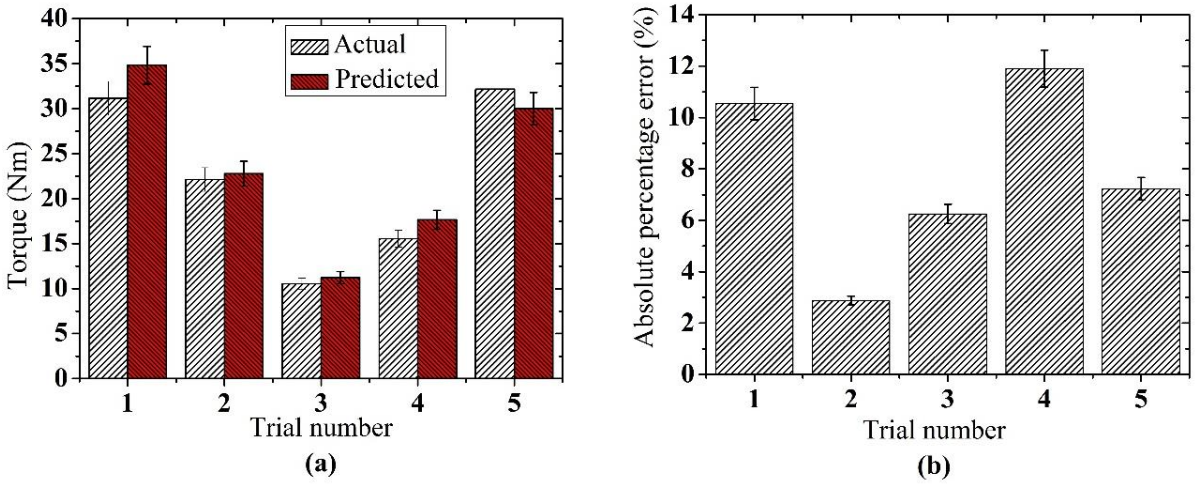

Fig. 7. 8 (a) Comparison of predicted and actual torque and (b) absolute percentage error of respective trials

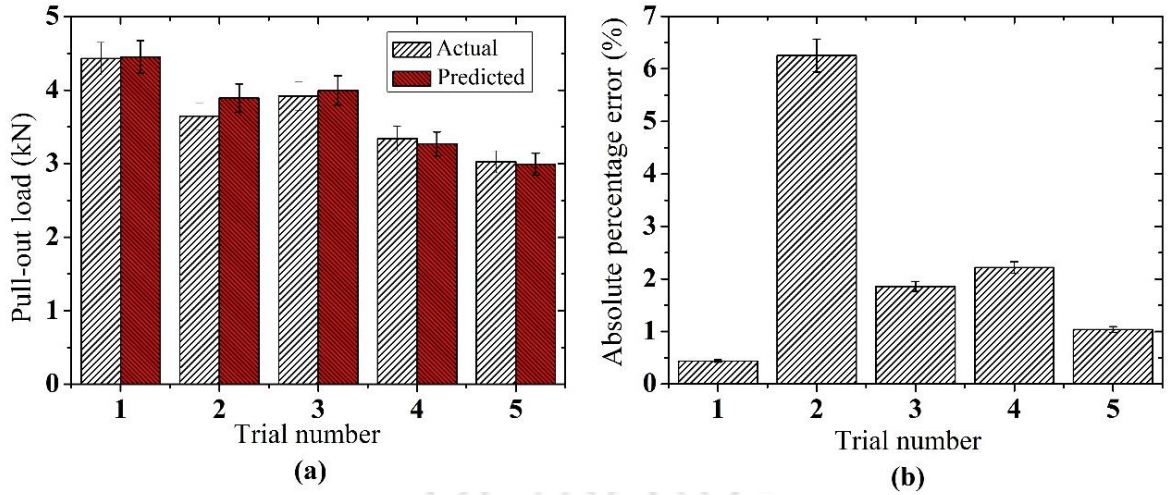

Fig. 7. 9 (a) Comparison of predicted and actual pull-out load and (b) absolute percentage error of respective trials

Predicted response variables from the fitted equations are in good agreement with the actual results, which shows maximum absolute percentage errors of less than 6% for pull-out load and 12% for torque. Therefore, strong evidence of the accuracy and adequacy of the fitted equations could be guaranteed.

The mean absolute percentage error (MAPE) is calculated by considering all points and found less than 1%. ANOVA can predict analytical values for both responses at a particular point which is different from testing points. Hence, this model is used for the discussion now onward to deal with the effects of each groove parameter and their interaction on joint quality.

7.4.3. Effect of Groove Parameters on Torque and Pull-out Load

Investigating the effect of each groove parameter on joint strength is the main objective of this chapter that is addressed in detail in the following subsections.

7.4.3.1. Effect of Groove Depth on Torque and Pull-out Load

Tube shearing and localized necking at the groove edge aggravated as groove depth increases beyond 2 mm. As groove depth increased, shearing off the tube at groove edge becomes severe as shown in Fig. 7.10 which can weaken the joint strength. The failure mode is well explained in section 7.4.3.5 that shows how a groove depth affects the load transferring capability of the manufactured joint.

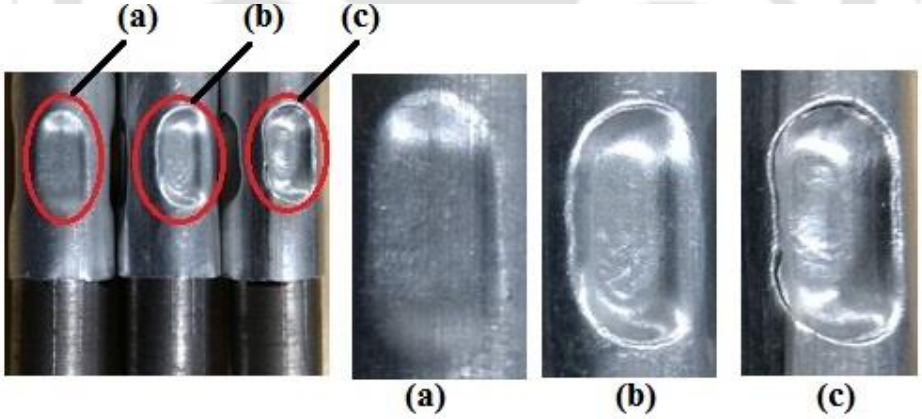

Fig. 7. 10 Tube shearing at groove edge for (a) 1 mm (b) 2 mm and (c) 3 mm groove depth

Localized cracks can be seen without using any magnification for the sample that has a 3 mm groove depth. This factor makes the joint to break easily with a lesser load. One of the significant groove parameters which have both positive and negative effect in torque and pull-out strength is groove depth and demonstrated in Fig. 7.11. Initially, torque and pull-out loads keep on increasing up to the maximum till groove depth reaches to 1.75 mm and 2 mm respectively and then start to decline.

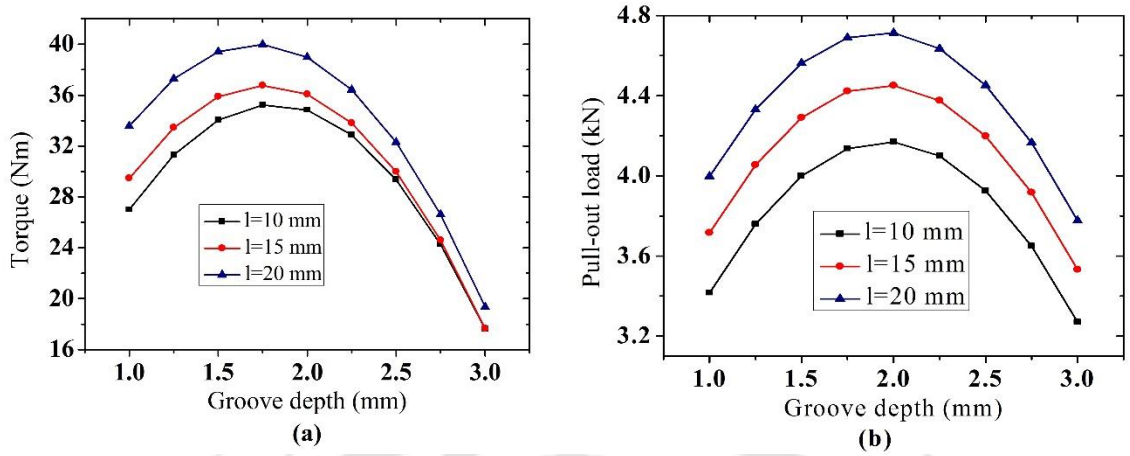

Fig. 7. 11 Effect of depth on (a) torque and (b) pull-out strength for 8 mm and 10 mm width

7.4.3.2. Effect of width on Torque and Pull-out strength

Figure 7.12 shows the effect of groove width on torque and pull-out load. Keeping a length and depth optimum (20 mm and 2 mm) based on previous analysis and varying width to investigate its effect on torque and pull-out strength.

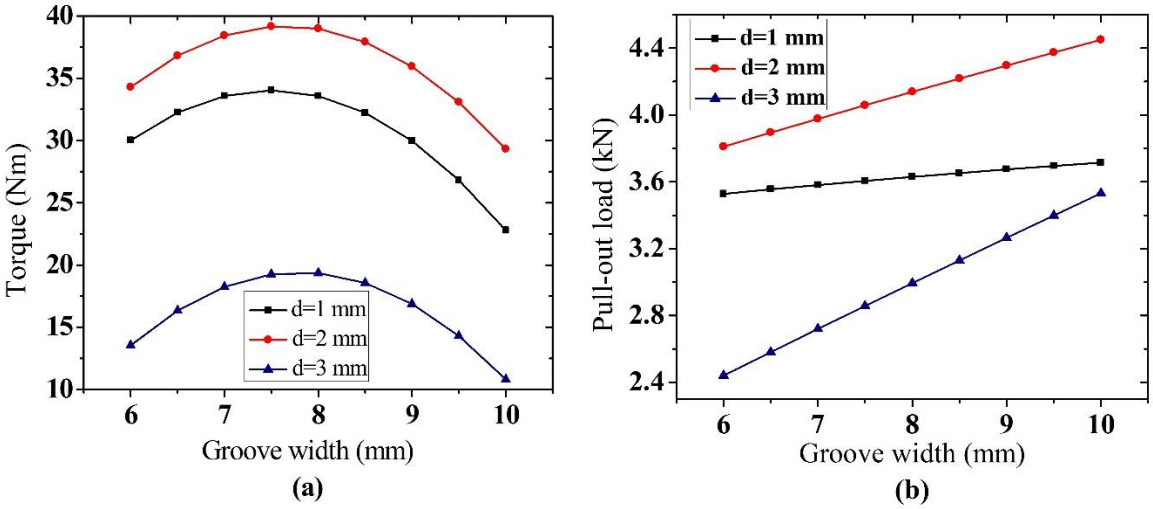

Fig. 7. 12 Effect of width on (a) torque and (b) pull-out strength

The two opposite effect of width on torque was investigated. Initially, the torque is rising as the width increases up to 7.5 mm and starts falling. The surface area between adjacent grooves which create interference fit is getting reduced while the width is increased. This factor is significantly minimizing the interlocking capability and weakening a torsional strength of the joint. However,

for the load applied axially, increasing groove width has a positive effect. Increasing a width leads to increase circumferential groove area which enhancing interlock of the tube especially for a load that is applied axially. Hence, pull-out strength which is highly dependent on the shearing of a tube at the groove edge shows linearly increasing as groove width increases.

7.4.3.3. Effect of Groove Length on Torque and Pull-out load

The two dominant joining mechanisms in EM crimping are interference-fit and form-fit which mainly depends on the contact area and mechanical interlocking due to the undercut of a rod. As groove length increase, the contact area will increase also, and the contribution of interference fit become significant. For optimum groove width and depth found from the previous analysis, the resistance to torsional and axial load increases as groove length increases and demonstrated in Fig. 7.13. The chance of creating wrinkles in the joining zone which have a negative effect on joint strength found less due to field-shaper. Therefore, groove length has a positive effect on both torque and pull-out strength regardless of groove width and depth. The optimum length determined by the effective working length of field-shaper which is 20 mm.

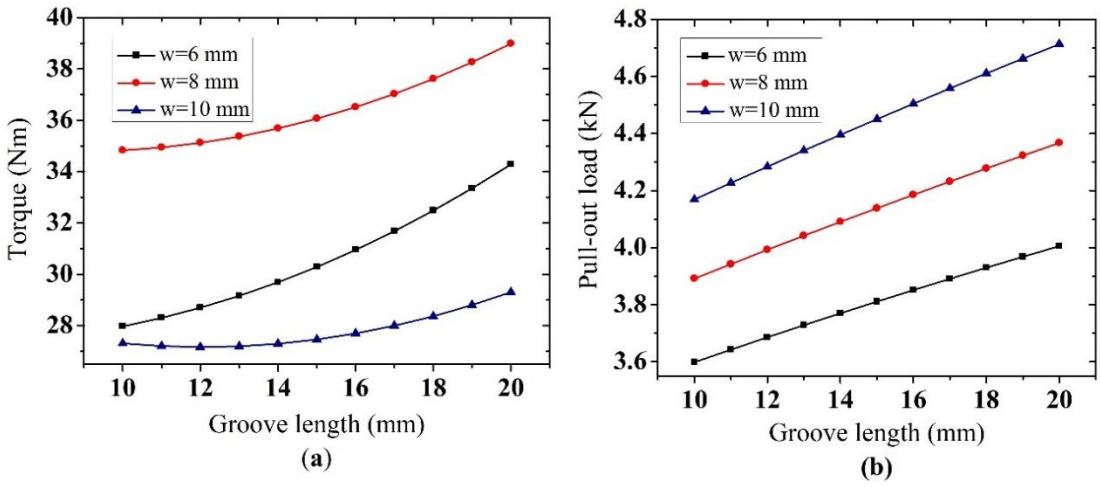

Fig. 7. 13 Effect of groove length on (a) torque and (b) pull-out strength

7.4.3.4. The Combined Effect of Groove Parameters on Joint Strength

The 2D representation of the combined effects of groove parameters on torque is shown in Fig. 7.14. The two opposite effect of width and linear effect of the length on torque is shown in Fig. 7.14 (a) by keeping the groove depth 2 mm which is optimum. Moreover, Fig. 7.14 (b) shows the

two opposite effects of depth and linear effect of length on torque by selecting the groove width of 8 mm which gives the maximum.

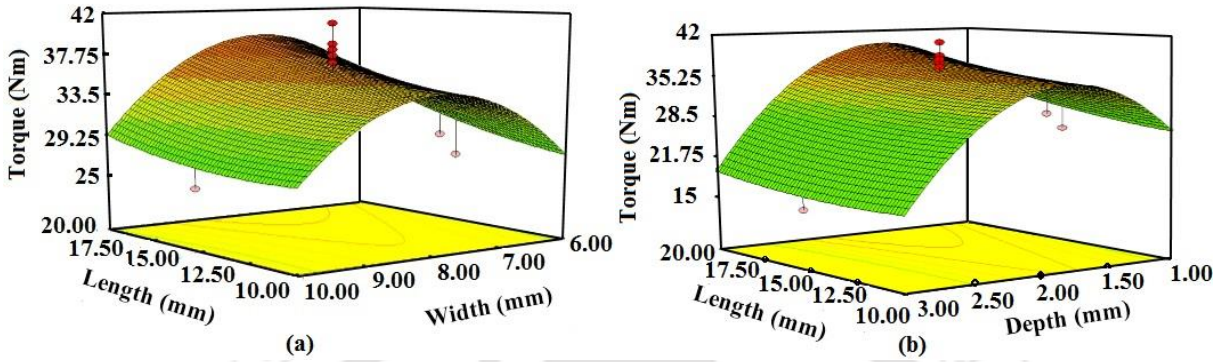

Fig. 7. 14 Response surface plot of the effect of groove parameters on torque

Similarly, Fig. 7.15 (a) shows the linear effect of length and width on pull-out strength keeping the groove depth of 2 mm. Fig. 7.15 (b) shows the two opposite effect of depth and the linear effect of length on pull-out strength by keeping the groove width of 8 mm

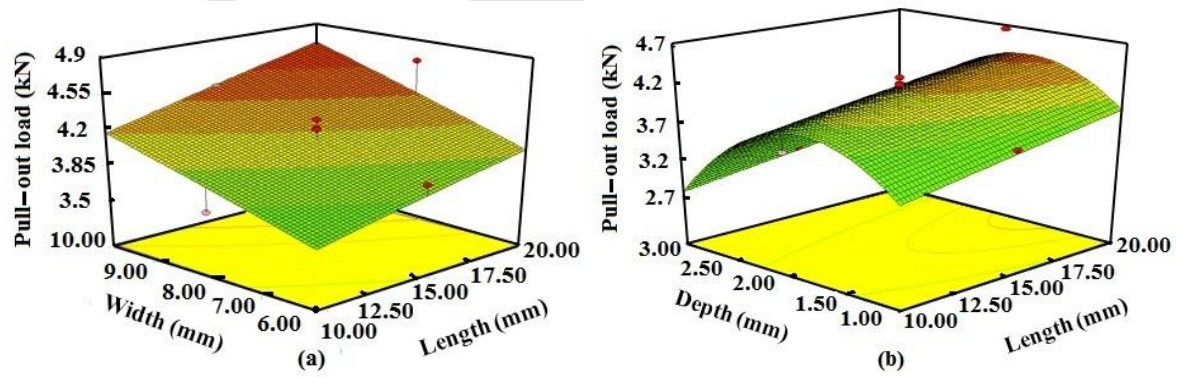

Fig. 7. 15 Response surface plot of the effect of groove parameters on pull-out load

7.4.3.5. Failure Mode in Torque, Pull-out and Transverse Load

Three modes of failure were observed during the torsional test, and better to discuss it based on the groove depth. The rod keeps rotating while the torsional load is applied for a sample that has 1 mm groove depth regardless of the width and the length as shown in Fig. 7.16 (a). However, the tube was twisted and finally cracked at the center for a sample which has 2 mm groove depth as shown in Fig. 7.16 (b). A deeper groove depth leads to tube shearing at the groove edge and failures

also initiate exactly at a point where thinning is critical with a less torsional load. Fig. 7.16 (c) shows how the tube is getting cracked at the joining zone for a sample that has a 3 mm groove depth.

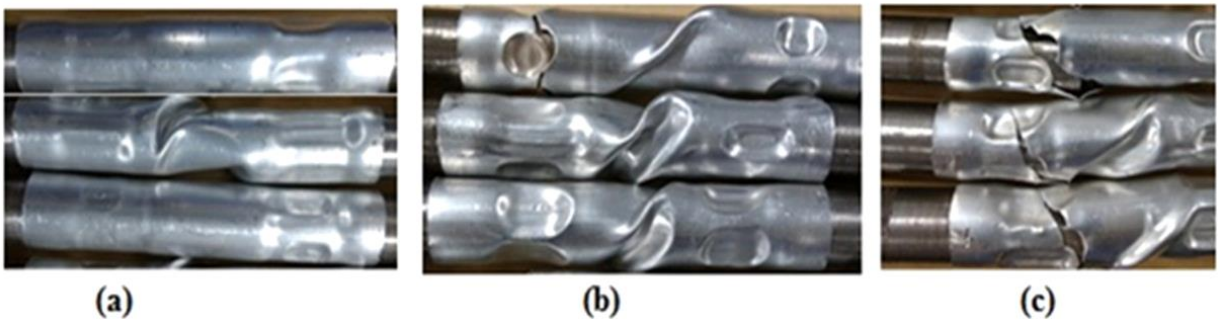

Fig. 7. 16 Failure mode in torsion test for (a) 1 mm (b) 2mm and (c) 3mm groove depth

In general, the three modes of failure were observed while the pull-out strength test was conducted. Similarly, the failure modes in the pull-out test are explained in terms of groove depth which is the most significant parameter in affecting joint strength than groove width or length. The rod keeps sliding after the joint is failing without crack for samples which has 1 mm groove depth as shown in Fig. 7.17 (a). The tube starts cracking nearby joining zone and propagates all around for those samples which have the groove depth of 2 mm as shown in Fig. 7.17 (b). For deeper groove depth, the groove edge is acting as a cutting edge. Hence, the portion of the tube at the joining zone getting torn out during pull-out for the sample which has a 3 mm groove depth as shown in Fig. 7.17 (c).

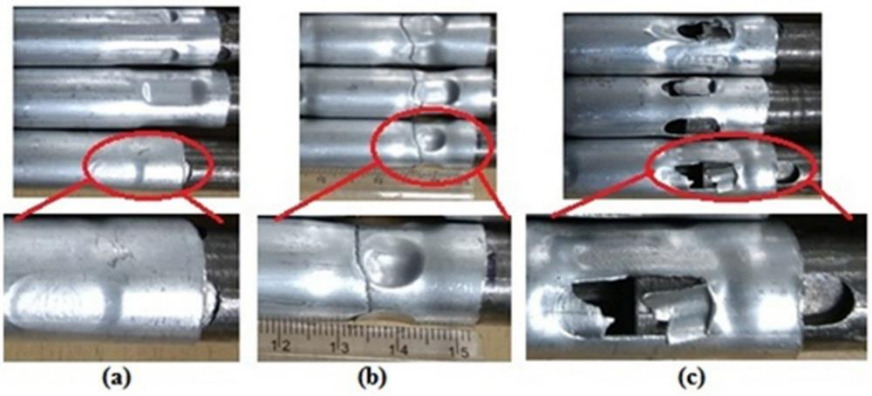

Fig. 7. 17 Failure mode in the pull-out test for (a) 1mm (b) 2 mm and (c) 3 mm groove depth

From the previous discussion, we found that the groove depth shouldn't be minimum or maximum to improve joint strength and to prevent the easy breakdown of the joint with a lesser load. However, only one type of failure mode was observed in the case of transverse loading regardless of groove parameters as shown in Fig. 7.18. This test and failure mode clearly explain that the effect of groove parameters on joint strength manufactured to support transverse load was insignificant. A maximum of 742 N was achieved as the load resistance from this test.

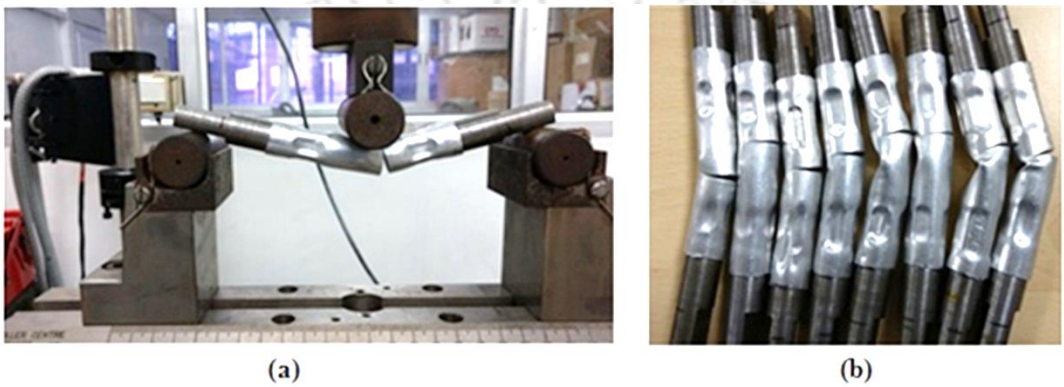

Fig. 7. 18 Three-point bending (a) setup and (b) failure mode

Finally, for the given dimensions of the rod, tube and process parameters, significant groove parameters in terms of rod diameter and tube thickness were represented to achieve maximum joint strength. If the groove designed based on this guideline for the same process parameters and material combination, maximum torque can be achieved. By keeping the groove length of $L=20$ *mm*, the following expression $D_0=2.2\ W$, $W=15t$, and $D=3.5t$ can be used as the design guideline where D_0, W, D, and t represents the outside diameter of the rod, groove width, groove depth, and tube thickness respectively. The most significant parameter in supporting axial load for the groove geometry introduced is the groove depth, and it should be $D=4t$ for the highest joint quality.

7.5. Summary

In this study, EM crimping experiment was carried out to investigate the effects of groove parameters on joint quality with the help of design of experiment method. Torsional joint strength, pull-out strength, and failure mode were analyzed and discussed in detail. The CCD and RSM which is the newly adopted tool in EM crimping were found to be very useful for the optimization of groove parameters. Relies on the result found, a guideline to design a rectangular groove to

transfer torsional and pull-out load simultaneously was proposed. The design of experiment method based on CCD and RSM is introduced in analyzing the effect of groove parameters on joint quality manufactured by EM crimping process. The following conclusions are drawn based on results found from the detailed experimental investigation.

- The model developed using CCD and RSM is used to predict the effect of each groove parameters on joint quality efficiently and economically with a limited number of the experiment.
- The developed mathematical model which describe torque and pull-out load in terms of groove parameters used to identify which groove parameter is the most significant in affecting the joint quality.
- Groove depth was found the most significant groove parameters for the considered material configuration to affect joint strength. However, groove length and width also has a significant effect on joint quality. Hence, a grove that has 2 mm, 20 mm and 8 mm of depth, length, and width is optimum to transfer both torsional and pull-out load.
- A guideline which is proposed in this study can be used to design a rectangular groove to transfer maximum torsional and axial load respectively.
- Three failure mode was observed during torsion and pull-out test. At optimum groove parameters, the tube is showing localized necking at the center which signifies the quality of the joint. Only one type of failure mode was observed in the case of a three-point bending test. Hence, there is no direct effect of groove parameters in supporting the transverse load.
- This kind of joint is commonly used in the aircraft seat structure and the drive shaft of automotive with different grade of aluminum tube and steel rod.

CHAPTER 8

CONCLUSIONS AND FUTURE SCOPE OF THE WORK

8 Conclusions and Future Scope of the Work

8.1. Conclusions

Electromagnetic crimping is one of the advanced manufacturing technologies used to join lightweight material including metals with different metallurgical and thermal properties. A new era of the manufacturing process is looking for developing advanced techniques for joining lightweight materials. Joining methods like fusion welding has several limitations like the creation of intermetallic compound, crack, voids, etc. that needs to be addressed. Advanced techniques like solid-state joining become the best options to overcome existed limitations. Joining metals that have a high aspect ratio for lightweight applications requires advanced techniques. A method that can provide enhanced joint strength without being affected by thermal property variations between the mating parts becomes the best option. The following conclusions are drawn from this work.

I. Collecting and analyzing different research findings related to electromagnetic forming and joining was done initially to understand the working principle and how this process becomes advantageous over conventional methods. The dissimilar metal combination, green, defect-free joint, repeatability, highest joint quality, and producing a ready to use product was found as the advantage of EMF and joining process over the conventional process. Different studies regarding electromagnetic forming and joining processes are systematically reviewed to find out the research gap.

II. LS-DYNA is a 3D FEM model used to predict different process parameters for the highest joint strength. The numerical model was validated with the experimental results to predict the interaction of several parameters using a single rectangular groove. Quality of joint manufactured using 4.1kJ was evaluated and 95% joint strength was found compared to the strength of the undeformed tube. The feasibility of electromagnetic crimping between the aluminum tube and a steel rod was studied using a single rectangular groove. The results revealed that the mechanical interlocking was found the main joining mechanism. The effect of energy on radial displacement, tube thickness reduction, and joint strength was found significant.

III. The EM crimping of the aluminum tube on a steel rod was investigated that can be used as a pre-study for an application for automotive and spaceframe structure. For the analysis, a

combined experimental investigation and numerical strategy have been chosen. A 3D coupled simulation of electromagnetic crimping is carried out using an EM-module of LS-DYNA^{TM} structural explicit code. A radial displacement, tube thickness reduction, and groove filling obtained from the simulation were compared with the experiment for model validation. The e ffect of energies on several process parameters are also predicted numerically using the devel oped model.

IV. More than 72 % load transferring capability of crimped samples was achieved compared to the strength of the aluminum tube. Moreover, 95 % of joint strength were found based on samples failed at joining zone compared to the aluminum tube. A joint manufactured in this investigation relies on the mechanical interlocking at the edge of the groove.

V. A simulation was used to predict the failure zone for the double rectangular groove. Radial displacement for different groove depth along the joining zone is measured numerically and experimentally and found in a good agreement with a percentage error of 5.13%. Parameters challenging to measure while conducting an experiment like pressure, shear strain, von-Mises stress, resultant velocity, effective plastic strain, magnetic field, resultant velocity, and Lorentz force are easily predicted from 3D coupled simulation. The more the groove depth, the more wrinkling.

VI. Deformation of the tube at the joining zone was found uniform while using field-shaper regardless of a groove profile. A single-stepped field-shaper was found better than tapered field-shaper to achieve the highest joint strength. The torque resistance achieved between aluminum tubes and a steel rod was found higher even for lower discharge energies as compared to aluminum to the aluminum joint. Torsion and pull-out test result reveals the knurled profile enhances the joint strength compared to plain profile. The contact length should be higher for better joint strength without significant tube thickness reduction. Three modes of failure are observed during torsional test, i.e., rod rotating, tube sheared off at the center and tube sheared off at the joining zone. At its best energy and profile failure of the basic tube material occur. Besides that, the rod is sliding and keeps coming out during the pull-out test with different load-bearing capacity regardless of material configuration and groove profile.

VII. The model developed using CCD and RSM is used to predict the effect of each groove parameters on joint quality efficiently and economically with a limited number of the experiment. For the given dimensions of the rod, tube and process parameters, we represent significant groove parameters in terms of rod diameter and tube thickness to achieve maximum joint strength. By keeping the groove length of $L=20\ mm$, the following expression $D_0=2.2\ W$, $W=15t$, and $D=3.5t$ can be used as the design guideline. The most significant parameter in supporting axial load for the groove geometry introduced is the groove depth, and it should be $D=4t$ for the highest joint quality. If the groove designed based on this guideline for the same process parameters and material combination, maximum torque and pull-out strength can be achieved.

8.2. Future Scope of the Work

- Study the effect of field-shaper geometry numerically and experimentally for crimping steel to steel configuration and propose the optimum parameters. The feasibility and applicability of novel field-shaper which can perform multiple crimping at the same time to increase the rate of production also not addressed.
- A phenomenological analysis of the EM machine + filed-shaper response in terms of magnetic field variance (magnitude + frequency) could be a helpful solution to well characterize the machine capability as well as the crimping response using the predictive computational model.
- Design and develop an adjustable fixture which can be used to reinforce different size coil and avoid unnecessary deformation while performing successive crimping process.
- Study the effect of different adhesive materials that can be used as a filler to achieve airtight joint between tube and rod.
- Study the combined effect of discharge energy and width-to-depth ratio on joint strength, and propose a design guideline using the DOE method and numerical simulation for the double rectangular groove.
- Develop an instrument that is capable of measuring the magnetic field at the joining zone for coils that have a different cross-section.

9 References

Areda, G., and S. Kore. 2017. "Finite Element Modeling and Simulation of Electromagnetic Crimping of Al6016-T6 Tube with Steel Rod." *ICCASP/ICMMD-2016. Advances in Intelligent Systems Research, 137*, pp. 83-88,

Baaten, T., Nicolas Debroux, Wim De Waele, and K. Faes. 2010. "Joining of Copper to Brass using Magnetic Pulse Welding." *Presented at Proceedings of the 4th International Conference on High Speed Forming—ICHSF*, March 9th-10th, 2010 Columbus, Ohio, USA: Institut für Umformtechnik-Technische Universität Dortmund, pp.83-96.

Bahmani, M.A., Niayesh, K. and Karimi, A., 2009. "3D Simulation of Magnetic Field Distribution in Electromagnetic Forming Systems with Field-shaper." *Journal of materials processing technology*, *209*(5), pp.2295-2301.

Barreiro, P., Beerwald, C., Homberg, W., Kleiner, M., Löhe, D., Marré, M. and Schulze, V., 2006. "Strength of tubular Joints made by Electromagnetic Compression at quasistatic and cyclic loading." *Presented at Proceedings of the 4th International Conference on High Speed Forming*—ICHSF, 20th and 21th of March 2006, pp. 107-116, Dortmund Germany.

Bogaert, D., De Waele, W., Faes, K. and Zaitov, O., 2012. "Torque Resistance of Joints made by Magnetic Pulse Crimping." *Sustainable Construction and Design*, *3*, pp.234-242.

Chaharmiri, R. and Arezoodar, A.F., 2016. "The Effect of Sequential Coupling on Radial Displacement Accuracy in Electromagnetic Inside-bead Forming: Simulation and Experimental Analysis using Maxwell and ABAQUS Software." *Journal of Mechanical Science and Technology*, *30*(5), pp.2005-2010.

Chu, Y.Y. and Lee, R.S., 2013. "Effect of Field shaper Geometry on the Lorentz Force for Electromagnetic Sheet Impact Forming Process." *Proceedings of the Institution of Mechanical Engineers, Part B: Journal of Engineering Manufacture*, *227*(2), pp.324-332.

Demir, O.K., Psyk, V. and Tekkaya, A.E., 2010. "Simulation of Tube Wrinkling in Electromagnetic Compression." *Production Engineering*, *4*(4), pp.421-426.

Dhar, N.R., Kamruzzaman, M. and Ahmed, M., 2006. "Effect of Minimum Quantity Lubrication (MQL) on Tool Wear and Surface Roughness in Turning AISI-4340 Steel." *Journal of materials processing technology*, *172*(2), pp.299-304.

Faes, K., De Waele, W., Müller, M. and Cramer, H., 2014. "Design of Electromagnetic Pulse Crimp Torque Joints." Universitätsbibliothek Dortmund, pp. 39-50.

Faes, K., O. Zaitov, and W. De Waele., 2012. "Electromagnetic Pulse Crimping of Axial Form Fit Joints." *Presented at Proceedings of the 5th International Conference on High Speed Forming*, April 24th – 26th, 2012, Dortmund, Germany, pp.229-242.

Faes, K., W. De Waele, M. Müller, and H. Cramer., 2014. "Design of Electromagnetic Pulse Crimp Torque Joints." *Presented at Proceedings of the 6th International Conference on High Speed Forming*, March 27th-29th, 2014, Daejeon, Korea, pp.38-50.

Golovashchenko, S., 2006. "Electromagnetic Forming and Joining for Automotive Applications." *Presented at Proceedings of the 2nd International Conference on High Speed Forming*, March 20th - 21st, 2006, Dortmund, Germany, pp.201-206.

Golovashchenko, Sergey F., 2007. "Material Formability and Coil Design in Electromagnetic Forming." *Journal of Materials Engineering and Performance*, *16*(3), pp. 314-320.

Hammers, T., Marré, M., Rautenberg, J., Barreiro, P., Schulze, V., Biermann, D., Brosius, A. and Tekkaya, A.E., 2009. "Influence of Mandrel's Surface and Material on the Mechanical Properties of Joints Produced by Electromagnetic Compression." *steel research international*, *80*(5), pp.366-375.

Homberg, W., Marré, M., Beerwald, C. and Kleiner, M., 2006. "Joining by Forming of Lightweight Frame Structures." In *Advanced Materials Research, 10*, pp. 89-100. Trans Tech Publications.

Hwang, W. S., J. S. Lee, N. H. Kim, and H. S. Sohn., 1993. "Joining of Copper Tube to Polyurethane Tube by Electromagnetic Pulse Forming." *Journal of Materials Processing Technology*, *37*(1), pp. 83-93.

Hwang, W. S., N. H. Kim, H. S. Sohn, and J. S. Lee. 1992. "Electromagnetic Joining of Aluminum Tubes on Polyurethane Cores." *Journal of Materials Processing Technology*, *34*(1), pp. 341-348.

Imbert JM, Winkler SL, Worswick MJ, Oliveira DA, Golovashchenko SS.2005. "The Effect of Tool–Sheet Interaction on Damage Evolution in Electromagnetic Forming of Aluminum Alloy Sheet." *ASME. Journal of Engineering Materials and Technology*, *127*(1), pp.145-153.

Itoh, T., 1973. "Damped Vibration Mode Superposition Method for Ddynamic Response Analysis." *Earthquake Engineering & Structural Dynamics*, *2*(1), pp.47-57.

Johnson, G.R. and Cook, W.H., 1985. "Fracture Characteristics of three Metals Subjected to Various Strains, Strain rates, Temperatures and Pressures." *Engineering fracture mechanics*, *21*(1), pp.31-48.

Johnson, Gordon R., and William H. Cook. 1983. "A Constitutive Model and Data for Metals Subjected to Large Strains, High Strain Rates and High Temperatures." *In Proceeding of the 7th International Symposium on Ballistics*, *21*(1), pp. 541-547.

Kamal M, Daehn GS.2006. "A Uniform Pressure Electromagnetic Actuator for Forming Flat Sheets." *ASME. Journal of Manufacturing Science and Engineering*, *129*(2), pp.369-379.

Karimi, A., Niayesh, K. and Bahmani, M.A., 2010. "Magnetic Field Enhancement in Electromagnetic Forming Systems using Anisotropic Materials." *International journal of material forming*, *3*(3), pp.205-208.

Kleiner, M., Beerwald, C. and Homberg, W. 2005. "Analysis of Process Parameters and Forming Mechanisms within the Electromagnetic Forming Process." *CIRP Annals-Manufacturing Technology*, *54*(1), pp. 225-228.

Kleiner, M., Marré, M., Beerwald, C., Homberg, W., Löhe, D., Barreiro, P. and Schulze, V., 2006. "Investigation of Force-fit joints Produced by Electromagnetic Tube Compression." *Annals of the German Academic Society for Production Engineerin*g, WGP, *13*(1), pp. 227-230.

Kumar, and R Kore, S.D.., 2017. "Electromagnetic Crimping in Tube-to-Cylinder Configuration: Influence of the Base Profiles on the Joint Quality." *Journal of Testing and Evaluation*, *46*(3), pp.1064-1075.

Kumar, R. and Kore, S.D., 2017. "Effects of Surface Profiles on the Joint Formation during Magnetic Pulse Crimping in Tube-to-rod Configuration." *International Journal of Precision Engineering and Manufacturing*, *18*(8), pp.1181-1188.

L'Eplattenier, Pierre, Grant Cook, Cleve Ashcraft, Mike Burger, Jose Imbert, and Michael Worswick., 2009. "Introduction of an Electromagnetism Module in LS-DYNA for Coupled Mechanical-Thermal-Electromagnetic Simulations." *Steel research international*, *80*(5), pp. 351-358.

Li, F., Mo, J., Zhou, H. and Fang, Y., 2013. "3D Numerical Simulation Method of Electromagnetic Forming for Low Conductive Metals with a Driver." *The International Journal of Advanced Manufacturing Technology*, *64*(9-12), pp.1575-1585.

Li, J. and Cheng, G.J., 2009. "Multiphysics Simulation on Electromagnetic Peening of Predrilled Holes." *International Journal of Mechanical Sciences*, *51*(11-12), pp.825-836.

Mamalis A, Manolakos D, Kladas A, Koumoutsos A. 2005. "Electromagnetic Forming and Powder Processing: Trends and Developments." *ASME. Applied Mechanics Reviews*, *57*(4), pp.299-324.

Marré, M., Brosius, A. and Tekkaya, A.E., 2008. "Joining by Compression and Expansion of (none-) Reinforced Profiles." *In Advanced Materials Research*, *43*, pp. 57-68. Trans Tech Publications.

Marré, M., Ruhstorfer, M., Tekkaya, A. E. and Zaeh, M. F.2009. "Manufacturing of Lightweight Frame Structures by Innovative Joining by Forming Processes." *International Journal of material forming*, *2*(1), pp. 307-310.

Melby, E.A. and Eide, H.O.S., 2013. "Blast Loaded Aluminium Plates: Experiments and Numerical Simulations." (Master's thesis, Institutt for konstruksjonsteknikk).

Mori, K.I., Bay, N., Fratini, L., Micari, F. and Tekkaya, A.E., 2013. "Joining by Plastic Deformation." *CIRP Annals*, *62*(2), pp.673-694.

Mynors, D.J. and Zhang, B., 2002. "Applications and Capabilities of Explosive Forming." *Journal of materials processing technology, 125,* pp.1-25.

Neugebauer, R., V. Psyk, and C. Scheffler., 2012. "Simulation of Electromagnetically Formed Joints." *In Proceedings of the 5th International Conference on High Speed Forming–ICHSF 2012,* April 24th – 26th, pp. 219-228, Dortmund U-Tower.

Oliveira, D.A., Worswick, M.J., Finn, M. and Newman, D., 2005. "Electromagnetic Forming of Aluminum Alloy Sheet: Free-form and Cavity Fill Experiments and Model," *Journal of Materials Processing Technology, 170(1-2),* pp.350-362.

Park, Y.B., Kim, H.Y. and Oh, S.I., 2005. "Design of Axial/Torque Joint made by Electromagnetic Forming." *Thin-walled structures, 43(5),* pp.826-844.

Patel, C., Ghatule, P. and Kore, S.D., 2017. "Finite Element Analysis of Effect of Process Parameters on Electromagnetic Free Expansion of Aluminium Tube." *International Journal of Materials and Product Technology, 54(1-3),* pp.165-178.

Psyk, Verena, D. Risch, B. L. Kinsey, A. E. Tekkaya, and M. Kleiner., 2011. "Electromagnetic Forming—A Review." *Journal of Materials Processing Technology, 211(5),* pp.787-829.

Rajak, A.K. and Kore, S.D., 2017. "Experimental Investigation of Aluminium–copper Wire Crimping with Electromagnetic Process: Its Advantages Over Conventional Process." *Journal of Manufacturing Processes, 26,* pp.57-66.

Rajak, A.K. and Kore, S.D., 2018. "Application of Electromagnetic Forming in Terminal Crimping using Different types of Field-shapers." *Journal of Mechanical Science and Technology, 32*(9), pp.4291-4297.

Rajak, A.K. and Kore, S.D., 2018. "Comparison of Different Types of Coil in Electromagnetic Terminal-wire Crimping Process: Numerical and Experimental Analysis." *Journal of Manufacturing Processes, 34,* pp.329-338.

Rajak, A.K. and Kore, S.D., 2018. "Numerical Simulation and Experimental Study on Electromagnetic Crimping of Aluminium Terminal to Copper Wire Strands." *Electric Power Systems Research, 163,* pp.744-753.

Rajak, A.K., Kumar, R., Basumatary, H. and Kore, S.D., 2018. "Numerical and Experimental Study on Effect of Different Types of Field-shaper on Electromagnetic Terminal-Wire Crimping Process." *International Journal of Precision Engineering and Manufacturing*, *19*(3), pp.453-459.

Schäfer, R., and P. Pasquale., 2010. "Electromagnetic Pulse Forming Technology Keys for Allocating the Industrial Market Segment." *Presented at Proceedings of the 4th International Conference on High Speed Forming*—ICHSF, 9th and 10th of March 2010, pp.16-25, Columbus, Ohio, United States of America.

Schäfer, R., P. Pasquale, and S. Kallee., 2009. "Industrial Application of the Electromagnetic Pulse Technology." *PST products* Gmbh, Alzenau, Germany.

Schäfer, Ralph, Pablo Pasquale, and Stephan Kallee. , 2014. "The Electromagnetic Pulse Technology (EMPT): Forming, Welding, Crimping and Cutting." Biuletyn Instytutu Spawalnictwa w Gliwicach, *58*(2), pp. 50-57.

Seth, M., Vohnout, V.J. and Daehn, G.S., 2005. "Formability of Steel Sheet in High Velocity Impact." *Journal of materials processing technology*, *168*(3), pp.390-400.

Shang, J., L'Eplattenier, P., Wilkerson, L. and Hatkevich, S., 2010. "Numerical Simulation and Experimental Study of Electromagnetic Forming." In *11th International LS-DYNA Users Conference, Detroit*, pp. 10-27.

Shin, C., Jin, H.H., Lee, J.G., Lee, D.J., Rhee, C.K. and Hong, J.H., 2008. "Expansion of a Low Conductive Metal Tube by an Electromagnetic Forming Process: Finite Element Modeling." *Metals and Materials International*, *14*(1), pp.91-97.

Silva, C.M., Nielsen, C.V., Alves, L.M. and Martins, P.A., 2015. "Environmentally Friendly Joining of Tubes by their Ends." *Journal of Cleaner Production*, *87*, pp.777-786.

Song, F.M., Zhang, X., Wang, Z.R. and Yu, L.Z., 2004. "A Study of Tube Electromagnetic Forming." *Journal of materials processing technology*, *151*(1-3), pp.372-375.

Sun, Z. and Karppi, R., 1996. "The Application of Electron Beam Welding for the Joining of Dissimilar Metals: An Overview." *Journal of Materials Processing Technology*, *59*(3), pp.257-267.

Suzuki, H., Murata, M. and Negishi, H., 1987. "The Effect of a Field shaper in Electromagnetic Tube Bulging." *Journal of Mechanical Working Technology*, *15*(2), pp.229-240.

T. Hammers Barreiro, P., A. Brosius, D. Löhe, M. Marré, J. Rautenberg, V. Schulze, and A. E. Tekkaya. 2008. "Influence of Mandrel Surface on the Mechanical Properties of Joints Produced by Electromagnetic Compression," *Presented at Proceedings of the* 3rd International Conference on High-Speed Forming, March 11 - 12, 2008, pp.245-256, Dortmund Germany.

Unger, J., Stiemer, M., Schwarze, M., Svendsen, B., Blum, H. and Reese, S., 2008. "Strategies for 3D Simulation of Electromagnetic Forming Processes." *Journal of materials processing technology*, *199*(1-3), pp.341-362.341-362.

Vanhulsel, P., Van Wonterghem, M., De Waele, W. and Faes, K., 2011. "Groove Design for Form Fit Joints made by Electromagnetic Pulse Crimping." In *Sustainable Construction and Design 2011 (SCAD)*, *2*(3), pp. 432-441. Ghent University, Laboratory Soete.

Varis, J.P., 2002. "The Suitability of Round Clinching Tools for High Strength Structural Steel." *Thin-Walled Structures*, *40*(3), pp.225-238.

Vedantam, K., Bajaj, D., Brar, N.S. and Hill, S., 2006." Johnson-Cook Strength Models for Mild and DP 590 Steels." In *AIP conference proceedings*, *845*(1), pp. 775-778). AIP.

Vivek, A., Kim, K.H. and Daehn, G.S., 2011. "Simulation and Instrumentation of Electromagnetic Compression of Steel Tubes." *Journal of Materials Processing Technology*, *211*(5), pp.840-850.

Watanabe, H., Tsutsui, H., Mukai, T., Kohzu, M., Tanabe, S. and Higashi, K., 2001. "Deformation Mechanism in a Coarse-Grained Mg–Al–Zn Alloy at Elevated Temperatures." *International Journal of Plasticity*, *17*(3), pp.387-397.

Weddeling, C., 2015. "*Electromagnetic Form-Fit Joining." Dr.-Ing* (Doctoral dissertation, Dissertation, Dortmund, Germany).

Weddeling, C., Demir, O.K., Haupt, P. and Tekkaya, A.E., 2015. "Analytical Methodology for the Process Design of Electromagnetic Crimping." *Journal of Materials Processing Technology*, *222*, pp.163-180.

Weddeling, C., Gies, S., Nellesen, J., Kwiatkowski, L., Tillmann, W. and Tekkaya, A.E., 2012. "Influencing Factors on the Strength of Electromagnetically Produced Form-Fit Joints using Knurled Surfaces." In *Proceedings of the 5th International Conference on High Speed Forming–ICHSF2012*, April 24th – 26th, pp. 243-254, Dortmund U-Tower.

Weddeling, C., Walter, V., Haupt, P., Tekkaya, A.E., Schulze, V. and Weidenmann, K.A., 2015. "Joining Zone Design for Electromagnetically Crimped Connections." *Journal of Materials Processing Technology*, *225*, pp.240-261.

Weddeling, C., Woodward, S., Nellesen, J., Psyk, V., Marré, M., Brosius, A., Tekkaya, A.E., Daehn, G.S. and Tillmann, W., 2010. "Development of Design Principles for Form-Fit Joints in Lightweight Frame Structures." *Presented at Proceedings of the 4th International Conference on High Speed Forming*—ICHSF, 9th and 10th of March 2010, pp. 137-148, Dortmund Germany.

Weddeling, C., Woodward, S.T., Marré, M., Nellesen, J., Psyk, V., Tekkaya, A.E. and Tillmann, W., 2011. "Influence of Groove Characteristics on Strength of Form-Fit Joints." *Journal of Materials Processing Technology*, *211*(5), pp.925-935.

Weddeling, C., Woodward, S.T., Marré, M., Nellesen, J., Psyk, V., Tekkaya, A.E. and Tillmann, W., 2011. "Influence of Groove Characteristics on Strength of Form-Fit Joints." *Journal of Materials Processing Technology*, *211*(5), pp.925-935.

Woodward, S., Weddeling, C., Daehn, G., Psyk, V., Carson, B. and Tekkaya, A.E., 2010. "Agile Production of Sheet Metal Aviation Components using Disposable Electromagnetic Actuators." *Presented at Proceedings of the 4th International Conference on High Speed Forming*—ICHSF, 9th and 10th of March 2010, pp. 34-46, Dortmund Germany.

Yu, H., Li, C., Zhao, Z. and Li, Z., 2005. "Effect of Field shaper on Magnetic Pressure in Electromagnetic Forming." *Journal of Materials Processing Technology*, *168*(2), pp.245-249.

Zia, M., Fazli, A. and Soltanpour, M., 2017. "Warm Electrohydraulic Forming: A Novel High Speed Forming Process." *Procedia engineering*, *2017*, pp.323-328.

Zittel, g., 2010. "A Historical Review of High-speed Metal Forming." *Presented at Proceedings of the 4th International Conference on High Speed Forming*—ICHSF, 9th and 10th of March 2010, pp. 2-15, Dortmund Germany.

10 Publications Out of this Work

International Journals

[1] **Areda, G.T.** & Kore, S.D., "Numerical Study and Experimental Investigation on Electromagnetic Crimping for Tube-to-Rod Configuration*," Int. J. Precis. Eng. Manuf.* Vol. 20, No.2, 2019, pp 181–191, https://doi.org/10.1007/s12541-019-00083-3.

[2] **Areda, G.T.** & Kore, S.D., "Mechanical Interlock Made by Electromagnetic Crimping for Axial Load Resistance using Aluminum Tube and Steel Rod" *International Journal of Testing and Evaluation* **(Recommended for publication).**

[3] **Areda, G.T.** & Kore, S.D., "Magnetic Pulse Crimping of Tube-to-Rod Using Double Rectangular Groove: Experiment and Numerical Simulation" *International Journal of Materials and Product Technology* **(Under review).**

[4] **Areda, G.T.** & Kore, S.D., "Analysis of Effect of Groove Parameters on Joint Strength Made by Electromagnetic Crimping" *International Journal of Materials and Product Technology* **(Communicated).**

[5] **Areda, G.T.** & Kore, S.D., "Effect of Field-shaper and Groove Profile on Joint Strength Made by Electromagnetic Crimping" *International Journal of Precision Engineering Manufacturing – Green Technology* **(To be submitted).**

Book chapter

[1] **Areda, G.T. and** Kore, S.D., "Numerical Study on Electromagnetic Crimping of Aluminium Tube and Steel Profiled Rod." *Advances in Computational Methods in Manufacturing. Springer, Singapore*, 2019, pp. 271-282, https://doi.org/10.1007/978-981-32-9072-3_23.

International Conference

[1] **Areda, G.,** and S. Kore. 2017 "Finite Element Modeling and Simulation of Electromagnetic Crimping of Al6016-T6 Tube with Steel Rod." ICCASP/ICMMD-2016. Advances in Intelligent Systems Research. Vol. 137, pp. 83-88, https://doi.org/10.2991/iccasp-16.2017.14.

[2] **Areda, G.,** and Sachin D. Kore, 2016 "Axial Load Resistance of Joints Made by Electromagnetic Pulse Crimping." Proceedings of 6th International & 27th All India Manufacturing Technology, Design, and Research Conference (AIMTDR-2016), College of Engineering, Pune, Maharashtra, India, pp.621-625.

National Conference

[1] **Areda, G**., and Sachin D. Kore, 2017 "FEM Study of Electromagnetic Crimping for Defence Application." presented at the 2nd National Conference on Emerging Technologies' Contributi on in Promoting Defence and Industry Capabilities (NCETCPDIC – 2017), July 18th-20th, 201 7, Defence University, College of Engineering, Bishoftu, Ethiopia.